Deltares

Enabling Delta Life

# Risk Analysis for Flood Protection Systems

## Main Report

TNO

Delft Cluster, Veiligheid tegen overstromingen

# Risk analysis for flood protection systems

Main Report

A.C.W.M. Vrouwenvelder (TNO)
M.C.L.M. van Mierlo (Deltares)
E.O.F. Calle (Deltares)
A.A. Markus (Deltares)
T. Schweckendiek (Deltares)
W.M.G. Courage (TNO)

## Verantwoording

Dit rapport bevat een verslag van werkzaamheden die zijn uitgevoerd als onderdeel van het Delft Cluster DC04.30 projectplan van 2005. Het betreft het onderdeel Systeemwerking van Deelproject C “Gevolgen van Overstroming”. De afronding van het project na 2008 heeft plaats gevonden onder de supervisie van Deltares. In dit project is samengewerkt tussen Deltares en TNO-Bouw, waarbij intern de volgende projectnummers zijn gehanteerd:

| | | |
|---|---|---|
| Deltares: | 1202140.008 | SO: Nieuwe Normering - Systeemwerking |
| TNO: | 034.67189 | 35.11 WP C: Probabilistic calculation / VP8B-18 DC CT04.30 Overstromingen |

Tijdens de uitvoering is regelmatig contact onderhouden met de Waterdienst van RWS, die ook de externe financiering voor zijn rekening heeft genomen.

Delft Cluster, Veiligheid tegen overstromingen

# Risk analysis for flood protection systems

Main Report / version 5 (d.d. 20-05-2010)

## Table of Contents

# 1 Introduction

## 1.1 Context of the research

Detailed assessment of flood risk, both on regional as well as on national scale, has been a topic of extensive research in the Netherlands since the early nineties of the past century. Effects of river system behaviour on flood risk (see definition in section 1.2) were usually neglected. For Dutch conditions, however, these effects of system behaviour are of importance (see section 1.3).

Nowadays, in the Netherlands it is commonly acknowledged that a flood risk-based safety approach is indispensable to support decision-making on flood protection strategies and measures. In this report a computational framework is described, that allows for assessing flood risk, while accounting for effects of river system behaviour. The computational frame work comprises of state-of-the-art modelling techniques of hydrodynamic loads and geotechnical resistance, a module for estimating flood consequences, and a module for estimating the occurrence probability of flooding and its associated annual flood risk. The computational framework was successfully applied on a case study area in the Netherlands (see section 1.4).

## 1.2 Definition of river system behaviour

River system behaviour refers to the fact that the flood risk (or safety) of a particular area may depend on the safety of other adjoining areas. It is possible that a measure to improve safety from flooding of a particular area might increase or decrease the safety of other areas, located within the same hydrological system. Effects of river system behaviour can be *beneficial* (increase of safety levels) or *adverse* (decease of safety levels):

- For instance, the failure of a local embankment in a single river system might result in the attenuation of the flood hydrograph and hence in reduced hydraulic loads along downstream located embankments. Reduced hydraulic loads means an *increase* of the safety (i.e. *beneficial* effect) along downstream located embankments.
- For more complex river networks, a local dike failure along a river carrying a high discharge, may result in the fact that its river water flows over flood prone areas into another river, that might have a small discharge conveying capacity only. Such situation may result in increased hydraulic loads and hence in a *decrease* of the safety (i.e. *adverse* effect) of areas located along the receiving river.

It might be clear from the examples above, that the driving mechanism in river system behaviour is the mutual interaction between the failure of flood protection works as result of exerted hydraulic loads and the hydrodynamic response (e.g. changes in river levels) of the river system to such failure.

It can be stated that neglecting effects of river system behaviour means that possibly a less accurate safety level for a particular area might be determined. Further more in case of prevailing effects of river system behaviour, the safety level (or safety norm) of all effected areas are to be considered jointly.

## 1.3 Importance of river system behaviour in the Netherlands

Van Mierlo (2005) and Van Mierlo&Van Buren (2006a, 2006b) made an inventory of hydraulic effects of system behaviour, resulting from the local failure under design conditions of primary

flood protection works (i.e. primary protection works, category a en b) in the Netherlands. It was assumed that flood protection works, being overtopped due to the local failure of a flood protection work elsewhere in the system, did not collapse. This is a conservative assumption. The hydraulic effects are defined as differences in maximum river levels under design conditions (i.e. design sea-levels and design upstream flood waves) between the situation without any failure and the situation with one local dike failure.

Figure 1-1 and Figure 1-2 show the findings for the *river dominated part* of the river Rhine and Meuse basin, located in the Eastern part of the Netherlands. The geographical area covered by these two figures is the same as the area, covered by the present case study (see Figure 1-6). Figure 1-1 depicts the type of system behaviour, that results from a local failure in a primary dike, category a (*green*: only reduced maximum river levels at other locations; *red:* increased and reduced maximum river levels; *black:* no significant changes; *grey:* not a primary dike, category a). Figure 1-2 depicts the spatial distribution of hydraulic effects of system behaviour, induced by the failure of the left river Waal dike near Weurt (*green and red*: respectively decrease and increase in maximum river levels; *black:* no significant changes; *blue:* water depths in flooded areas). The local dike failure at Weurt results, except for the flooding of dike ring 41 also in the overtopping of Meuse dikes (i.e. water of river Waal flows into river Meuse). This overtopping results in a rise in maximum water levels on river Meuse, which finally results in the flooding of the downstream located dike ring 36 and 38 (see Figure 1-2). Weurt coincides with potential breach location Dr41L1, considered in the present case study (see Figure 1-6). In both Figure 1-1 and Figure 1-2, darker colours green, red and blue indicate larger values.


Figure 1-1: Type of system behaviour due to a local dike failure

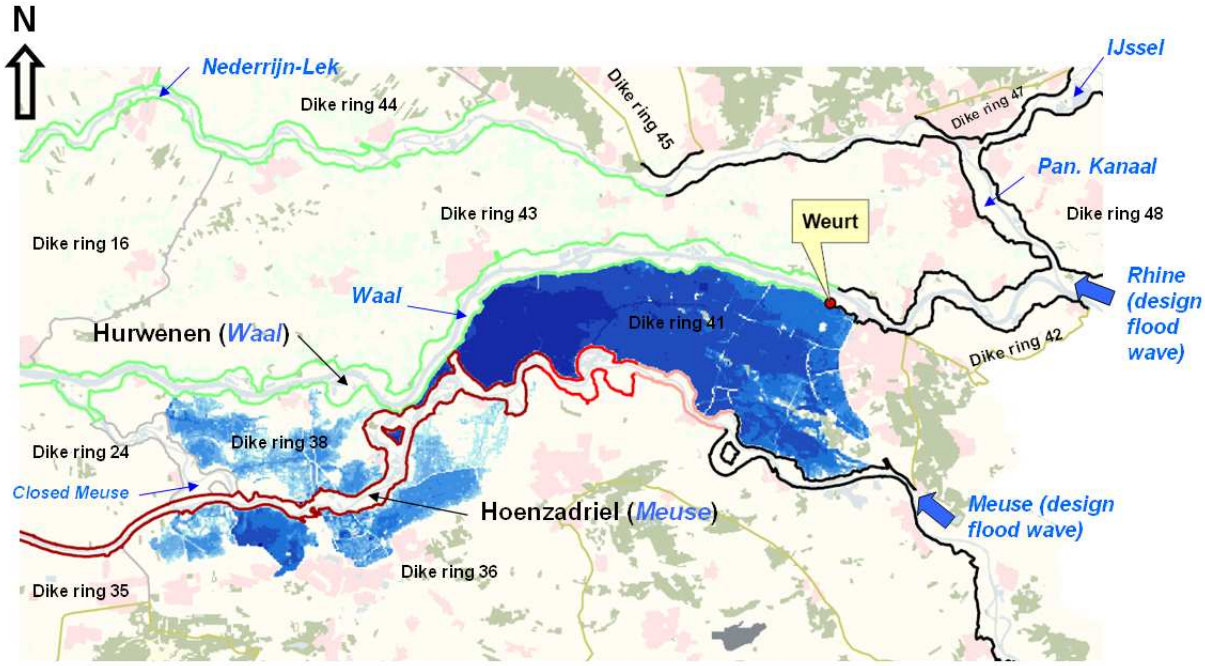


Figure 1-2: Hydraulic effects of system behaviour induced by a breach in the left river Waal dike near Weurt (i.e. location Dr41L1 depicted in Fig 1.6)

As an example hydraulic effects of river system behaviour at Hurwenen (Waal) and Hoenzadriel (Meuse) due to a local dike failure at Weurt under design conditions are shown in Figure 1-3 and Figure 1-4. The depicted river levels were determined in hydrodynamic computations, having design flood waves with frequency of occurrence of once in 1250 year at Lobith (Rhine) and Vierlingsbeek (Meuse). Figure 1-3 and Figure 1-4 show that a local dike failure at Weurt results in a decrease of 0.05 m in the maximum river level at Hurwenen and an increase of 0.96 m in the maximum river level at Hoenzadriel. The decrease (*beneficial* effect) of 0.05 m at Hurwenen means that a river level with a return period of once in 1019 years occurs, instead of river level with a design return period of once in 1250 years. The increase (*adverse* effect) of 0.96 m at Hoenzadriel means that a river level with a return period of once in 19608 years occurs, instead of a river level with a design return period of once in 1250 years. From a statistical point of view design flood waves at Lobith and Vierlingsbeek often coincide (Diermanse and Van Vuren, 2002). Hence, the occurrence of the adverse effect of 0.96 m rise in maximum river level at Hoenzadriel is not that unlikely, given that a local dike failure at Weurt occurs.

Conclusions from the inventory were that effects of river system behaviour cannot be neglected in determining flood risk in the Netherlands. Beneficial effects are negligible compared to adverse effects, and emphasis should, therefore, be paid in avoiding adverse effects.

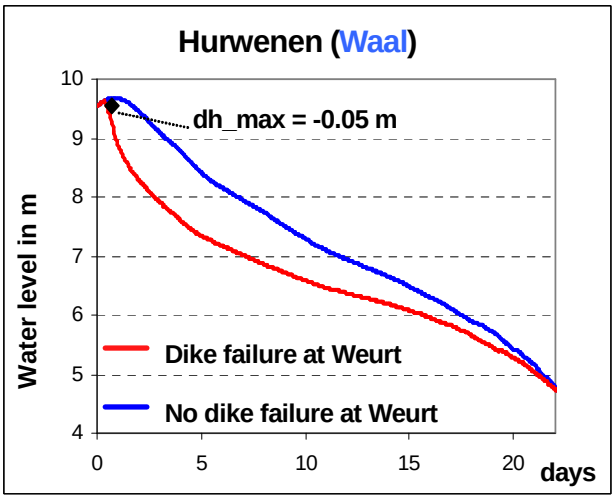


Figure 1-3: Hydraulic effects at Hurwenen(Waal) due to local dike failure at Weurt (see Fig 1.2) under design conditions.

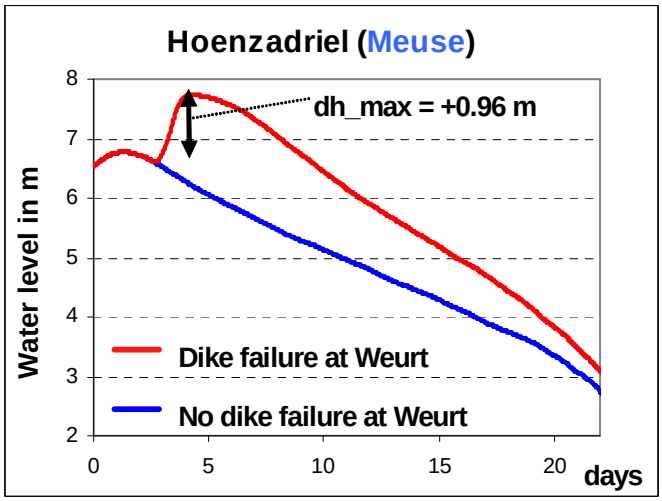


Figure 1-4: Hydraulic effects at Hoezadriel (Meuse) due to local dike failure at Weurt (see Fig 1.2) under

## 1.4 Scope of present study

The present study is a follow up of an earlier study carried out in the *Delft Cluster* research project in the Netherlands (*Van Mierlo et al 2003 and 2007*). In this project a conceptual framework for the evaluation of interaction effects in the case of inundations caused by rivers. A numerical demonstration was presented for a very simple geometrical configuration (Figure 1-5).

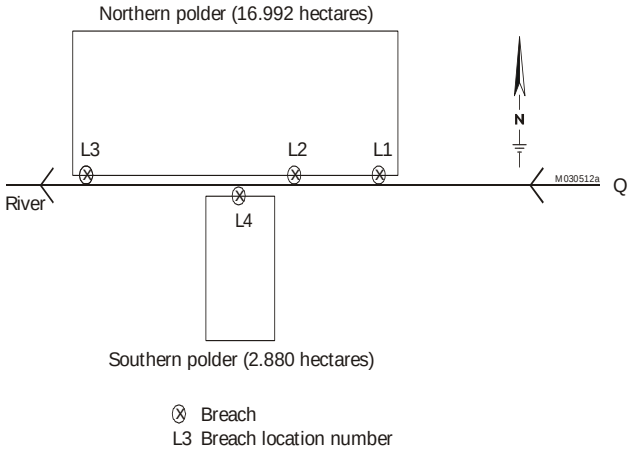


Figure 1-5: Example case in DC-1 study.

In the current study the same basic concept, with a number of technical extensions, is applied to a real flood protected area in the Netherlands situated between the rivers Rhine and Meuse (see Figure 2). The aim is to test, extend and improve those concepts as well as considering the possible implications for our safety policy. Intended items for improvements are:

1. Hydraulic models (efficiency, accuracy, parallel processing)
2. Geotechnical and structural aspects (mechanisms, second line structures)
3. Probabilistic calculation aspects

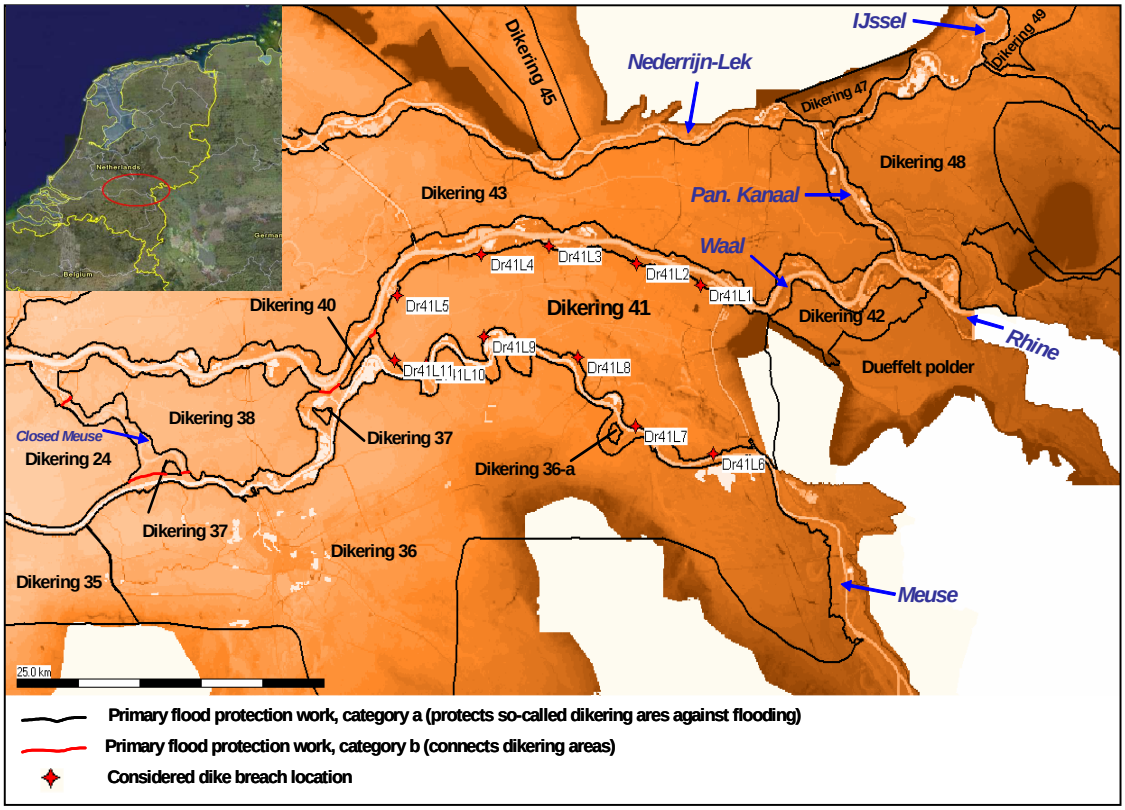


Figure 1-6: Present case study area

This report gives an outline on the various ideas for an efficient approach. It is based on ideas developed (but not tested) during the first stage of Delft Cluster. The basic issue is that a probabilistic analysis usually requires a large number of deterministic computer runs. As long as relatively simple models are used, this is no problem. However, the behaviour of a set of dike rings under flood conditions is so complex that a single run for a deterministic scenario may already cost quite some calculation time. So efficient programming is a key issue. However, in this project main attention has been given to the effort to perform such an analysis anyhow. In order to keep computation time within acceptable limits some simplifications have been made, rather then making highly sophisticated shortcuts. Possible extensions of the computational framework in combination with possible refinements of the calculation procedure will be discussed in chapter 7.

## 1.5 Publications

Next to a number of presentations, the follwing publications are realized:

- Markus, A.A., Courage, W.M.G., van Mierlo, M.C.L.M., *A computational framework for flood risk assessment in the Netherlands*, Scientific Programming, in Press.
- Schweckendiek, T., Vrouwenvelder A.C.W.M., van Mierlo, M.C.L.M., Calle, E.O.F., Courage, W.M.G., *River System Behaviour Effects on Flood Risk*. ESREL, Valencia, Spain, 2008.Martorell et al. (eds): Safety, Reliability and Risk Analysis: Theory, Methods and Applications. CRC Press, Taylor & Francis Group, London, ISBN 978-0-415-48513-5.
- Van Mierlo, M.C.L.M., Schweckendiek, T. and Courage, W.M.G., 2008 *Importance of River System Behaviour in Assessing Flood Risk*, Flood Risk Management: Research and Practice - Samuels et al (eds.), 2009, Taylor & Francis Group, London, pp 327-337, ISBN 978-0-415-48507-4.
- Wim Courage, Ton Vrouwenvelder, Thieu van Mierlo and Timo Schweckendiek, *River System Behaviour Effects in Flood Risk Calculations*, 2010 , in Press.
- Ton Vrouwenvelder, Wim Courage, Thieu van Mierlo and Timo Schweckendiek, *Berekening inundatierisico voor systemen van waterkeringen,* 2010 , in Press

In addition, a wokshop was organized for a broad audience of people from the field on June 3rd 2010 at Deltares, Delft.

# 2 Hydraulic and geotechnical models

## 2.1 Hydraulic model

Flood risk analysis naturally considers hydraulic respectively hydrodynamic aspects as the main load components on the flood defences, like river heads or wave conditions. For assessing effects of river system behaviour it is necessary, in addition to predicting extreme loads throughout the considered system, to model the effects of local failures on the further development of the flood pattern. For this is the main driving mechanism in river system behaviour. Therefore, in each SOBEK computational time-step (±30 s), except for flood propagation also the failure mechanisms (see section 2.2) assigned to each defence structure (e.g. dike section) are evaluated. Furthermore, in case of dike failure, the hydrodynamic model initiates dike breach. Thereafter the hydrodynamic model computes breach growth as function of the actual flow through the dike-breach (see section 2.3). Evaluation of failure mechanisms as well as breach development is effected through the Real-time control (RTC) module in SOBEK.

As mentioned above flood modelling is done using SOBEK (Dhondia, J.F. and G.S. Stelling, 2004), being a one (1D) and two (2D) dimensional hydrodynamic software package developed at Deltares (until 2007 WL|Delft Hydraulics). The SOBEK models (see section 5.1), applied in the case study, comprise of a 1D and a 2D hydrodynamic part. The entire considered geographical area (i.e. rivers, dikes as well as dike ring areas) is modelled as 2D hydrodynamic flow, having a grid cell size of 100m. A local dike breach is modelled as a 1D branch, which is connected to 2D grid cells, respectively located at the river side and at the dike ring side of a potential breach location. The 1D branch accommodates a weir, which is lowered and broadened in accordance with the applied Verheij and Van der Knaap (2002) breach growth formula (see section 2.3). Hence, dike breaches can only occur at “1D potential breach branches”, while “2D river dike grid cells” cannot fail but are overtopped as soon as river levels exceed local crest levels.

The main output of the hydrodynamic model is the flood pattern of each scenario. For each 2D grid cell, SOBEK provides its maximum water depth, its maximum flow velocity and the speed at which water levels rise. This output data is used for determining the flood consequence (i.e. damage and victims) of each scenario (see section 2.4).

The system considered in our study of river system behaviour is a geographically defined (river) flood prone area. It includes rivers (or river branches) within this area and (natural or man made) flood protection structures. Interactions between river flow and the possible failure of flood protection works are to be accounted for within the area. The boundaries of the area must be chosen such that:

1. flood risk within the area solely depends on the hydraulic properties of its river system and the strength characteristics of its flood protections,
2. water levels and discharges at the boundaries of the area are to be autonomous, i.e. not influenced by potential flood events within or outside the area.

## 2.2 Geotechnical failure mechanisms

### 2.2.1 Introduction

The modular structure of the developed computational framework allows the implementation of virtually any structural model to represent the resistance of the flood defences.

For the area treated in the presented case study we are dealing mainly with river dikes. Previous risk analyses have shown that the dominant (most probable) failure mechanisms in the area are 'heave and piping' and 'overflow and erosion of the inner slope' (*see VNK 2005*). For sake of simplicity, analytical and semi-empirical expressions are used as descriptions for the failure mechanisms. Other mechanisms are neglected for the time being and their contribution to the failure probability is speculated to be small. More detailed analyses in the future will also have to consider other structures, like locks, that form part of the flood defence system.

Each mechanism is formulated as a performance function Z:

$$Z = R(\underline{x}) - S(\underline{x}) \tag{2.1}$$

with:

$R(\underline{x})$ resistance part of the mechanism
$S(\underline{x})$ load part of the mechanism

Both $R$ and $S$ are functions of the considered random variables $\underline{x}$. It implies that if $Z<0$, this is considered as failure and vice versa.

The described mechanisms are initiating mechanisms in a sense that they initiate failure of the dike. Once an initiating mechanism occurs, we assume that breach development occurs (see 2.3).

### 2.2.2 Heave and Piping

**Description**

Heave and piping are consecutive mechanisms that can occur in sand layers below dikes. Both are caused by large pore pressure gradients. A typical situation is sketched in Figure 2-1, where a permeable sand layer in contact with the river follows the increase of water pressure directly whereas the pore pressure in the clay top layer in the hinterland remain considerably lower. If the pore pressure exceeds the weight of the top layer, this layer is lifted up and as a consequence vertical cracks occur. The groundwater flows out in vertical direction. This phenomenon is called heave.

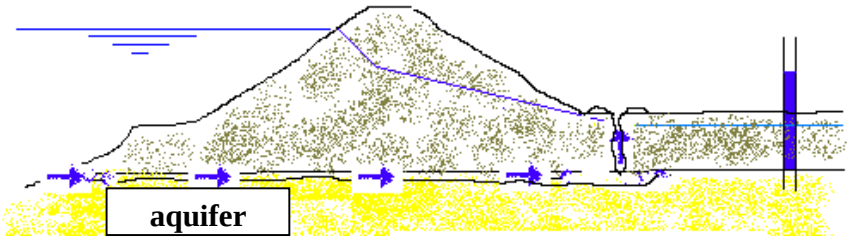


Figure 2-1: Heave and Piping

Heave can be followed by piping. The vertical groundwater flow can cause erosion and initiate the transport of sand. This erosion process can initiate the formation of tubular holes (pipes) below the dike, the development of which starts at the heave crack and grows towards the river. These pipes can endanger the dike stability as a whole by virtually undermining the structure.

The mechanisms leading to heave and piping are certainly time dependent. However, for sake of simplicity, time dependence has not explicitly been modelled at this stage. It is suggested to take up this issue in subsequent studies (see also Appendix A).

**Formulation**

Heave and piping mechanisms have to be considered simultaneously. Piping can only occur, given that heave has occurred beforehand, and if a critical head is exceeded. As stated before. time dependence is not considered in this project explicitly. Reasonable assumptions about the time dependence are made in the failure mechanism descriptions implicitly.

For heave we can determine a critical head difference and thereby a critical river head $h_{crit,heave}$, for which the pore pressure in the aquifer exceeds the weight of the top layer (in case of an aquitard: an almost or completely impermeable layer) by:

$$\mathrm{h}_{\mathrm{crit,heave}} = \frac{\gamma_{sat} - \gamma_w}{\gamma_w} d + \mathrm{h}_{\mathrm{hinter}} \tag{2.2}$$

where:

| | | |
|---|---|---|
| $\gamma_{sat}$ | = | saturated volumetric weight of the top layer [kN/m3] |
| $\gamma_w$ | = | volumetric weight of water [kN/m3] |
| d | = | thickness of the top layer [m] |
| $\mathrm{h}_{\mathrm{hinter}}$ | = | hydraulic head in the hinterland [m+NAP] |

(If no top layer with low permeability is present, heave occurs when the critical gradient $i_c$ is exceeded. This relation requires knowledge about the geometry of present piping screens and is therefore neglected here in first instance.)

The limit state function for heave is formulated as:

$$\mathrm{Z} = \mathrm{m}_0 \Delta \mathrm{h}_{\mathrm{crit,heave}} - \mathrm{m}_{\Delta \mathrm{h}} \left( h - h_{h\,\mathrm{int}\,er} \right) = m_0 \left( \frac{\gamma_{sat} - \gamma_w}{\gamma_w} d \right) - \mathrm{m}_{\Delta \mathrm{h}} \left( h - h_{h\,\mathrm{int}\,er} \right) \tag{2.3}$$

The model factors $\mathrm{m}_0$ and $\mathrm{m}_{\Delta \mathrm{h}}$ reflect the uncertainties in the determination of the critical head difference $\Delta \mathrm{h}_{\mathrm{crit,heave}}$ [m] for heave and the amount of damping respectively.

The critical river head for piping $h_{crit,piping}$ *[m+NAP]* can be determined by the rule of Sellmeijer:

$$h_{crit,piping} = h_{hinter} + \left( \frac{D}{L} \right)^{\frac{0.28}{((D/L)^{2.8} - 1)}} \eta d_{70} \left( \frac{g}{\nu k L} \right)^{1/3} L \left( \frac{\gamma_g}{\gamma_w} - 1 \right) \left[ 0.68 - 0.1 \cdot \ln \left\{ \eta d_{70} \left( \frac{g}{\nu k L} \right)^{1/3} \right\} \right] \tan\theta + 0.3 d \tag{2.4}$$

The limit state function for piping can be formulated as:

$$Z = m_p \Delta h_{crit,piping} - \left(h - 0.3d - h_{h\,int\,er}\right) \quad (2.5)$$

The model factor $m_p$ reflects the uncertainties in the determination of the critical head difference $\Delta h_{crit,piping}$ for piping (rule of Sellmeijer).

The choices of the input parameters are somewhat situation-dependent (e.g. on flooding of the protected area). The exact implementation and decision criteria whether a dike fails or breaches in the calculation model depending on the circumstances are explained in Appendix B.

### 2.2.3 Overtopping and Subsequent Inner Slope Erosion

**Description**
The mechanism overtopping is contemplated as a combination of the river head exceeding the dike height and the consequences of overflow on the dike stability. The water level exceeding the crest level of the dike height is considered as failure in the sense of overtopping. For the hydraulic calculations in this scheme it is furthermore important to implement a criterion for the creation of a dike breach. This criterion will be dependent on the overtopping discharge and the quality of the inner slope protection with respect to erosion. The influence of waves is neglected at this stage. The influence in the case study regions is speculated to be negligible.

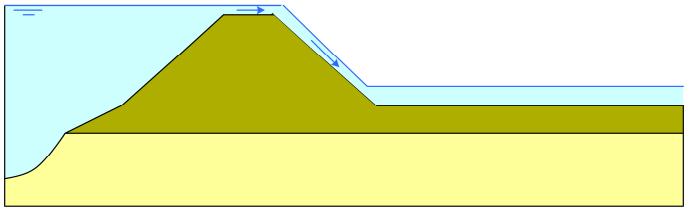

Figure 2-2: Failure Mechanism Overflow

**Implementation**
Overflow occurs when the water level exceeds the dike height. The subsequent flow over the dike slope can cause erosion and failure of the slope. The limit state function is therefore:

$$Z = h_d - h \quad (2.6)$$

where:
$h_d$ = dike height [m+NAP]

The amount of overflow and the quality of the slope protection determine the inner slope stability with respect to erosion. For this project we will adopt a relation from a CIRIA-research which is also used in the theoretical manual of PCRing (Vrouwenvelder 2003) to determine the critical overflow discharge $q_c$:

$$q_c = \frac{v_c^{5/2} k^{1/4}}{125 \tan \alpha_i^{3/4}} \qquad (2.7)$$

where:

| | | |
|---|---|---|
| $v_c$ | = | critical flow velocity over the protection layer [m/s] |
| $\alpha_i$ | = | slope angle [rad] |
| k | = | roughness coefficient according to Strickler [$m^{1/2}s^{3/2}$] |

In case of lacking data, we assume a default value of k = 0.015 with a 25% variation coefficient. The critical flow velocity $v_c$ is given by:

$$v_c = f_g \frac{3.8}{(1 + 0.8 \cdot \log_{10} t_e)} \qquad (2.8)$$

where:

$f_g$=quality of the (grass) protection layer (bad: 0.7,medium:1.0;good: 1.4)[-]

(if given in terms of ersion resitance coefficient $c_g$: $f_g = \left( \frac{c_g}{6 \cdot 10^5} \right)^{2/3}$ )

| | | |
|---|---|---|
| $t_e$ | = | duration of exceedance of the critical flow velocity [h] |

In the current study the time effects are not modelled explicitly. Therefore we choose the exceedance duration $t_e$ = 100 h, which is a best guess estimate for river flood waves. Figure 2-3 shows that in this order of duration the critical velocity is not very sensitive.

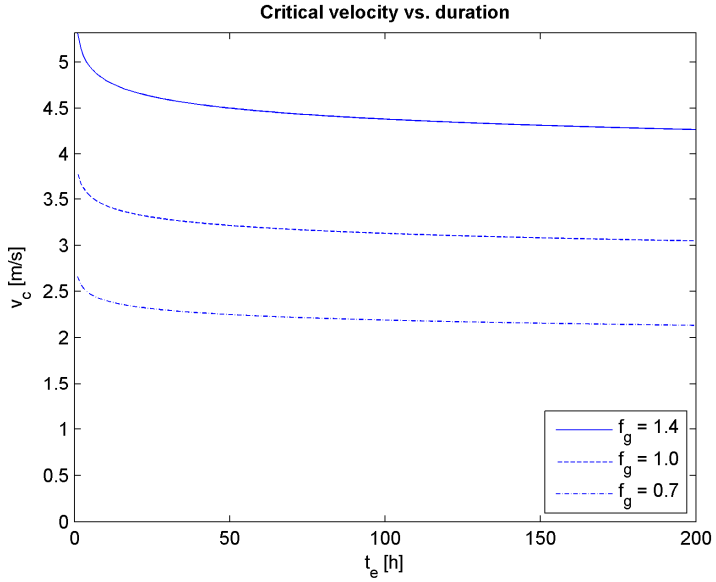


Figure 2-3: Critical velocity as function of grass quality and exceedance duration

In the hydraulic calculations the control variable will be the local water level. In order to transform formula 2.8 from discharge- to water-level dependence, basic fluid mechanics relations can be applied and the relation changes to the critical head difference for erosion in the following form:

$$\Delta h_e = \sqrt[3]{\frac{q_c^{\,2}}{0.36 \cdot g}} \tag{2.9}$$

The limit state function can be formulated as:

$$Z = h_d + m_e h_e - h = h_d + m_e \sqrt[3]{\frac{q_c^{\,2}}{0.36 \cdot g}} - h \tag{2.10}$$

The model factor $m_e$ reflects the uncertainty in the erosion model.

The influence of overflow / overtopping on micro stability is not considered.

### 2.2.4 Slope Instability

**Description**
The most typical failure mechanism in terms of slope stability in river regimes is the failure of the inner slope of the dike. The outside water level rises and causes an increase of the pore pressures inside the dike[1]. This leads to a decrease of effective stresses and thereby of the shear resistance of the soil and failure can occur as indicated in Figure 2-4.

Uncertainties of pore pressures relate to uncertainties of the geohydrological characteristics and parameters, as well as to the initial saturation level of the dike body, as a result of weather conditions prior to the extreme river discharge event. Both, uncertainties regarding pore pressures as well as uncertainties of shear strength properties play a role in the probability of inner slope failure.

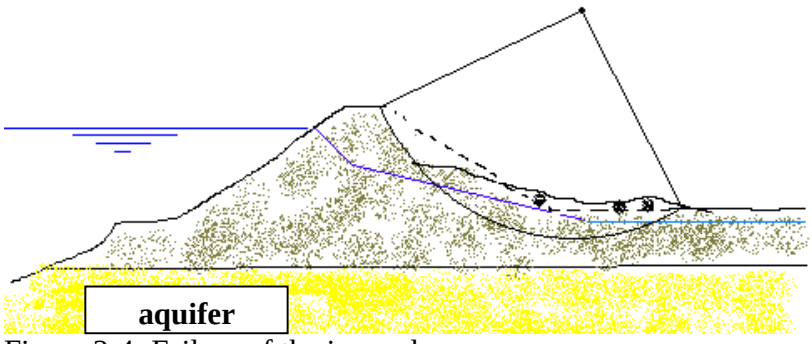

Figure 2-4: Failure of the inner slope

At present several methods are being used for assessing the safety of river dikes:

- analytical methods like Bishop's slip circle analysis (e.g. Mstab),
- probabilistic techniques using the analytical methods (e.g. Mprostab),
- Finite Element Analysis (e.g. Plaxis).

[1] As in the previous section, the influence of infiltration of overtopping water in not considered.

The pore pressures can be determined in different manners. For design and safety assessment there are technical recommendations that can be consulted (e.g. 'Technisch Rapport Waterspanningen bij Dijken'). These recommendations comprise conservative approaches for the determination of phreatic lines and pore pressures. Usually they consider the steady-state situation[2].

The flood wave duration, however, may be insufficient to develop a steady-state situation in the dike. For a more realistic pore pressure field considering the time aspect, transient groundwater flow calculations can be carried out. Time-dependent flow calculations are not state-of-the-art in dike design yet, but the potential benefits of such an approach can be demonstrated by example calculations as carried out by Van Esch 1994 (internal report GeoDelft: 'Tijdsafhankelijke stabiliteit van dijken').

The classical methods for slope stability assessment do not consider residual strength. In practice, it is possible that e.g. the failure of the inner slope does not necessarily mean that the dike loses its water retaining function.

As described in section 2.2.2, the heave phenomenon can cause a situation with zero effective stress under a top layer with low permeability. That means that also the shear strength in that zone is practically zero. In this case the failure plane can be of a different shape with respect to classical slip circle models, following the layer separation below the top layer (see Figure 2-5). The consequence is that with rising outside water levels the safety factor may drop suddenly, when reaching a critical level – the heave potential.

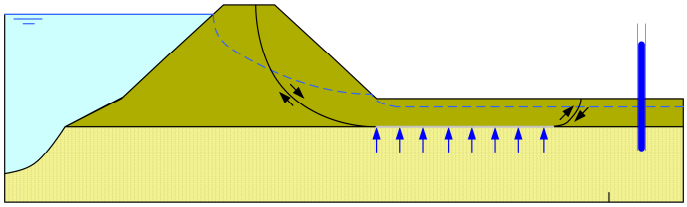

Figure 2-5: Heave Causing Instability

**Implementation**

Slope instability is not considered in the present case study. Nevertheless, a possible way to implement this mechanism is the following.

For this mechanism, there is no simple explicit formulation. This problem can be circumvented by carrying out several reliability calculations (e.g. with Mprostab) at different local water levels, from which we obtain conditional reliability indices $\beta(h)$ and influence coefficients $\alpha_i(h)$. With these we formulate an equivalent limit state function in the following form:

$$\tilde{Z} = \beta(h) + \sum_{i=1}^{\#\,variables} \alpha_i(h)\frac{(X_i - \mu_{X_i})}{\sigma_i} \qquad (2.11)$$

where:

$X_i$ = relevant variables (e.g. soil strength or permeability)

[2] Virtually infinite duration of the maximum water level for schematization of pore pressures and pore water flow.

$\mu_{Xi}$ = expected values of the variables

Between the discrete calculated values of the conditional $\beta(h)$ and $\alpha_i(h)$ we apply linear interpolation, respectively extrapolation outside the investigated range.

The model factor is already included in the calculated values using a model factor on the uncertainties in the Bishop slip circle approach.

### 2.2.5 Fault Tree

The following fault tree illustrates the dependencies between the mechanisms for the chosen scheme (including slope stability):

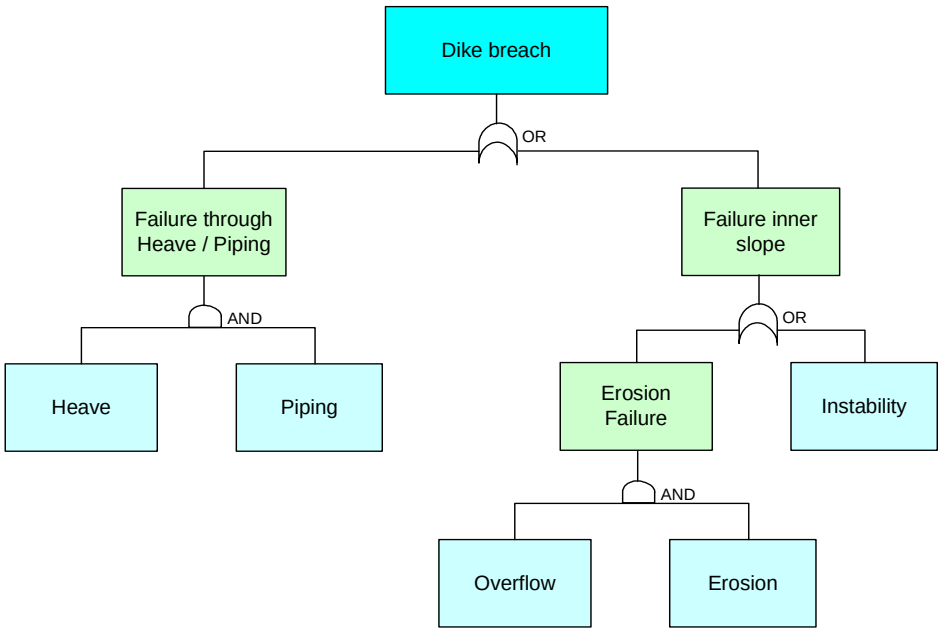


Figure 2-6: Fault tree for dike breach criteria

This fault tree is not suited for the determination of the failure probability in the total calculations scheme, but merely a representation of the criterion to decide whether a dike breach is to be initiated in the hydraulic calculations.

*Remark: The fault tree in Figure 2-6 illustrates the decision scheme for dike breach initiation, if all above described mechanisms are used. In the case studies presented in this report sometimes reduced fault trees with a smaller number of mechanisms have been used.*

## 2.3 Dike Breach modelling

The previously described mechanism descriptions are used to detect the initiation of failure, i.e. the loss of integrity of the dike. Once this occurs, a time-dependent breach growth formulation is applied (e.g breach development as function of the flow passing through the dike breach) and the geometrical model is adapted accordingly (dike crest level decreases locally and the breach grows in width). This influences the further hydrodynamic development as well. In the present study a different breach growth concept was used than in the earlier Delft Cluster research project.

### 2.3.1 Dike breach growth concept in the DC1 research project

In the earlier Delft Cluster research project (hereafter referred to as the DC1 project), both overflow and piping failure mechanisms were evaluated. If failure occurred, the dike-breach process started immediately. Hence, any kind of residual strength was neglected. Further on, the dike-breach process occurred irrespective of actual river levels and flow velocities through the dike-breach. More precisely, the dike-breach process comprised of two steps:

1. In the *1st step*, the initial dike height was lowered towards local surface level. The lowering occurred in 1 hour for a constant breach width of 20 m.
2. In the *2nd step*, only the width of the dike-breach was increased. More precisely, a final breach width ($B_{final}$) was attained in $T_{breach}$ hours. Both $B_{final}$ and $T_{breach}$ were stochastic model parameters.

*Resuming*: In the DC1 project residual strength was neglected and dike-breach developed irrespective of the magnitude of the flow through the dike-breach. Hence, the height of the dike was always lowered to local surface level and the final breach width was always attained.

### 2.3.2 Dike breach growth concept in the present (DC2) research project

In the present Delft Cluster research project (hereafter referred to as the DC2 project), the failure mechanisms described in section 2.2. are evaluated. Residual strength should preferably be considered. In the DC2 project, residual strength was, however, not considered due to the lack of adequate formulations that describe remaining residual strength after the occurrence of a particular failure mechanism. In the DC2 project breach growth was a function of the magnitude of the actual flow through the dike-breach. This is important, since the magnitude of changes in hydraulic loads elsewhere in the river system depend on the magnitude of flows through dike breaches. In return, flows through dike breaches depend on governing hydraulic boundary conditions and the time-dependent growth of dike breaches.

Irrespective of which failure mechanism occurred at a potential breach location, the same breaching formulation was applied in the present (DC2) project. The breaching formulation comprises of two steps:

1. **The *1st step*:**
   Once failure occurs, the dike-height at the concerning potential breach location is instantaneously lowered to a level that is 0.10 m below the maximum of the adjacent river level and the adjacent water level in the protected area (i.e. dike ring). This means that any kind of residual strength is neglected.
   Thereafter, if the actual flow-velocity through the dike-breach exceeds a critical flow-velocity ($u_c$), the dike-height decreases with a constant LoweringSpeed and for a constant breach width ($B_o$) till the maximum of the local surface level ($Z_{min}$) is attained.

$$LoweringSpeed = (z_0 - z_{\min}) / T_0 \quad (2.12)$$

*where:*
LoweringSpeed = velocity in which the dike height is lowered in m/hr
$Z_0$ = initial dike height (i.e. before failure occurred) in m.
$Z_{min}$ = maximum of the local surface level at both side of the dike in m.
$T_0$ = Time period during which the dike-breach, having a constant initial width ($B_o$) is lowered from its initial crest level ($z_{crest\ level}$) to its final crest level ($z_{min}$) [hr]

The critical flow-velocity ($u_c$), the constant breach width ($B_o$), the initial dike height ($Z_0$) and time period (To) are stochastic parameters.

2. **The *2nd step:***
The 2nd step starts as soon as $Z_{min}$ is attained. ($t>t_o$). In the 2nd step, the dike height remains equal to $Z_{min}$. However, as long as the actual flow-velocity through the dike-breach exceeds the critical flow-velocity ($u_c$), the width of the dike breach develops in accordance with the Verheij-vdKnaap formula.
In the Verheij-vdKnaap formula the breach-width tends to an asymptotic analytical solution. However, there is no physical limitation for the maximum breach width. The Verheij-vdKnaap formula reads:

$$B(t_{i+1}) = B(t_i) + \frac{\partial B}{\partial t}\Delta t \quad (2.13)$$

and:

$$\left(\frac{\partial B}{\partial t}\right)_{t_i} = \frac{f_1 f_2}{\ln 10}\frac{\{g(h_{up} - h_{down})\}^{1.5}}{u_c^2}\frac{1}{1 + \frac{f_2 g}{u_c}(t_i - t_0)} \quad (2.14)$$

*Conditions:*
If $h_{down} < Z_{min}$ than yields $h_{down} = Z_{min}$
If $B(t_i) < B(t_{i-1})$ than yields $B(t_i) = B(t_{i-1})$

***Where:***
B(t) : Width of the breach at point-in-time t,
$\Delta t$ : time step [s]
$f_1$ : Constant factor [-]
$f_2$ : Constant factor [-]
g : Acceleration due to gravity [$m/s^2$]
$h_{up}$ : Upstream water level at point-in-time t [m]
$h_{down}$ : Downstream water level at point-in-time t [m]
$t_i$ : Point-in-time [hr]
$t_o$ : Point-in-time [hr] at which the local surface level ($Z_{min}$) is attained

$u_c$ : Constant critical flow-velocity sediment/soil [m/s]

Verhey and van der Knaap propose following default values and range:

| **Parameter** | **Default** | **range** |
|---|---|---|
| $f_1$ | 1,3 | 0,5 – 5 |
| $f_2$ | 0,04 | 0,01 – 1 |
| $B_0$ | 10 m | 1 – 100 m |
| $T_o$ | 0.1 hr | 0.1 – 12 hr |
| $u_c$ | 0,2 m/s | 0,1 - 10 m/s |

$T_o$ : Time period during which the dike-breach, having a constant initial width ($B_o$) is lowered from its initial crestlevel ($z_{crest\ level}$) to its final crest level ($z_{min}$) [hr]

Classification of soil-strength:

In the Verheij-vdKnaap (2002) formula, a value for $u_c$ should be defined. In the Table below values for $u_c$ and $\tau_c$ are given as function of the soil-type.

| **Soil type** | **$u_c$ (m/s)** | **$\tau_c$ (Pa)** | **Grondsoort** |
|---|---|---|---|
| Grass, good | 7 | 185 | gras, goed |
| Grass, moderate | 5 | 92.5 | gras, matig |
| Grass, bad | 4 | 62 | gras, slecht |
| Clay, very good (compacted) | 1.0 | 4 | klei, zeer goede (compact; $t_{ongedraineerd}$ = 80-100 kPa) |
| Clay, good (firm) | 0.80 | 2.5 | klei met 60% zand (stevig; $t_{ongedraineerd}$ = 40-80 kPa) |
| Clay, moderate, (little structure) | 0.70 | 2 | goede klei met weinig structuur |
| Clay, moderate (considerable structured) | 0.60 | 1.5 | goede klei, sterk gestructureerd |
| Clay, bad (weak) | 0.40 | 0.65 | slechte klei (slap; $t_{ongedraineerd}$ = 20-40 kPa) |
| Sand with 17% silt | 0.225 | 0.20 | zand met 17% silt |
| Sand with 10% silt | 0.20 | 0.15 | zand met 10% silt |
| Sand with 0% silt | 0.16 | 0.10 | zand met 0% silt |

For a known $\tau_c$ value, a value for $u_c$ can determined using the formula given below

$$u_c = 0.5\sqrt{\tau_c} \qquad (2.15)$$

Further on $u_c$ might be determined using the following formula:

$$u_c = u_{c,zand}\left(1+0,01\alpha P_{clay}\right)+\beta\left(0,65-v\right) \quad (2.16)$$

***Where:***
Default values $\alpha$ = 15, $\beta$ = 1 and $u_{c,zand}$ = 0,2 m/s
v = n / (1-n ) with n = soil pore fraction (default n = 0.4),
$P_{clay}$ = percentage of clay

## 2.4 HIS-SSM damage module

The flood consequence (i.e. damage and victims) are determined using the '*HIS Damage and Victims Module'* (in Dutch, referred to as HIS-SSM, see *Huizinga 2004*). HIS-SSM is a commonly applied method for determining flood consequence in the Netherlands. HIS-SSM comprises, a computational engine, a database and so-called damage and victim functions (*Jonkman 2007*). The standard database contains detailed information on the land-use (agriculture, urban area, industry and so on) as well as the number of inhabitants, cost of houses and infrastructural works for each region in the Netherlands. Per land-use there are standard damage and victim functions available in HIS-SSM. The user can define its own database as well as its own damage and victim functions. In the case study (see chapter 5) the standard database and the standard damage and victims functions were applied in the HIS-SSM computations.
HIS-SSM is a GIS-based tool that requires per 2D grid cell of the hydrodynamic model schematisation, the characteristics of the flood pattern (for details, see section 2.1) as main input. Based on this hydraulic information and the selected damage and victim functions, HIS-SSM computes the expected economical damage and the expected number of victims. This is illustrated in Figure 2-7. HIS-SSM can provide flood consequence for the entire area as well as per user defined sub-areas (e.g. per dike ring area).

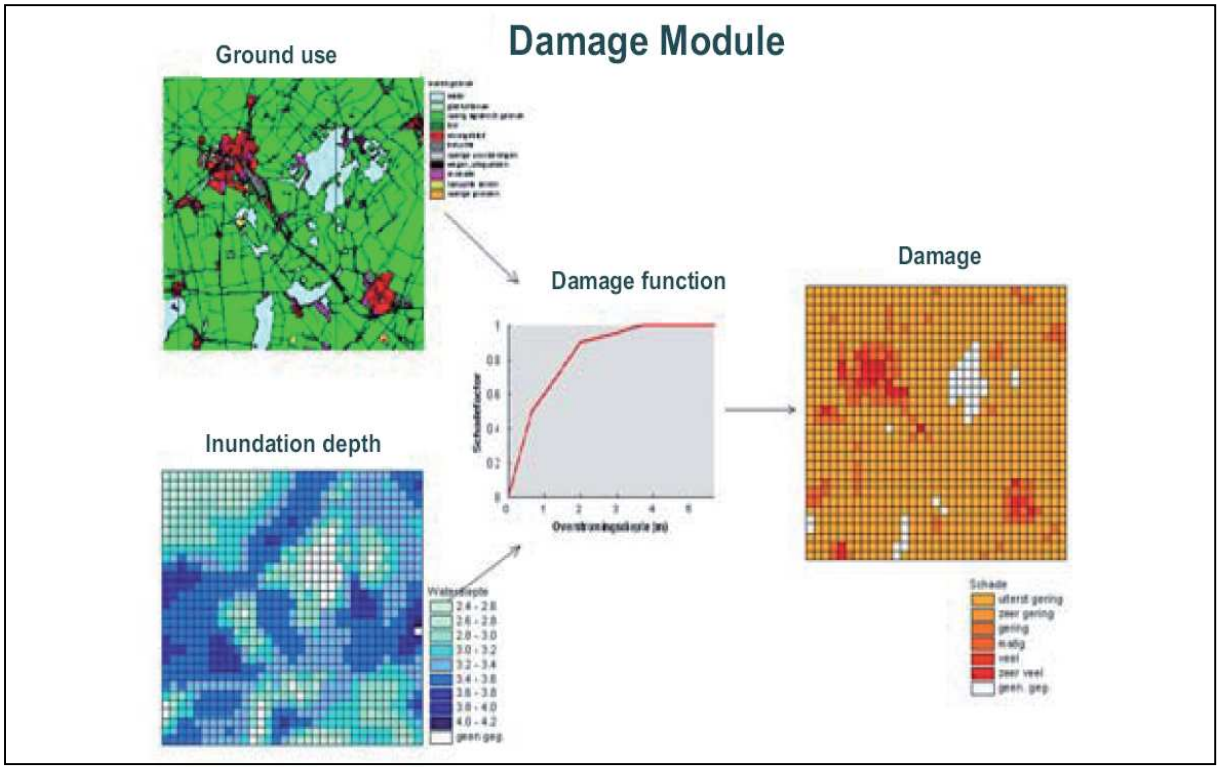


Figure 2-7: Flood damage determination with HIS-SSM (VNK 2005)

# 3 Statistical models

## 3.1 Hydraulic models

Important processes and variables for the load on rivers are:

- River discharge
- Duration and form of a high discharge
- Wind speed and direction
- Water level at the river mouth
- Duration of the storm onset

In the current study the basic concept is applied to a real flood protected area in the Netherlands, situated between the rivers Rhine and Meuse. For that area it is assumed, for the time being, that wind speed and direction, sea water level and the duration of the storm onset need not be modelled statistically. In fact, for down stream locations deterministic stage discharge relations are imposed. However, in future projects they can and should be taken properly into account. The simplified assumption in this project is based on the location of the area at hand (the east of the Netherlands) and the failure mechanisms that are looked at (overflow, heave and piping).

With respect to the river discharge, duration and form of the discharges, use is made of the PC-Ring implementation which accounts for the discharge statistics based on:

1. The distribution of the yearly extremes, which gives return times of the top discharges,
2. The arbitrary point in time distribution, which gives the average number of days per year that a certain level of discharge is exceeded.

In case of more than one river threatening the flood defence, the correlation between the discharges is used to account for the probability that an extreme discharge occurs on both rivers. Details of this modellation can be found in '*Theoriehandleiding PC-Ring, deel B statistische modellen' (Vrouwenvelder et al).*

In order to establish the physical relation between local water levels and river discharges, SOBEK calculations are used. These calculations are carried out for the chosen geographical model, assuming absence of river system behaviour effects. That is, the hydraulic loads on the dikes are computed assuming that the entire flood wave passes through the system without any dike failure or overtopping. The resulting hydraulic loads are calculated for a range of discrete peak flood waves:

from 500 to 7900 $m^3$/s with steps of 100 $m^3$/s for the river Meuse, and
from 2000 to 25000 $m^3$/s for the river Rhine (both with steps of 100 $m^3$/s).[3]

These relations are derived assuming the 50% value of the flood wave pattern.
As a result, a database is obtained with water levels per location as a function of the peak flood waves.

[3] The original statistics as described in '*Theoriehandleiding PC-Ring, deel B statistische modellen' (Vrouwenvelder et al)* and as implemented in PCRing were used. In order to speed up the calculations in findig failure scenarios, within the context of proof of concept, a pragmatic assumption of temporarely extending the upper bound for Lobith from 18000 to 25000 $m^3$/s was adopted. From a hydro-meteorological point of view, it is doubtful if such discharges can occur (see Deltares, 2008). Besides, the frequency of occurrence will be much smaller than the one derived from the applied joint probability density function (see Gudden and Overmars, 2004; Lammersen, 2004).

Prob2B draws of the random samples for the peak discharges of Rhine and Meuse (the latter conditionally on the first) and then obtains the water levels on the locations. When, in combination with the Mont Carlo realizations of the dike properties, failure and or overflow is calculated in one or more locations, the set of parameter values is saved to a file for use in the 2-D Sobek inundation simulations. The latter will again make use of the high water waves as already generated by the water wave generator in deriving the MHW database.
The time delay between discharges at Rhine (Lobith) and Meuse (Vieringsbeek) is based on 'Het samenvallen van pieken op Rijn en Maas in het benedenrivierengebied' (Diermanse et al) and is modelled as:

0 hour if $Q_{Lobith}$>=8000$m^3$/s OR $Q_{Vieringsbeek}$>=2000$m^3$/s
-36 hour in all other cases.

With the minus sign indicating that the peak discharge at Vierlingsebeek on river Meuse occurs 36 hours before the peak discharge at Lobith on river Rhine occurs.

## 3.2 Dike properties

The following list gives an overview of the variables involved in the currently described failure mechanisms, except slope instability:

Table 3.1: Variables overview

| **Variable** | **in code** | **Unit** | **Description** | **Mechanism(s)** |
|---|---|---|---|---|
| h | h | [m+NAP] | water level | all mechanisms |
| D | D | [m] | aquifer thickness | piping |
| L | L | [m] | piping length | piping |
| d | d | [m] | impermeable top layer thickness | heave, piping |
| $h_{hinter}$ | h_hinter | [m+NAP] | hydraulic head hinterland | heave, piping |
| $h_d$ | h_d | [m+NAP] | dike height | overflow, erosion |
| $\tan(\alpha_i)$ | tanalphai | [-] | inner slope angle | erosion |
| $\gamma_{sat}$ | gamma_sat | [kN/m3] | saturated volumetric weight of the impermeable top layer | heave |
| $\gamma_w$ | gamma_w | [kN/m3] | volumetric weight of water | heave, piping |
| k | k | [m/s] | specific permeability | piping |
| $d_{70}$ | d70 | [m] | 70th percentile of the grain distribution (sieve curve) | piping |
| $\nu$ | nu | [m2/s] | kinematic viscosity | piping |
| $\eta$ | eta | [-] | White constant (sleepkrachtfactor) | piping |
| $\theta$ | theta | [rad] | rolling resistance angle | piping |
| $\gamma_g$ | gamma_g | [kN/m3] | volumetric weight of the grains | piping |
| $c_g$ | cg | [-] | grass quality coefficient | erosion |
| $t_e$ | te | [h] | critical velocity exceedance duration | erosion |
| K | K | [m] | roughness coefficient by Strickler (inner slope) | erosion |
| $m_0$ | m0 | [-] | model uncertainty critical head difference for heave (damping) | heave |
| $m_h$ | mh | [-] | model uncertainty head difference for heave (damping) | heave |
| $m_p$ | mp | [-] | model uncertainty Sellmeijer | piping |
| $m_e$ | me | [-] | model uncertainty erosion inner slope | erosion |

Data on the probability density functions for the dike (resistance) parameters were taken from the FLORIS project (VNK 2005). For the case studies presented in chapter 5 and 6, the parameters are presented in Appendix C.

# 4 Computational Framework for the Risk Analysis

## 4.1 System calculation procedure

Uncertainties are present in the loads on and properties of flood protection systems as well as in the characteristics of the area under consideration. In addition to the uncertainties in the properties there are modelling uncertainties and also the degree of detailing is a factor contributing to scatter. In principle, it is possible to model every house for collapse, every person for drowning and every car for evacuation. But these refined models will be too time consuming in the first place and may even be not reliable. The best strategy is probably to use the refined models for calibrating the simpler ones. At the same time these models should be calibrated to real world data as far as possible.

In cost benefit based decision analysis it is usually sufficient to calculate the expectation of the damage. The final scatter in the damage is in principle little used. This, however, does not mean that we can neglect uncertainties in the various random variables. In the first place, neglecting uncertainties may lead to incorrect estimates of expectation, as in general E(g(**X**)) is not equal to g(E(**X**)), except for linear relationships.

The general expression for a flood-risk R for a certain time interval (0,t) is given by:

$$R = E(D) = \int D(\underline{x})\, f(\underline{x}) d\underline{x} \qquad (4.1)$$

Where

$\underline{x}$ the vector with all the stochastic parameters
$f(\underline{x})$ is the joint probability distribution function of $\underline{x}$.
$D(\underline{x})$ is the capitalised value of the damage in (0,t)
$E(..)$ is "expected value"

Elements of the vector x which play a role in the problem are: the river discharge, the wind speed, the sea level, soil properties, dike lining, emergency measures, polder roughness, behaviour of secondary dams, etc. These quantities, in principle, are defined for every point in time in (0,t) and for every point in space.

## 4.2 Scenario approach

If the consequences conditional upon failure are deterministic and do not depend on the particular failure scenario, the risk may be written in the well known standard from:

$$R = P_F\, C. \qquad (4.2)$$

where $P_F$ is the (annual) failure probability and $C$ is a numerical number representing the consequences of failure, for instance expressed in monetary units. In most cases, however, consequences are not deterministic and may also depend on the failure scenario, which then leads to:

$$R = \sum_i P_i \; E\{ C_i \mid F \} \tag{4.3}$$

Here $P_i$ is the annual probability for branche $i$ or failure scenario $i$ and E($C_i$|F) is the expected value that may be associated with the corresponding adverse consequences, conditional upon failure. In this study $C_i$ is supposed to be positive. Negative values of $C$ (indicating benefits) are treated separately. A worked example can be found in (Van Manen and Brinkhuis, 2003). Note that branches or scenarios represent exclusive sequences of events. Consequently, the sum of $P_i$ is equal to the probability of failure: $P_F = \Sigma P_i$.

Usually, a standard reliability analysis does not lead to a set of scenario probabilities, and it may be necessary to do some post processing. Consider as an example a small system of two dike elements. In that case, we would have to calculate:

$$R = P_1 C_1 + P_2 C_2 + P_{12} C_{12} \tag{4.4}$$

where $P_1$ is the probability that only element 1 fails, $P_2$ the probability that only element 2 fails and $P_{12}$ the probability that both elements fail. If inundation does not change the physical conditions, we simply have ($Z$ being the limit state function for failure):

$$P_1 = P\,(Z_1<0 \cap Z_2>0) = P\,(Z_1<0) - P\,(Z_1<0 \cap Z_2<0) \tag{4.5a}$$
$$P_2 = P\,(Z_1>0 \cap Z_2<0) = P\,(Z_2<0) - P\,(Z_1<0 \cap Z_2<0) \tag{4.5b}$$
$$P_{12} = P\,(Z_1<0 \cap Z_2<0) \tag{4.5c}$$

However, in most cases the conditions for each scenario depend on the physical circumstances. For instance, if the weakest element fails first in time, it may unload the other element. As a result that element will not fail at all and consequently $P_{12} = 0$. This is a reasonable scenario for river dikes. In that case the values of $P_1$ and $P_2$ follow from:

$$P_1 = P\,(Z_1<0 \cap Z_1<Z_2) \tag{4.6a}$$
$$P_2 = P\,(Z_2<0 \cap Z_2<Z_1) \tag{4.6b}$$

indicating that one element fails and the other element is stronger. Note that this formulation requires a similar metric for both mechanisms $Z_1$ and $Z_2$ that enables a direct comparison. For other types of dike failure mechanisms, the downstream elements may be unloaded, but not the upstream ones. In that case we have, element 1 being the upstream element:

$$P_1 = P(Z_1<0) \tag{4.7a}$$
$$P_2 = P(Z_2<0 \cap Z_1>0) \tag{4.7b}$$

Actually, we should also include the hydraulic circumstances, as they may influence the course of events. This approach has been used (or is used) in projects like Picaso[4], VNK1[5] and VNK2[6]. For

[4] Bouwdienst Rijkswaterstaat en Dienst Weg- en Waterbouwkunde Rijkswaterstaat, Pilot Case Overstromingsrisico, Deel VI: Eindrapport, Delft, 2001.
[5] Projectbureau Veiligheid Nederland in Kaart, Hoofdrapport Onderzoek Overstromingsrisico's, 2005 SBN-90-369-5604-8.
[6] VNK-2, http://www.helpdeskwater.nl/projectvnk/project_vnk2

complex dike rings the amount of relevant scenarios may become very large. Additionally, to limit calculation time, consequence estimates in those calculations are based on the design point of the scenario. As the scenarios were mostly dictated by the consequences, the scenarios themselves were compound events, not always possessing a unique and physically well defined design point For that reason a new method was looked for, as described in the next section.

### 4.3 Direct Risk estimate using Monte Carlo

The integral (4.1) can also be evaluated using a Monte Carlo procedure. In such a calculation a set of random variables $\underline{x}$ is generated and the series of events that takes place in the flood area, are determined. This is a complex but fully deterministic analysis. All the water levels, the waves, the dike strengths etc. in the entire area are known for the period under consideration. If the combination $\underline{x}$ leads to an initiation of flooding somewhere in the area, all consequences of this event for the rest of the area can be considered.

The basic formula for a direct Monte Carlo estimate for the risk or unconditional damage expectation is given by:

$$R = E(C) = \frac{1}{N} \sum C(x) \tag{4.8}$$

The summation is over all runs, N is their total number or runs, $C(x)$ is the damage (which is zero in case of no inundation), and x is the vector of random variables with probability density function f (x).

Applying importance sampling can often approve the efficiency:

$$R = E(C) = \frac{1}{N} \sum C(x)( f(x) / h(x)) \tag{4.9}$$

where $h(x)$ the density function for the importance sampling. This formulation (4.9), however, still requires many simulations in order to get sufficient certainty.

In many cases there are more efficient ways to estimate the failure probability, for instance the combination of FORM and System Analysis. In that case we estimate the risk from:

$$R = \mathrm{E}(C) = P_F \, \mathrm{E}(C|F) \tag{4.10}$$

where the conditional damage (assuming importance sampling) expectation follows from:

$$E(C \mid F) = \frac{\sum C(x) f(x) / h(x)}{\sum I(x) f(x) / h(x)} \tag{4.11}$$

The functions h(x) may be inspired by the results of the failure probability calculations. In the case of normal sampling, of course, $h(x) = f(x)$.

The point is that the determination of E(C|F) is not so time consuming as (4.8) as the numerator and denominator in (4.11) are heavily correlated (see subsequent example)). Note for instance that in the case of C being deterministic, only one run is necessary. In order to assess how many Monte Carlo runs are necessary; assume that we accept an error of 10 percent. A sufficient number of runs is then obtained if:

$$\sigma(C|F) / \sqrt{(N)} < 0.10 * E(C|F) \tag{4.12}$$

Here N is the number of runs leading to inundation and E(C|*F*) and $\sigma$(C|*F*) are the estimators of the conditional mean and standard deviation following from the importance sampling.
If P(F) has been calculated by Monte Carlo (both crude and importance sampling) we may use directly the runs where failure occurred.

**Example**

To show the advantage of the proposed procedure, consider the case where the limit state function is given by:

$$Z = 2 - x_1 \tag{4.13}$$

and the consequences in case of failure by:

$$C = 100 (1+0.1 x_1+0.1 x_2+ 0.1 x_3+ 0.1 x_4 +0.3 x_5) \tag{4.14}$$

All variables $x_i$ are standard normal. We perform an Importance sampling on $x_i$ with an increased standard deviation equal to 2.0. The number of samples is equal to N= 100. Repeating this simulation for 10 times we find the following result:

| **simulation number** | **Risk using (4.9 )** | **Risk using (4.10/4.11)** |
|---|---|---|
| 1 | 0.65 | 3.37 |
| 2 | 7.50 | 3.49 |
| 3 | 0.03 | 3.89 |
| 4 | 1.80 | 3.06 |
| 5 | 1.41 | 2.94 |
| 6 | 8.42 | 3.22 |
| 7 | 4.24 | 2.28 |
| 8 | 4.11 | 2.73 |
| 9 | 4.18 | 3.13 |
| 10 | 0.30 | 2.82 |
| | | |
| Mean | 3.26 | 3.09 |
| stand dev | 2.96 | 0.44 |

It is obvious that the analysis based on (4.9) has a large scatter and N=100 is not enough to get a reliable result. The column based on (4.10) and (4.11) shows much les scatter and the result for N=100 is acceptable. P(F) is equal to $\Phi(-2) = 0.023$.

## 4.4 The procedure used in chapter 5 and 6.

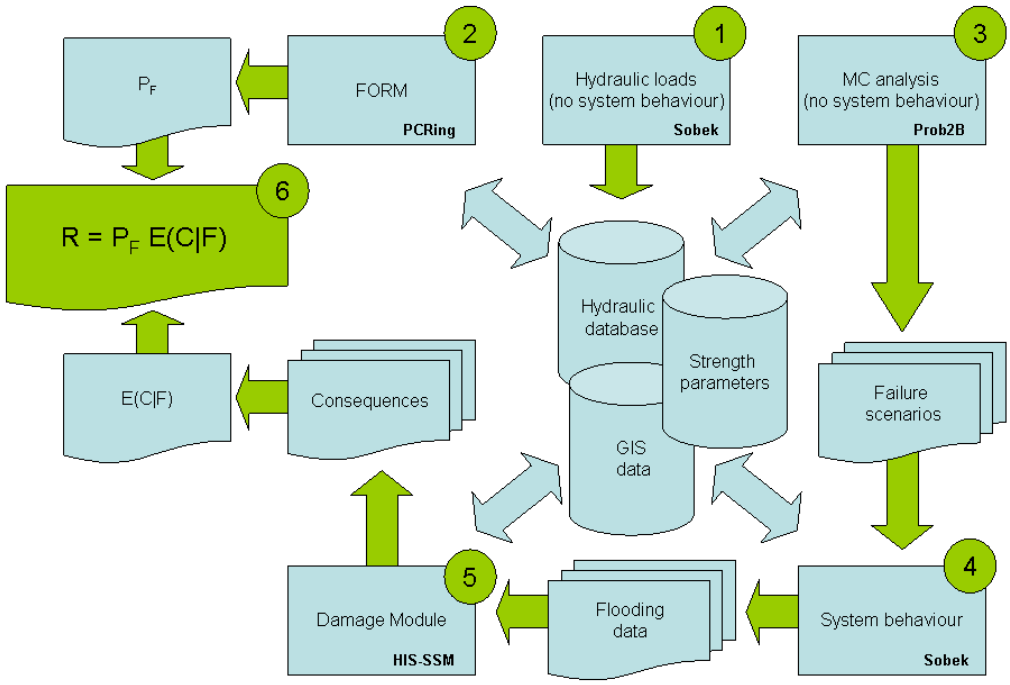


Figure 4-1 Schematic representation of the computational framework

Following the path of separately calculating failure and failure scenario based consequences; a computational framework as shown in figure 2 has been developed and used in the present analysis (case studies in chapter 5 and chapter 6). The six basic steps of the framework, as enumerated in Figure 4-1 are described below.

*Step 1: Determination of hydraulic loads without considering effects of river system behaviour*

Initially, hydrodynamic calculations are carried out for the chosen geographical model, assuming absence of river system behaviour effects. That is, the hydraulic loads on the dikes are computed assuming that the entire flood wave passes through the system without any dike failure. These computations are carried out for a range peak discharges at the upstream boundary of the system. The results are stored in the so-called Step 1 hydraulic data base.

*Step 2: calculating the probability of failure for the system.*

For the dike ring system at hand a reliability calculation is performed. The result is the probability $P_F$ that at least one dike (section) within the system fails. A method is chosen that efficiently calculates this $P_F$. For the Netherlands, the PC-Ring software (*Steenbergen et al, 2004, and Vrouwenvelder, 2001*) is available. It is able to calculate failure probabilities per dike ring (comprised of sections) but also systems of dike rings can be evaluated. Combinations of reliability methods, e.g. FORM, and System Analysis (e.g. *Hohenbichler et al, 1983*) can be chosen. The analysis comprises properties of the dikes regarding the considered failure mechanisms as well as peak discharges at the upstream boundary of the geographical model. The load on the analyzed dike sections are interpolated using the Step 1 hydraulic database. Loads and resistances are compared using performance functions with respect to the failure mechanisms considered, such as piping or overflow.

*Step 3: A representative set of Monte Carlo realisations, conditional upon failure*

At prefixed potential breach locations reliability analyses per section are carried out using Crude Monte Carlo runs. The realizations comprise properties of the dikes regarding the considered failure mechanisms as well as peak discharges at the upstream boundary of the geographical model. The load on the analyzed dike sections are interpolated using the Step 1 hydraulic database. Loads and resistances are compared using performance function as described in Chapter 2.

The results of this step are the probability that at least one dike (section) fails, a representative set of realizations conditional upon failure (at least one dike section fails) and the complementary set of realizations, in which no failure occurs.
If there is a failure, all data will be stored for the third step. The data consist of:

- Discharge time function of the river Rhine at Lobith
- Discharge time function of the river Meuse at Vierlingsbeek,
- Wind direction and velocity (uniform over the case study region)
- Resistance properties for all potential second, third etc breach locations.
- Breach properties, including possible random quantities
- The location of the failure
- The failure mechanism

The MC was continued until about a 100 failure runs were found. The advantage of this procedure is that Step 3 can be made with a relative simple and quick calculation procedure. The efficiency of this step may even be increased by Importance Sampling, possibly in combination with a FORM step.
The 100 runs are primarily based on a first assessment of the variation in the systems probability of failure. Results will have to show whether such a number of scenarios will also suffice for a proper assessment of the consequences and risk.

*Step 4: Hydrodynamic calculations, allowing for effects of system behaviour*

In Step 4 the hydrodynamic consequences (i.e. determination of the flooding pattern) including the effects of dike failures and overflow of dikes are determined for the representative set of

realisations with failure obtained in Step 3. This was done by means of SOBEK computations as described in section 2.1

*Step 5: Determination of flood consequence (damage & victims)*

In Step 5, flood consequence is determined for the representative set of realizations conditional upon failure (i.e. the findings of Step 3). More precisely for the Step 3 representative set of realizations, the direct economic damage as well as the expected number of human casualties is computed with HIS-SSM (see section 2.4) using the flooding patterns determined in Step 4 as main input .
No damage and no victims are assumed for the set of Monte Carlo realizations from Step 3, in which no dike failure occurred (i.e. the complementary set of realizations).

*Step 6: Determination of Flood Risk*

Determine the risk from:

$$R = E(D \mid F)\, P(F) \tag{4.14}$$

D is the damage for an arbitrary scenario, P(F) is the system failure probability, which follows from the PC-Ring calculation in step 2 and $E(D \mid F)$ is the average damage following from step 5. The conditional risk was estimated by (4.11) where in this case simply:

$$\mathrm{E}(D|F) = 1/N \, \Sigma \, C_i \tag{4.15}$$

An important question is how many runs are necessary in steps 3 to 5. For the time being it was assumed that we needed about 100 failure cases to get a reliable result. We will return to this issue after discussion of the results of the case study. We will also discuss some options to reduce the calculation time.

## 4.5 Fluctuations in time and space

Some parameters fluctuate every year or even more often, others are constant in time. In the analysis we only look at one event with a total time span of about 1 month. The sampling will be either a pure importance sampling (increased variance or shifted mean) or a constrained sampling. The stretching to a longer period will be made by the outcrossing approach. This means that we calculate the probability of failure (F) in one month and survival (S) in the month before. Then the outcrossing approach gives:

$$P_F(t) = P(F_1) + (N(t)-1)\, P(S_1 \cap F_2) \tag{4.16}$$

Where N(t) is the number of reference periods (months) in the period t under consideration, e.g. one year or several years. The longer period is necessary for economic optimization, but also for the Individual and Social Risk criteria. TAW has proposed that an averaging of these risks over a period of say 10 year would be appropriate.

Another issue is the length effect. It is proposed to use also there an analytical solution based on the outcrossing approach, similar as in PC-Ring.

The above scheme holds for some relatively short time span, one year or a part of it. The results need to be expanded to a period of say 50 years. If there are no time depending loads or deteriorating effects, we may use a transformation of the standard out crossing method to the risk domain:

$$R(T)= R(1)+(T-1)\,(R(2)- R(1)) \tag{4.17}$$

where $R$(T) is the risk for a period T (in years) and $R$(1) and $R$(2) are risks for 1 and 2 year periods respectively. Additionally corrections for discounting, deterioration and climate changes should be included.

# 5 Case study 1

## 5.1 Description

The described computational framework (section 4.4) has been applied to the upper (river dominated) part of the Rhine and Meuse river basin, in the eastern part of the Netherlands (see Fig 5.1). The model area or studied region includes eighteen Dutch dike ring areas as well as two German polders located along the Niederrhein. The case study area covers 4600 square kilometres.
In this case study potential dike breach locations were only considered in one dike ring, called "Dijkring 41: Land van Maas en Waal" (see Fig. 5.2). At all other locations dike-sections cannot fail, but may be overtopped as soon as river levels exceed dike levels. More precisely 5 dike sections along river Waal (Dr41L1 - Dr41L5) and 6 dike sections along river Meuse (Dr41L6 - Dr41L11) were considered. These dike sections were selected based on the flooding characteristics of the concerned area.

Fig. 5.1 Location of case study area

In the current case study, these eleven potential dike breach locations are assumed to be appropriate for the characterization of the flood risk. In chapter 6 (case study 2) this assumption will be checked by increasing the number of locations. The analysis used $N = 7\ 10^6$ Monte Carlo realizations of the input parameters. (Crude Monte Carlo).

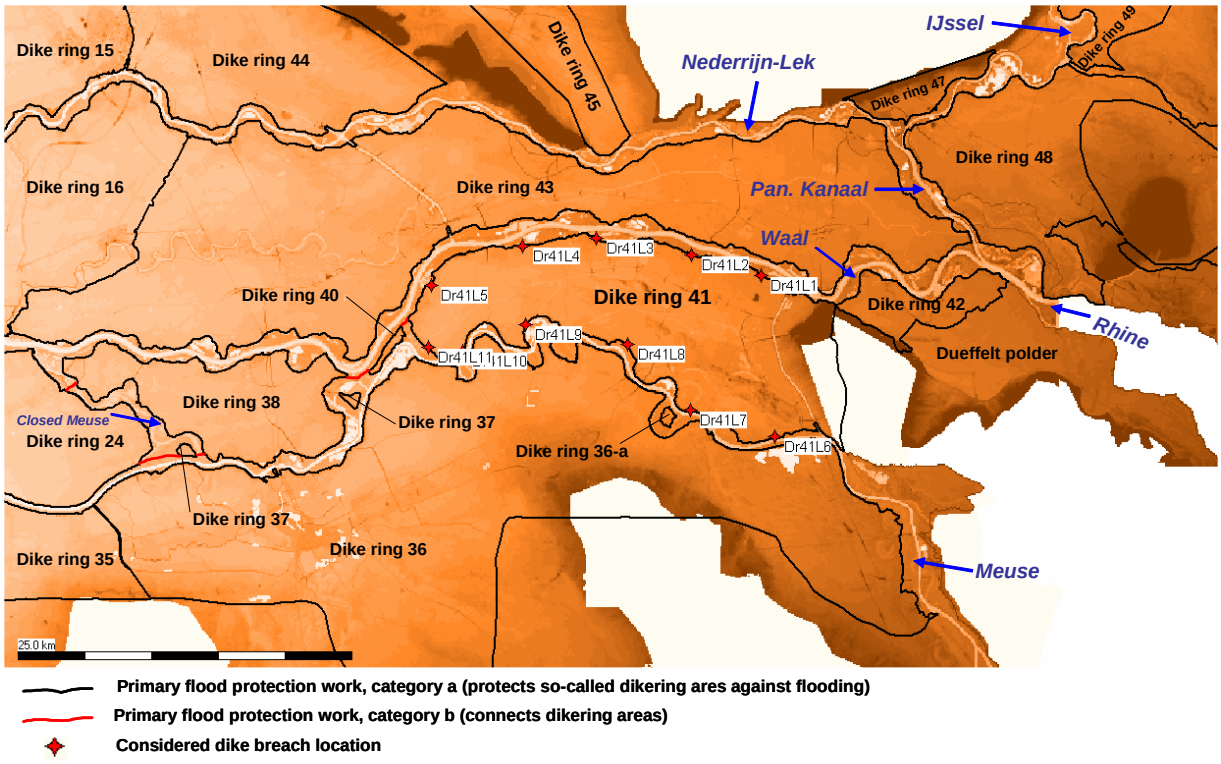

Fig 5.2 The case study area

## 5.2 Initial and boundary conditions

Upstream at river Rhine (e.g. at Lobith) and upstream at river Meuse (e.g. at Vierlingsbeek) flood hydrographs ($Q=f(t)$) with a certain return period were imposed. Flood waves on river Rhine and Meuse are mutually correlated. Therefore, a joint probability density function was used (see section 3.1). In some of the scenarios (see Table 5.1), very large discharges are applied (e.g. 25000 $m^3/s$ on river Rhine and 5300 $m^3/s$ at river Meuse). From a hydro-meteorological point of view, it is doubtful if such discharges can occur (see Deltares, 2008). Besides, the frequency of occurrence will be much smaller than the one derived from the applied joint probability density function (see Gudden and Overmars, 2004; Lammersen, 2004). The shape of the flood hydrograph were determined, using the flood wave generator (HKV, 2004). Presently only median flood wave shapes were considered. Downstream at the Meuse as well as on the river Rhine branches (deterministic) stage-discharge relationships were used.

Table 5.1 Maximum discharges on river Rhine and Meuse

| Scenario No. | Max. discharge $m^3/s$ | | Scenario No. | Max. discharge $m^3/s$ | | Scenario No. | Max. discharge $m^3/s$ | |
|---|---|---|---|---|---|---|---|---|
| | Rhine | Meuse | | Rhine | Meuse | | Rhine | Meuse |
| Scen 1 | 18700 | 4600 | Scen 23 | 20100 | 4200 | Scen 45 | 19500 | 3500 |
| Scen 2 | 18900 | 4300 | Scen 24 | 21300 | 5300 | Scen 46 | 18700 | 4800 |
| Scen 3 | 18800 | 4300 | Scen 25 | 17900 | 3900 | Scen 47 | 18400 | 4500 |
| Scen 4 | 18400 | 4200 | Scen 26 | 19600 | 4400 | Scen 48 | 17900 | 4400 |
| Scen 5 | 13500 | 3300 | Scen 27 | 17900 | 3900 | Scen 49 | 19800 | 4500 |
| Scen 6 | 17900 | 3600 | Scen 28 | 18600 | 4500 | Scen 50 | 11400 | 2500 |
| Scen 7 | 18900 | 4200 | Scen 29 | 12100 | 2500 | Scen 51 | 9800 | 1800 |
| Scen 8 | 19600 | 4200 | Scen 30 | 25000 | 5100 | Scen 52 | 18700 | 3700 |
| Scen 9 | 18700 | 4200 | Scen 31 | 20300 | 4000 | Scen 53 | 18600 | 4200 |
| Scen 10 | 18300 | 4100 | Scen 32 | 18800 | 3800 | Scen 54 | 19400 | 4200 |
| Scen 11 | 20700 | 5100 | Scen 33 | 20300 | 4500 | Scen 55 | 17800 | 3800 |
| Scen 12 | 23000 | 5300 | Scen 34 | 17800 | 4400 | Scen 56 | 20700 | 5000 |
| Scen 13 | 14100 | 3600 | Scen 35 | 18900 | 4500 | Scen 57 | 8600 | 1400 |
| Scen 14 | 13500 | 2600 | Scen 36 | 19100 | 4000 | Scen 58 | 20500 | 4900 |
| Scen 15 | 10300 | 1500 | Scen 37 | 11700 | 2300 | Scen 59 | 19600 | 4500 |
| Scen 16 | 19800 | 4800 | Scen 38 | 20800 | 4500 | Scen 60 | 11300 | 2400 |
| Scen 17 | 20400 | 4800 | Scen 39 | 25000 | 5700 | Scen 61 | 18500 | 3800 |
| Scen 18 | 21100 | 4700 | Scen 40 | 18100 | 3900 | Scen 62 | 14600 | 2800 |
| Scen 19 | 20200 | 4200 | Scen 41 | 18700 | 4200 | Scen 63 | 12200 | 2600 |
| Scen 20 | 11800 | 1800 | Scen 42 | 20200 | 4500 | Scen 64 | 20600 | 4800 |
| Scen 21 | 18500 | 4100 | Scen 43 | 12600 | 3100 | Scen 65 | 19900 | 4000 |
| Scen 22 | 15100 | 3400 | Scen 44 | 16000 | 3700 | Scen 66 | 13300 | 3000 |

## 5.3 Dike characteristics

Dike sections can fail at so-called potential breach locations only (see section 5.1 and Fig 5.1). More detailed information on the considered potential breach locations is given in Table 5.2

Dike sections in the model can fail as a result of loads exerted on its river side as well as on its dike ring side, i.e. the dike is considered symmetric in terms of failure mechanisms for sake of simplicity.

As already mentioned, for all the other dike rings in the system it is assumed that its surrounding dikes cannot fail. However, these dikes can overflow as soon as river levels exceed dike levels. Data on the probability density functions for the dike (resistance) parameters in the model region were available from the FLORIS project (VNK 2005).

Table 5.2 Overview of considered potential breach locations.

Dr41Lx is considered potential breach location number Dr41Lx

- coding Dr41, means dike ring 41 ("Dijkring 41: Land van Maas en Waal")
- *coding Lx, means potential breach location number Lx*

| Breach Location | x-coord. RDM[1] | y-coord. RDM[1] | Dike height in metres | River name and relative position |
|---|---|---|---|---|
| Dr41L1 | 183050 | 431050 | 14.95 | Waal, kilometre 889_4 |
| Dr41L2 | 177850 | 432650 | 14.06 | Waal, kilometre 895_1 |
| Dr41L3 | 170750 | 433850 | 13.20 | Waal, kilometre 902_3 |
| Dr41L4 | 165250 | 433250 | 12.80 | Waal, kilometre 908_5 |
| Dr41L5 | 158450 | 430350 | 11.75 | Waal, kilometre 917_3 |
| Dr41L6 | 184150 | 419050 | 12.83 | Maas, kilometre 169_6 |
| Dr41L7 | 177750 | 421050 | 12.42 | Maas, kilometre 177_2 |
| Dr41L8 | 173050 | 425950 | 10.77 | Maas, kilometre 184_8 |
| Dr41L9 | 165450 | 427450 | 10.09 | Maas, kilometre 192_3 |
| Dr41L10 | 160850 | 425450 | 8.73 | Maas, kilometre 199_3 |
| Dr41L11 | 158050 | 425850 | 8.91 | Maas, kilometre 203_7 |

Notes:

1. x and y coordinates according to Rijksdriehoekmeting (RDM), the Dutch geographical coordinate system

### 5.4 SOBEK model schematisations

Two different SOBEK models were used

1. ***SBK_1***: SOBEK model that only covers the river network and Dike ring 41 (see Fig 5.1),
2. ***SBK_2***: SOBEK model that covers the entire case study area (see Fig 5.2).

Both SOBEK models consider the same potential dike breach locations (see section 5.1 and 5.3) and have spatially uniform (2D) grid cell size of 100m.

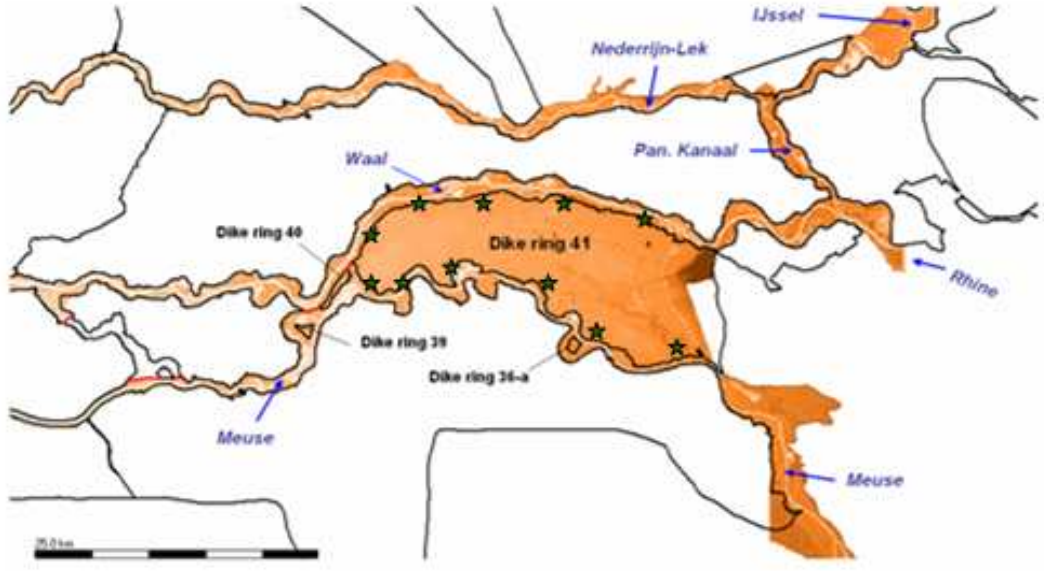


Fig 5.1 The SBK_1 model schematisation

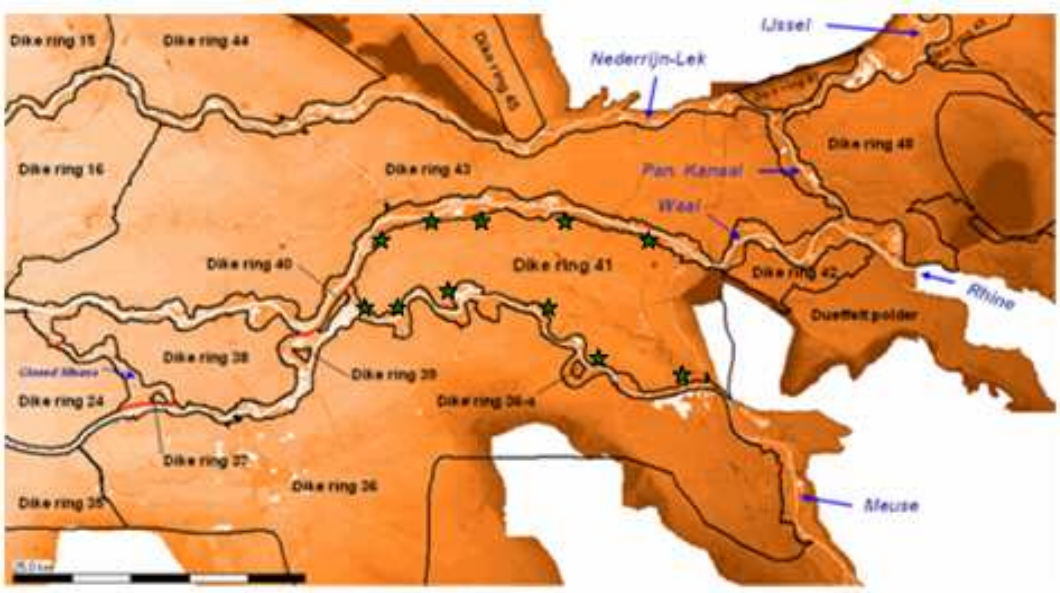


Fig 5.2 The SBK_2 model schematisation

## 5.5 Results

Results of the case study are given in line with Steps 1 to 5, discussed in section 4.1.

### 5.5.1 Step 1 results

For STEP 1 a number of hydrodynamic model runs was carried out for a range of flood waves ($Q=f(t)$) on river Rhine and Meuse. The result of step 1 is a hydraulic database, containing per potential breach location the river levels for different upstream flood waves, having increments in the peak discharge of 100 $m^3/s$.

### 5.5.2 Step 2 results

A PC-Ring calculation is made for dike ring 41. In the PC-Ring schematization the dike ring is divided into 80 sections. The annual failure probability for dike ring 41, $P_F$, is calculated:

$P_F = 0.02$ [-/year]

### 5.5.3 Step 3 results

The evaluation of the 7 $10^6$ Monte Carlo realizations in STEP II in the simplified model, neglecting system effects and using the water levels determined in STEP I, led to 65 scenarios, in which at least one dike section failed in the system. As the Monte Carlo simulations make use of realizations for discharges based on 48 hours statistics, this leads to an estimate of the failure probability for the dike ring of $P_f = 9.4\ 10^{-6}$ *[1/48hrs],* i.e. the probability per 48 hours of a flood event in the area as a consequence of a dike failure

*Remarks:*
*a. The absolute value of the failure probability as estimated by the above Monte Carlo simulations is not considered to be representative for this dike ring, since in the calculations made no length effects were accounted for and only eleven infinitesimally small locations were chosen. It is only of indicative nature.*
b. *When transforming the failure probabilities to a period of 1 year, the change will roughly be in the order of a factor 90 (1 year ~1 season ~180 days ~90*48 hrs). The corresponding probability of failure would thus be approximately 0.001 [1/year]. The full PCRing calculationof step 2 for dike ring 41 leads to a total failure probability of 0.02 [1/year] (β = 2).*

The variation coefficient of the failure probability estimate is about:

*$COV(P_f) = 1/sqrt(65) = 12\ \%$*

That is sufficiently precise for the present purpose. By the way, this failure probability is not influenced by effects of river system behaviour. The calculation time for STEP 3 on a standard issue 2 GHz Windows PC was about 12 hours.

### 5.5.4 Step 4 results

In STEP 4, SOBEK computations with the SBK_1 model and the SBK_2 model (see section 5.4) were made for the Step 3 representative set of scenarios (i.e. the Step 3 scenarios that resulted in at least one dike failure). For each such scenario yields that the same hydraulic boundary conditions and the same strength properties for the considered potential dike breach locations (i.e. Monte Carlo realization) are used in computations with the SBK_1 and the SBK_2 model. Computational efforts on a standard issue 2 GHz Linux PC varied from 140 to 580 hours (6 to 24 days) per model run. The required computational time is roughly a linear function of the maximum discharges imposed at the upstream boundaries. Recently the computational procedure has been optimized, resulting in computational effort of 50 to 150 hours (2 to 6 days) per run.

Table 5.3 gives the total number of failures per dike ring 41 breach location, which occurred in the sets of 65 scenarios. In Step 3, locations failed due to exerted hydraulic river loads only. For Step 4, a distinction is made between failures induced by river loads (river side) and by hydraulic loads exerted at the dike ring side, that occur due to the flooding of dike ring 41. Table 5.4 gives a classification of scenarios with respect to dike failure locations.

Both Table 5.3 and 5.4 indicate effects of river system behaviour. The general trend in Table 5.3 is that the number of failures per location, induced at the river side decreases with the degree in which river system behaviour is enabled. System behaviour was not enabled in Step 3. In Step 4&SBK_1 system behaviour was enabled for dike ring 41 only, and in Step 4&SBK_2 it was enabled in the entire case study area. One can see that, downstream breach locations, except for Dr41L10 and Dr41L11, benefit more from system behaviour effects than the upstream ones. Resuming, Table 5.3 and 5.4 provides indications that effects of system behaviour are of importance. Hereunder, more detailed observations are given for justifying the above statement.

*Important* to mention is that all 66 Step 3 scenarios, computed in Step 4 with the SBK_1 and SBK_2 model, resulted in flooding (e.g. dike ring 41 and/or other dike rings). For *1* (one) scenario it yields that no failures occurred in Step 4&SBK_2 (more details, given hereafter). For 38 scenarios yields that failures as result of exerted hydraulic river loads, occur in Step 3 and Step 4&SBK_2 at exactly the same location, and are induced by the same failure mechanism. For *17* scenarios yields that along downstream locations more failures occurred in Step 3 than in Step 4&SBK_2, since, due to flood, water levels in Step 4&SBK_2 were lower than in Step 3. For *2* scenarios yields that in Step 4&SBK_2_a Meuse dike failed due to high river levels, while this was not the case in Step 3. The reason for the high Meuse river levels was that in Step 4&SBK_2 water from river Waal flowed into river Meuse, while this is just not possible in Step 3. In *8* Step 4&SBK_2 scenarios, in contradiction to Step 3 scenarios, no failure occurred either along a Waal dike or Meuse dike. This can be explained as follows. In Step 4&SBK_2 no Meuse dike failed, since river levels were reduced by the flooding of upstream areas along river Meuse. In such scenario, however, a Waal dike failed both in Step 3 and Step 4&SBK_2. In other scenarios it was the other way around, meaning that for the same reasons a Waal dike did not fail in Step 4&SBK_2, while both in Step 3 and Step 4&SBK_2 a Meuse dike failed.

Detailed analysis of the Step 4&SBK_2 scenario set revealed that in 56 out of the 62 scenarios in which at least one Waal dike breach location failed, flooding of dike rings along river Meuse occurred. An example is scenario 24 (see Fig 5.3), where the left Waal dike at location Dr41L1 (Weurt) failed for Rhine discharges of 18900 $m^3/s$. As a result Waal water flows through dike ring 41 towards locations Dr41L10 and Dr41L11. Successively, the right Meuse dikes at locations Dr41L10 and Dr41L11 failed as result of loads, exerted on their dike ring side. Consequently, a large volume of Rhine water flows towards river Meuse, that is conveying an upstream flood wave with a peak discharge of 4300 $m^3/s$. The inflow of river Rhine water results in the overtopping of dikes along dike-rings 36, 38 and 39. Hence, although the dikes along the latter three dike rings cannot fail in the model setup, flooding of these three dike rings occurs as result of river system behaviour (*adverse* effect).

In Step 4, in contrast to Step 3 analysis, no breaching occurred in scenario 13 (see Table 5.4). The reason is that in Step 4 hydraulic loads at breach locations were reduced (*beneficial* effect) due to minor flooding of upstream dike rings 42 and 43 (see Fig 7) and minor flooding of dike ring 41 (i.e. overtopping of dikes in between dike breach locations).

The above detailed analysis demonstrates the true complex behaviour of river system behaviour. It also demonstrates that beneficial and adverse effects can occur simultaneous or in separate flood occurrences, that contribute to the overall flood risk. Hence, a method, as the one used in

the present study, is needed to determine the statistically weighted contribution of both beneficial and adverse aspects of river system behaviour both on failure probability as well as on flood risk.

Table 5.3: Failures of dike ring 41 breach locations

| Location | Step 3 | Step 4 & SBK_1 | | Step 4 & SBK_2 | |
|---|---|---|---|---|---|
| | River side | River side | Dike ring side | River side | Dike ring side |
| Dr41L1 | 34 | 27 | 0 | 27 | 0 |
| Dr41L2 | 32 | 17 | 0 | 17 | 0 |
| Dr41L3 | 27 | 11 | 0 | 11 | 0 |
| Dr41L4 | 19 | 4 | 0 | 3 | 0 |
| Dr41L5 | 28 | 10 | 0 | 9 | 0 |
| Dr41L6 | 13 | 11 | 0 | 11 | 0 |
| Dr41L7 | 1 | 0 | 0 | 0 | 0 |
| Dr41L8 | 11 | 2 | 0 | 2 | 0 |
| Dr41L9 | 1 | 2 | 0 | 0 | 0 |
| Dr41L10 | 3 | 0 | 53 | 0 | 53 |
| Dr41L11 | 1 | 1 | 44 | 1 | 44 |

Table 5.4 Classification of scenarios with respect to failure locations

| *Waal failure*: One or more failures at potential breach locations Dr41L1 to Dr41L5<br>*Meuse failure*: One or more failures at potential breach locations Dr41L6 to Dr41L11<br>*Failures*: Both induced by loads exerted at river side or loads exerted at the dike ring side | | | |
|---|---|---|---|
| Step 4 & SBK_1 | | Step 4 &SBK_2 | |
| *Scenario classification* | *No* | *Scenario classification* | *No* |
| a. No dike failure | 1 | a. No dike failure | 1 |
| b. Only Waal failure | 6 | b. Only Waal failure | 6 |
| c. Only Meuse failure | 2 | c. Only Meuse failure | 3 |
| d. Waal&Meuse failure | 57 | d. Waal&Meuse failure | 56 |

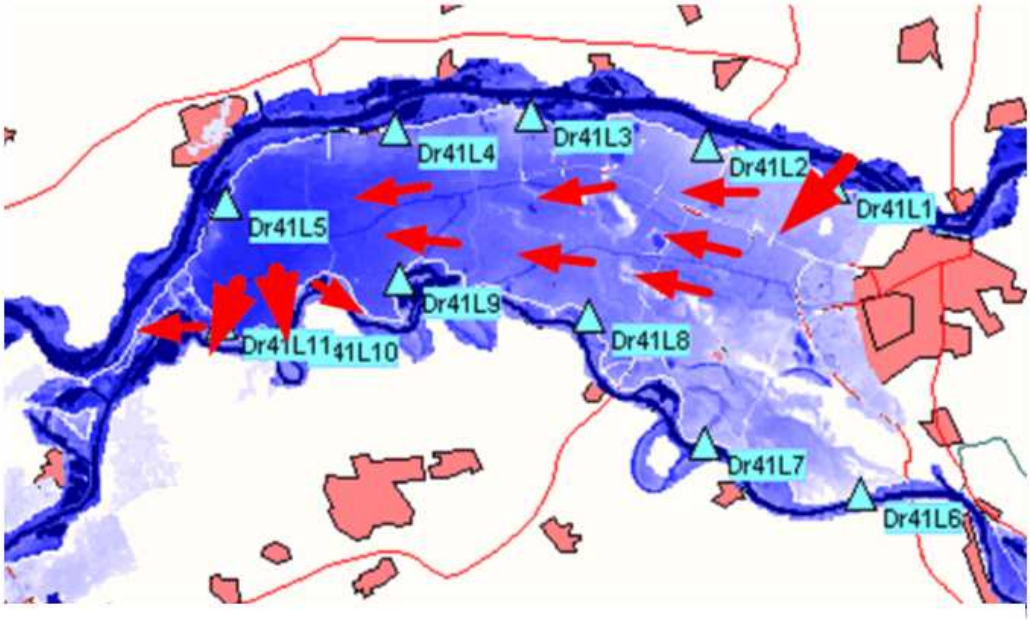


Fig 5.3 Flooding pattern in scenario 24 of the Step 4 & SBK_2 set

### 5.5.5 Step 5 results

The computational framework determines flood risk using the HIS-SMM Damage and Victims module (see section 2.4) and the hydraulic output, computed in Step 4 for the SBK_1 and SBK_2 models (see section 5.4). The computational framework makes flood consequence (both expected damage and expected number of casualties) available as:

- *A flood risk map* with spatial discretization equal to the SOBEK grid cell size (i.e. 100m in the present case study), and
- *Tables* of aggregated flood consequence per dike ring area

The flood consequence (i.e. damage and victims) of the 65 Step 3 scenarios are given in Table 5.5. Total area, refers to all flood prone areas, except the river network. The variation coefficients (standard deviation divided by mean; SBK_2 model) for dike ring 41 are smaller than for the total area (see Table 5.5). Due to the considered breach locations, dike ring 41 is flooded more often (i.e. in each scenario). Flooding of other dike rings occurs only if dikes are overtopped. As a result the mean flood consequence in dike ring 41 is relatively larger and its standard deviation smaller than for the other dike rings.

For the SBK_1 and SBK_2 model, flood consequences in dike ring 41 are of the same order of magnitude (see Table 5.5). Considering the SBK_1 model only, means neglecting considerable flood consequences in other flood prone areas. Flood consequences along downstream located flood prone areas will become larger in case breaching along these areas occurs. Hence for a proper estimation of flood risk in the river basin, it is essential to consider the entire river basin (e.g. to account for effect of river system behaviour). To make this more explicit, consider that one determines flood risk for dike ring 36, while only considering breaching and overtopping of Meuse dikes along dike ring 36. This will result in an ***underestimating*** of the flood risk in dike ring 36, since the failure of a left Waal dike along dike ring 41 contributes to the flood consequence (and hence flood risk) in dike ring 36 (as shown in Table 5.5).

As illustration, for the Step 4&SBK_2 scenario set, the expected flood damage and expected victims in dike ring 41 are respectively depicted as histograms (see Fig 5.4). As illustrated in Fig 5.4 the mean value of the damage, considering only the runs that lead to damage, was *5.8 $10^9$ € per year* with a variation coefficient of 0.29 (e.g. standard deviation divided by the mean). That suggests that there is something like a typical damage value in case of an inundation of this dike ring, regardless of the way it is realised. This aspect requires further investigation. The histogram for casualties in Fig. 5.4 shows that the representative scenarios do not yield a symmetric distribution (mean = 730) of casualties and a relatively high variation coefficient of about 0.50. In Fig. 5.5 the corresponding histograms for the Step 4 &SBK_1 scenario set are shown for comparison.

Table 5.5 Flood consequences of the 65 Step 3 scenarios

| Area | SOBEK model schematisation | | | |
|---|---|---|---|---|
| | SBK_1 | | SBK_2 | |
| ***Dike ring 41*** | *Mean* | *St.Dev* | *Mean* | *St.Dev* |
| • *Victims (-)* | 792 | 436 | 730 | 371 |
| • *Damage (€)* | $6.2 \times 10^9$ | $2.2 \times 10^9$ | $5.9 \times 10^9$ | $1.7 \times 10^9$ |
| ***Total area***[1)] | *Mean* | *St.Dev* | *Mean* | *St.Dev* |
| • *Victims (-)* | - | - | 979 | 832 |
| • *Damage (€)* | - | - | $8.9 \times 10^9$ | $7.9 \times 10^9$ |

1) Total area: all flood prone areas, except the river network

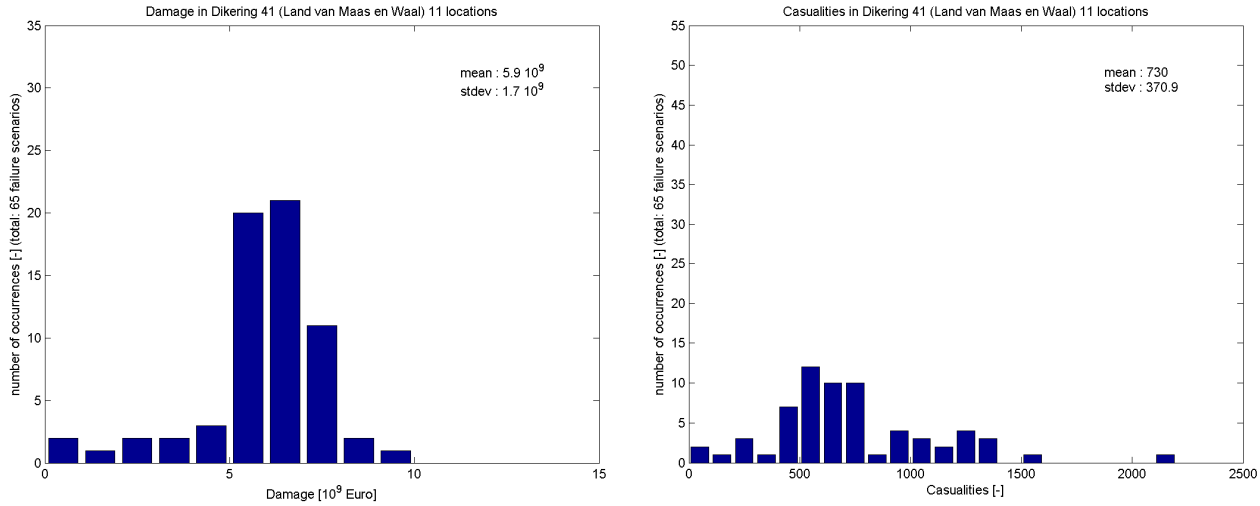


Fig 5.4 Histograms of damage and victims in dike ring 41 for the Step4&SBK_2 scenario set

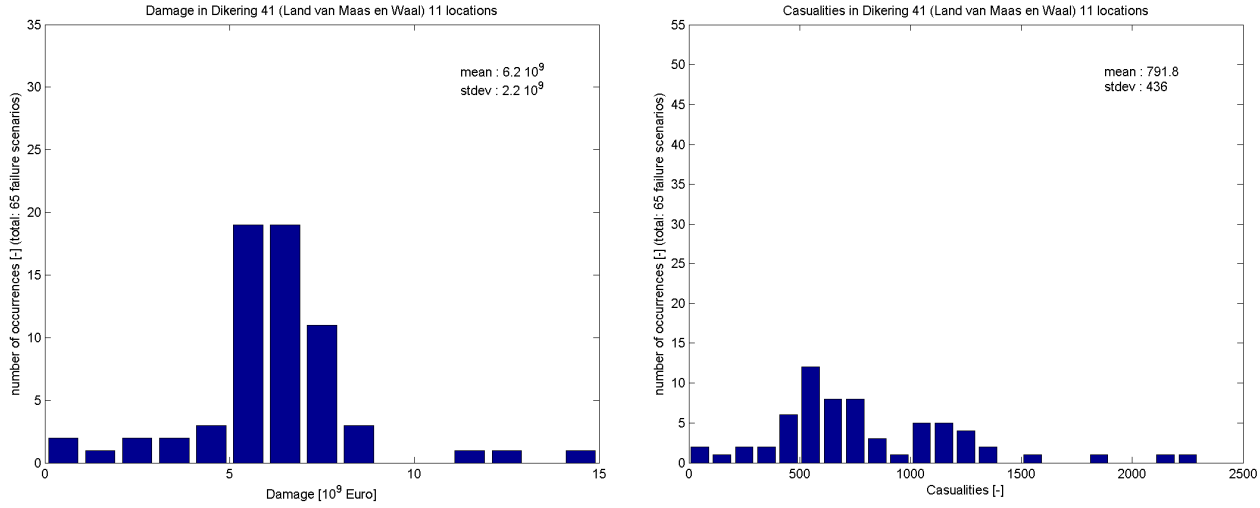


Fig 5.5 Histograms of damage and victims in dike ring 41 for the Step4&SBK_1 scenario set

### 5.5.6 Step 6 results

Finally in Step 6, annual flood risk is determined in the dimensions of direct economical damage and human casualties. It is assumed that each scenario represent a time span of one year. The annual flood risk for dike ring 41 and for the total area (e.g. all flood prone areas, except the river network) is given in Table 5.6. Since Crude Monte Carlo is used, the annual flood risk equals the mean flood consequence given in Table 5.5 multiplied by the probability of failure. (see section 4.4).
For the probability of failure the same value is assumed as calculated by a full PCRing calculation for dike ring 41. Thus, PCRing's value of $P_f = 0.02$ [1/year] is used for the probability of failure.
This leads to the indicative values for the flood risk as presented in Table 5.6.

Table 5.6 Estimated annual flood risk

| Flood consequence | SOBEK model schematisation | |
|---|---|---|
| | SBK_1 | SBK_2 |
| | ***Dike ring 41*** | ***Dike ring 41*** |
| • *Victims (1/Yr)* | 15.8 | 14.6 |
| • *Damage (€/Yr)* | $1.24 \times 10^8$ | $1.18 \times 10^8$ |
| | ***Total area[1)]*** | ***Total area[1)]*** |
| • *Victims (1/Yr)* | - | 19.6 |
| • *Damage (€/Yr)* | - | $1.78 \times 10^8$ |

Notes:

1. Total area: all flood prone areas, except the river network

.

## 5.6 Conclusions Case 1

In the past, the effects of river system behaviour were not taken into account in flood risk analyses. The presented computational framework enables us to assess these effects. In other words, it can determine the statistically weighted contribution of both beneficial and adverse effects of system behaviour. That effects of system behaviour are of importance in the case study area was shown in section 1.3.
Although breaching of dikes was only considered along dike ring 41, in the analysed case study, still the importance of considering effects of river system behaviour was demonstrated. Hence, the study is to be contemplated as proof of concept for a real Dutch situation. The effects of river system behaviour would be more pronounced in case dike failures along all dike ring areas were considered. However, for the sake of simplicity (e.g. for better understanding the phenomena involved), it was decided to start with allowing breaching of dikes along dike ring 41 only.

*Computational framework*
- The framework is suitable for including the effects of river system behaviour into flood risk analysis.
- The computational framework is a modular framework that allows for implementation of all kinds of modules concerning probabilistic calculation techniques, structural models of flood defences, hydrodynamic modelling, evacuation modelling and flood consequence assessment,
- The concept of the computational framework also allows for any kind of river basin and river network, any kind of flood defence structure and flood mitigating measure, any kind of failure mechanism and breach growth formulation.
- The manner in which flood risk is determined, combining information about the land use with the potential flood characteristics calculated in a hydrodynamic model, is far more realistic than earlier approaches as for example in the FLORIS project.
- In the Netherlands currently there is a discussion about the efficiency of segmenting dike rings into smaller units by building dikes within these flood protected areas in order to palliate consequences in case of flooding. The presented tool is suitable for evaluating the efficiency of such plans in terms of risk.

*Case Study*
- The case study showed that system effects can be significant and is considered a proof of concept.
- The effects of river system behaviour are expected to be more pronounced and complex, when larger regions and breaching along more dike rings is considered. This is supported by the effects found in the analysis.
- In the case study, in some scenarios the land side of a dike failed as a consequence of loads exerted on it from the inundated hinterland. As, mentioned earlier, the dikes were considered symmetric in terms of resistance parameters. The effect of this simplification has to be investigated in future studies.
- Even though a Crude Monte Carlo simulation is carried out, as in the case study, it was feasible to carry out the computations with reasonable time effort. This is because the computationally intensive hydrodynamic model has only to be run for scenarios that include at least one failure within the system. The efficiency could still be increased by applying Importance Sampling.
- An assumption for this case study was that the eleven chosen potential breach locations would give a representative image of the risk for the model region. This assumption will be verified by additional calculations with more of such locations in a second case study (chapter 6).

# 6 Case Study 2

## 6.1 Description

An assumption made for Case study 1, described in chapter 5, was to suffice with 11 breach locations along dike ring 41. In this chapter the influence of increasing the number of breach locations is investigated.
The geographical area covered in case study 2 is the same as the area considered in case study 1: it covers the upper (river dominated) part of the Rhine and Meuse river basin, in the eastern part of the Netherlands (see Fig. 5.1). The model area or studied region includes eighteen Dutch dike ring areas as well as two German polders located along the Niederrhein. Case study 2 area also covers 4600 square kilometres. Furthermore, in case study 2 (as in case study 1) potential dike breach locations were only considered along one dike ring, called "Dijkring 41: Land van Maas en Waal" (see Fig. 6.1a to Fig. 6.1c). At all other locations dike-sections cannot fail, but may be overtopped as soon as river levels exceed dike levels.

Main differences between case study 1 and case study 2 are:

1. Case study 1 considers in total 11 potential breach locations (Dr41L1 – Dr41L11), while case study 2 considers in total 38 potential breach locations (Dr41L1 – Dr41L38). The first eleven potential breach locations in case study 2 (i.e. Dr41L1 – Dr41L11) are identical with respect to location to the eleven potential breach locations in case study 1. With respect to strength parameters, 3 out of the first eleven breach locations differ when compared to case study 1 (Dr41L1, Dr41L2, Dr41L6). The reason for this is a different procedure followed in matching the breach locations to the dike sections in the PCRing database[7]. Furthermore, in case study 1, the model uncertainty in the head difference for heave (mh) was unintentionally taken as a constant value equal to 0.8. In case study 2, mh is implemented as a lognormal distribution: LOGN(0.8,0.08). Values for the strength parameters are given in Appendix C.
2. In case study 2, the evaluation of the limit-state-function of the piping failure mechanism (see section 2.2.2) was refined, see Appendix B. Among other parameters, in evaluating the piping failure mechanism a river level and a water level in the dike ring area (hereafter called the dike ring water level) are needed. Regarding the river level and the dike ring water level, following distinction can be made between case study 1 and case study 2 (see also appendix B):
    a. *Evaluating possible piping failure induced by river loads*:

        Both in case study 1 and 2, the river level corresponds to the water level (i.e. water depth above local surface level) just in front of the potential breach location. In case that there is no river water standing in front of a potential breach location, the river level is equal to the local surface level (i.e. water depth equals zero). It is assumed that in case of possible piping failure induced by river loads, river water is standing in front of the potential breach location. Hence, it is not necessary to make use of the river level in the low-water-bed channel (see also section b. below).

        In case study 2, the water level inside the dike ring is the phreatic level at a potential exit point for uplift and piping, e.g. the dike toe or the drainage ditch

[7] In case study 1, the breach locations were allocated to a dike section based on their distance towards the dike section's midpoint. In case study 2 the criterium was changed towards the breach loctation falling in between a section's begin and end point.

behind the dike, if present. If the phreatic level is not known, the surface level is assumed instead. If the dike ring is flooded, water level inside the dike ring is determined by SOBEK. In case study 1, the information on phreatic levels was not used, that means that without flooding of the dike ring, the water level inside the ring was always assumed as the surface level. In other words, the dike ring water levels applied in evaluating possible piping failure induced by river loads in case study 2, are usually below the ones applied in case study 1. Therefore, piping failures from the river towards the protected area may occur more often in case study 2 than in case study 1, since the water level difference is larger, if the phreatic level is known.

*b.* *Evaluating possible piping failure induced by dike ring loads:*

Both in case study 1 and 2, the dike ring water level is the one calculated in SOBEK. In case study 1, the river level corresponds to the water level just in front of the potential breach (dike) location. In case study 2, the river level was changed to the water level in the low-water-bed channel. That is because, if the river is constrained to the low-riverbed, using the surface level at the river side dike toe leads to underestimating the piping problem. Hence, also this aspect ma lead to more piping failures in case study 2 compared to case study 1.


Fig. 6.1a Location of potential breach location in case study 2

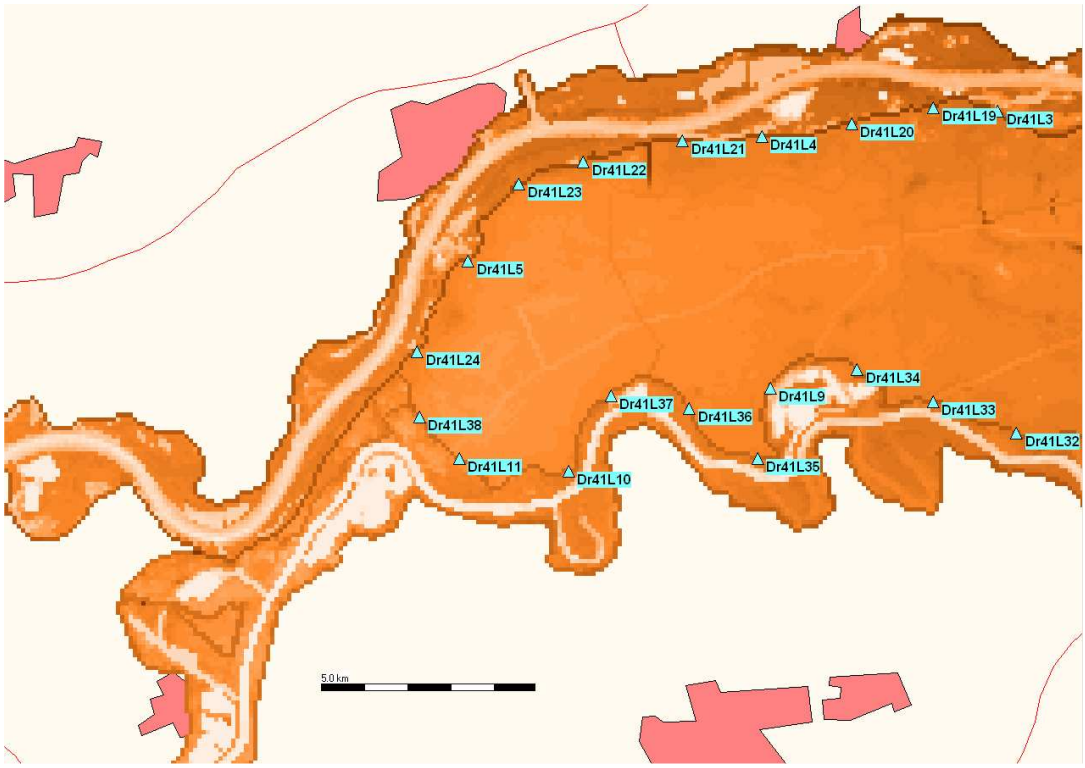


Fig. 6.1b Location of potential breach location in case study 2

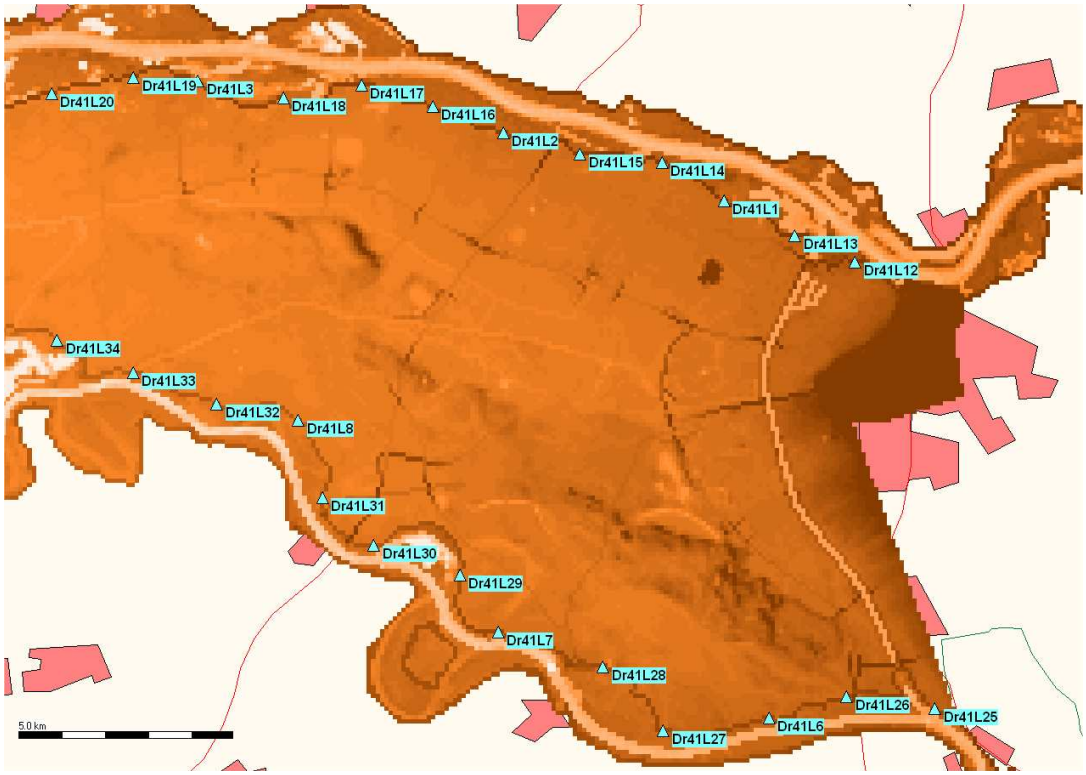


Fig. 6.1c Location of potential breach location in case study 2

## 6.2 Initial and boundary conditions

The same initial and boundary conditions were used as for case 1, see section 5.2. However, use is made of a new SOBEK executable for case 2, in which improvements regarding the computation of overland flow were made. Therefore, also a new Step 1 hydraulic database was constructed for case study 2.
The discharges of the newly derived scenarios are listed in Table 6.1. As for case 1, some scenarios show large discharges (e.g. 22324 $m^3/s$ on river Rhine and 5230 $m^3/s$ at river Meuse). With respect to this, reference is made to the comments as presented in section 5.2.

Table 6.1 Maximum discharges on river Rhine and Meuse Case Study 2

| Scenario No. | Max. discharge $m^3/s$ Rhine | Meuse | Scenario No. | Max. discharge $m^3/s$ Rhine | Meuse | Scenario No. | Max. discharge $m^3/s$ Rhine | Meuse |
|---|---|---|---|---|---|---|---|---|
| Scen 1 | 8938 | 1437 | Scen 35 | 7441 | 1984 | Scen 69 | 9962 | 2131 |
| Scen 2 | 16007 | 4028 | Scen 36 | 10562 | 2081 | Scen 70 | 6778 | 1366 |
| Scen 3 | 11032 | 2453 | Scen 37 | 10643 | 2714 | Scen 71 | 9088 | 1406 |
| Scen 4 | 10399 | 2301 | Scen 38 | 15294 | 3891 | Scen 72 | 17093 | 4032 |
| Scen 5 | 8754 | 1359 | Scen 39 | 13197 | 3105 | Scen 73 | 9114 | 1583 |
| Scen 6 | 10709 | 2105 | Scen 40 | 7565 | 1247 | Scen 74 | 16482 | 3848 |
| Scen 7 | 14541 | 3452 | Scen 41 | 10588 | 2788 | Scen 75 | 10136 | 2126 |
| Scen 8 | 11190 | 2262 | Scen 42 | 17651 | 3982 | Scen 76 | 16841 | 4105 |
| Scen 9 | 16895 | 3606 | Scen 43 | 10480 | 2369 | Scen 77 | 19881 | 4565 |
| Scen 10 | 14896 | 3136 | Scen 44 | 13487 | 2749 | Scen 78 | 10501 | 1621 |
| Scen 11 | 10347 | 2355 | Scen 45 | 16777 | 3955 | Scen 79 | 15771 | 3725 |
| Scen 12 | 10838 | 2453 | Scen 46 | 15138 | 3222 | Scen 80 | 16845 | 3942 |
| Scen 13 | 19293 | 4333 | Scen 47 | 9955 | 2013 | Scen 81 | 20793 | 4301 |
| Scen 14 | 22324 | 4990 | Scen 48 | 14794 | 2962 | Scen 82 | 14486 | 2794 |
| Scen 15 | 17185 | 4436 | Scen 49 | 17770 | 4012 | Scen 83 | 16948 | 4352 |
| Scen 16 | 7515 | 1722 | Scen 50 | 7019 | 1578 | Scen 84 | 11116 | 1973 |
| Scen 17 | 10607 | 1739 | Scen 51 | 16448 | 3813 | Scen 85 | 7935 | 1679 |
| Scen 18 | 18304 | 4712 | Scen 52 | 8592 | 1245 | Scen 86 | 8492 | 2072 |
| Scen 19 | 9148 | 1715 | Scen 53 | 18342 | 4039 | Scen 87 | 8558 | 1431 |
| Scen 20 | 7924 | 1147 | Scen 54 | 10536 | 1916 | Scen 88 | 15335 | 3659 |
| Scen 21 | 14467 | 4218 | Scen 55 | 20793 | 4414 | Scen 89 | 17239 | 3715 |
| Scen 22 | 12779 | 2690 | Scen 56 | 11627 | 2296 | Scen 90 | 9513 | 2392 |
| Scen 23 | 18056 | 4275 | Scen 57 | 12459 | 2563 | Scen 91 | 14222 | 3770 |
| Scen 24 | 16346 | 3445 | Scen 58 | 14595 | 3000 | Scen 92 | 15462 | 3731 |
| Scen 25 | 15162 | 3207 | Scen 59 | 17522 | 4131 | Scen 93 | 11389 | 2532 |
| Scen 26 | 10410 | 1771 | Scen 60 | 10098 | 2545 | Scen 94 | 8011 | 2180 |
| Scen 27 | 13649 | 3173 | Scen 61 | 9055 | 1941 | Scen 95 | 19192 | 4536 |
| Scen 28 | 10044 | 2662 | Scen 62 | 10929 | 3101 | Scen 96 | 21412 | 5230 |
| Scen 29 | 11323 | 2499 | Scen 63 | 14639 | 3692 | Scen 97 | 14990 | 3995 |
| Scen 30 | 10948 | 2595 | Scen 64 | 16984 | 3819 | Scen 98 | 12605 | 2449 |
| Scen 31 | 17746 | 3898 | Scen 65 | 8364 | 1878 | Scen 99 | 15894 | 2621 |
| Scen 32 | 13129 | 2746 | Scen 66 | 11190 | 2347 | Scen 100 | 8913 | 1906 |
| Scen 33 | 14722 | 3996 | Scen 67 | 7329 | 1401 | | | |
| Scen 34 | 11773 | 2665 | Scen 68 | 9857 | 2312 | | | |

### 6.3 Dike characteristics

Dike sections can fail at so-called potential breach locations only. Considered potential breach locations are depicted in Figs 6.1a to 6.1c. More detailed information on their location along river Waal and Meuse is given in Table 6.2

Dike sections in the model can fail as a result of loads exerted on its river side as well as on its dike ring side, i.e. the dike is considered symmetric in terms of failure mechanisms for sake of simplicity. Data on the probability density functions for the dike (resistance) parameters in the model region were available from the FLORIS project (VNK 2005). For more information on strength parameters and their probability density functions at each potential breach location, reference is made to Appendix C

As already mentioned, for all the other dike rings in the system it is assumed that its surrounding dikes cannot fail. However, these dikes can overflow as soon as river levels exceed dike levels.

Table 6.2 Overview of considered potential breach locations.

Dr41Lx is considered potential breach location number Dr41Lx

- coding Dr41, means dike ring 41 ("Dijkring 41: Land van Maas en Waal")
- *coding Lx, means potential breach location number Lx*

| Breach Location | x-coord. RDM[1] | y-coord. RDM[1] | Dike height in metres | River name and relative position |
|---|---|---|---|---|
| Dr41L1 | 183050 | 431050 | 14.95 | Waal, kilometre 889_4 |
| Dr41L2 | 177850 | 432650 | 14.06 | Waal, kilometre 895_1 |
| Dr41L3 | 170750 | 433850 | 13.20 | Waal, kilometre 902_3 |
| Dr41L4 | 165250 | 433250 | 12.80 | Waal, kilometre 908_5 |
| Dr41L5 | 158450 | 430350 | 11.75 | Waal, kilometre 917_3 |
| Dr41L6 | 184150 | 419050 | 12.83 | Maas, kilometre 169_6 |
| Dr41L7 | 177750 | 421050 | 12.42 | Maas, kilometre 177_2 |
| Dr41L8 | 173050 | 425950 | 10.77 | Maas, kilometre 184_8 |
| Dr41L9 | 165450 | 427450 | 10.09 | Maas, kilometre 192_3 |
| Dr41L10 | 160850 | 425450 | 8.73 | Maas, kilometre 199_3 |
| Dr41L11 | 158050 | 425850 | 8.91 | Maas, kilometre 203_7 |
| Dr41L12 | 186150 | 429650 | 15.27 | Waal, kilometre 885_5 |
| Dr41L13 | 184650 | 430250 | 15.27 | Waal, kilometre 887_3 |
| Dr41L14 | 181550 | 431950 | 14.33 | Waal, kilometre 891_2 |
| Dr41L15 | 179650 | 432150 | 14.21 | Waal, kilometre 893_0 |
| Dr41L16 | 176250 | 433250 | 13.82 | Waal, kilometre 896_6 |
| Dr41L17 | 174550 | 433750 | 13.69 | Waal, kilometre 898_5 |

| | | | | |
|---|---|---|---|---|
| Dr41L18 | 172750 | 433450 | 13.55 | Waal, kilometre 900_3 |
| Dr41L19 | 169250 | 433950 | 13.16 | Waal, kilometre 903_9 |
| Dr41L20 | 167450 | 433550 | 12.94 | Waal, kilometre 905_6 |
| Dr41L21 | 163350 | 433150 | 12.58 | Waal, kilometre 910_0 |
| Dr41L22 | 161050 | 432650 | 12.49 | Waal, kilometre 912_3 |
| Dr41L23 | 159550 | 432150 | 12.24 | Waal, kilometre 914_8 |
| Dr41L24 | 157150 | 428250 | 11.54 | Waal, kilometre 919_5 |
| Dr41L25 | 187950 | 419250 | 13.36 | Maas, kilometre 165_9 |
| Dr41L26 | 185950 | 419550 | 12.85 | Maas, kilometre 167_9 |
| Dr41L27 | 181550 | 418750 | 12.51 | Maas, kilometre 172_4 |
| Dr41L28 | 180250 | 420250 | 12.36 | Maas, kilometre 174_6 |
| Dr41L29 | 176850 | 422350 | 11.79 | Maas, kilometre 179_4 |
| Dr41L30 | 174850 | 423050 | 11.38 | Maas, kilometre 181_1 |
| Dr41L31 | 173650 | 424150 | 11.07 | Maas, kilometre 183_1 |
| Dr41L32 | 171250 | 426350 | 10.55 | Maas, kilometre 186_3 |
| Dr41L33 | 169250 | 427050 | 10.13 | Maas, kilometre 188_6 |
| Dr41L34 | 167450 | 427750 | 10.68 | Maas, kilometre 190_6 |
| Dr41L35 | 165150 | 425750 | 8.95 | Maas, kilometre 192_3 |
| Dr41L36 | 163550 | 426850 | 9.46 | Maas, kilometre 195_8 |
| Dr41L37 | 161750 | 427250 | 8.95 | Maas, kilometre 197_1 |
| Dr41L38 | 157350 | 426650 | 8.72 | Maas, kilometre 204_3 |

Notes:

2. x and y coordinates according to Rijksdriehoekmeting (RDM), the Dutch geographical coordinate system

### 6.4 Three different model configurations

Following distinction is made in model configurations:

1. One SOBEK model configuration:
   ***SBK_1***: SOBEK model that only covers the river network and Dike ring 41 (see Fig 6.2)
2. Three different sets of potential breach locations.

The SOBEK model has a spatially uniform (2D) grid cell size of 100m.

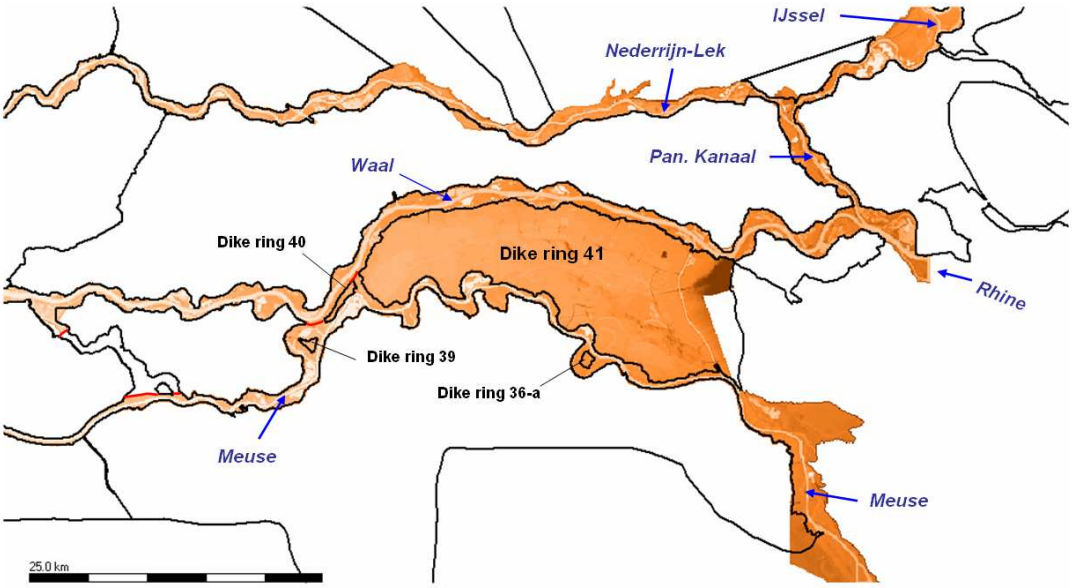


Fig 6.2 The SBK_1 Model schematization

Refering to the SBK_1 Model schematization from Case Study 1 as ***Set A,*** the following three new sets of potential breach locations are used:

- ***Set B***, comprising of in total *eleven* potential breach locations, being: Dr41L1 to Dr41L11,
- ***Set C***, comprising of in total *twenty-two* potential breach locations, being: Dr41L1 to Dr41L11, Dr41L12, Dr41L14, Dr41L17, Dr41L19, Dr41L22, Dr41L24, Dr41L25, Dr41L27, Dr41L30, Dr41L33 and Dr41L36,
- ***Set D***, comprising of in total *thirty-eight* potential breach locations: being: Dr41L1 to Dr41L38

For information on the potential breach locations Dr41L1 to Dr41L38, reference is made to section 6.3.

Table 6.3 gives an overview of the different SOBEK model configurations in Case Study 2.

Table 6.3 Overview of the model configurationsin Case Study 2

| Three different SOBEK model configuration applied in Case study 2 | | | |
|---|---|---|---|
| No | Code | Sobek Model | Considered potential breach locations |
| 1 | SBK_1 & Set B | Dike ring 41 only | Dr41L1 to Dr41L11 |
| 2 | SBK_1 & Set C | Dike ring 41 only | Dr41L1 to Dr41L11, Dr41L12, Dr41L14, Dr41L17, Dr41L19, Dr41L22, Dr41L24, Dr41L25, Dr41L27, Dr41L30, Dr41L33 and Dr41L36 |
| 3 | SBK_1 & Set D | Dike ring 41 only | Dr41L1 to Dr41L38 |

## 6.5 Results

### 6.5.1 Step 1 results

In case study 2 use was made of a new SOBEK executable, in which improvements regarding the computation of overland flow were made. It was, therefore, decided to construct a new Step 1 hydraulic database for case study 2.

### 6.5.2 Step 2 results

The annual failure probability $P_F$ for dikering 41 is equal to 0.02 [-/year] as already calculated using PC-Ring in Case study 1.

### 6.5.3 Step 3 results

In step 3 Monte Carlo realizations were obtained, neglecting system effects and using the water levels determined in Step 1, in which at least one dike section failed in the system.
This was realized by first deriving 100 fail scenarios for the set with 38 possible breach locations (set D).
The scenarios for the sets with less breach locations were defined as subsets of set D, by selecting the corresponding locations that are to be evaluated in step 4. Advantage is that the three sets (B to D) will have the same hydraulic boundary conditions (from table 6.1). Disadvantage will be that the resulting number of scenarios for set A (11 locations) and set B (22 locations) are substantially less than 100. Table 6.4 gives an overview of the number of scenarios per set.

Table 6.4 MC realisations, for different breach location sets

| Code | Nloc [-] | Number of MC realizations [-] | Number of failure scenarios [-] | Pf [1/48hrs] | β (48 hours) [-] |
|---|---|---|---|---|---|
| SBK_1 & Set B | 11 | 1384029 | 23 | $1.7\ 10^{-05}$ | 4.2 |
| SBK_1 & Set C | 22 | 1384029 | 72 | $5.2\ 10^{-05}$ | 3.9 |
| SBK_1 & Set D | 38 | 1384029 | 100 | $7.2\ 10^{-05}$ | 3.8 |

The Monte Carlo simulations make use of realizations for discharges based on 48 hours statistics. Hence the unit [1/48 hrs] as depicted in table 6.4.
With 100 scenarios for set C, the variation coefficient of the failure probability estimate is about:

*COV($P_f$) = 1/sqrt(100) = 10 %*

That is sufficiently precise for the present purpose.
When transforming the failure probabilities to a period of 1 year, the change will roughly be in the order of a factor 90 (1 year ~1 season ~180 days ~**90***48 hrs). For set C, this would account for an overall β equal to 2.5.
The full PCRing calculation for dike ring 41, with a total of 80 sections (step2) leads to a reliability index β = 2. The difference (approximately a factor 3 in terms of failure probability) is explained mainly by the number of breach locations and length effects accounted for in both modellations.

### 6.5.4 Step 4 results

In Step 4, SOBEK computations with the SBK_1 model were made for the Step 3 representative scenarios per set.

For set B (11 locations) all 23 scenarios from step 2 also led to corresponding failures in step 4 for the SOBEK calculations.
For set C (22 locations) 4 scenarios out of the 72 did not result in a failure scenario for step 4. This concerned scenario numbers 1, 15, 70 and 81.
For set D (38 locations) 3 scenarios out of the 100 were unsuccessful in reproducing failure in step 4, namely scenarios 1, 59 and 70.
A closer look at these scenarios shows that the origin of failures being absent in step 4 lies in crashed runs, rounded values for the river discharges, different implementation of dike ring phreatic water levels and a constant dike height in step 4 whereas in step 3 the dike height was modelled as a stochastic parameter.

In Step 3, locations failed due to exerted hydraulic river loads only. For Step 4, a distinction is made between failures induced by river loads (river side) and by hydraulic loads exerted at the dike ring side, that occur due to the flooding of dike ring 41.
Due to the refined modelling for heave and piping the number of failures as a result of piping increases when compared to case study 1. In Case study 2 a total number of 17 breach locations failed due to this mechanism within the 23 scenarios in the configuration with 11 locations (set B). In Case study 1 the number of failure locations due to heave and piping was equal to 19 (within 65 scenarios).

Tables 6.5a and 6.5b give the total number of failures per dike ring 41 breach location, which occurred in the sets of corresponding scenarios. Set A, from Case Study 1, is also included in these tables.
From Table 6.5a, one can see that for river loads the downstream locations benefit from system effects as, in the current simulations, failure locations seem to cluster towards the upstream locations. For (secondary) failures due to loads at the (flooded) dike ring side, a significant number of failures is found for locations Dr41L10, Dr41L11 (downstream locations at the Meuse). In general, most (primary) failures occur at the river Rhine.
Going from Table 6.5a towards Table 6.5b, the number of breach locations first increases from 11 to 22 (set C, left side of the table). Location Dr41L12 is the most upstream location at the Rhine. It shows a remarkable number of failures (predominantly due to ‘Heave&Piping’) and in terms of system effects it shelters the downstream locations. Other added breach locations at the Rhine behave comparable to the points from set A they are lying next to. For the locations at the

Meuse, the added location Dr41L30 shows to be present in a (relative) large number of failure scenarios. In contrast to the new scenarios of the Rhine, however, it is not the most upstream point. With respect to secondary failures, i.e. failures due to loads exerted from within the dike ring, there is hardly an increase in the number of scenarios in which this takes place. This indicates that compared to downstream failures at the Rhine, failures at Dr41L12 seem to be less severe.

For set D, the right part in Table 6.5.b, new breach locations are added. The new point at the Meuse, Dr41L35, adds a significant number of river induced failure scenarios, predominantly due to 'Overflow&Erosion'. Downstream at the Meuse, a significant number of dike ring induced failures are observed at location Dr41L38.

Table 6.5a Failures of dike ring 41, for scenarios with 11 breach locations
Grey marked cells indicate locations along Waal, otherwise locations along Meuse.

| | Set A (11 locations, 65 scenario's) | | | Set B (11 locations, 23 scenario's) | | |
|---|---|---|---|---|---|---|
| Location | Without system effects (step 3) | With system effects (step 4) | | Without system effects (step 3) | With system effects (step 4) | |
| | River side | River side | Dike ring side | River side | River side | Dike ring side |
| 'Dr41L1' | 34 | 27 | 0 | 14 | 12 | 0 |
| 'Dr41L2' | 32 | 17 | 0 | 13 | 8 | 0 |
| 'Dr41L3' | 27 | 11 | 0 | 5 | 2 | 0 |
| 'Dr41L4' | 19 | 4 | 0 | 4 | 0 | 0 |
| 'Dr41L5' | 28 | 10 | 0 | 8 | 2 | 0 |
| 'Dr41L6' | 13 | 11 | 0 | 4 | 3 | 0 |
| 'Dr41L7' | 1 | 0 | 0 | 0 | 0 | 0 |
| 'Dr41L8' | 11 | 2 | 0 | 3 | 1 | 0 |
| 'Dr41L9' | 1 | 2 | 0 | 2 | 2 | 0 |
| 'Dr41L10' | 3 | 0 | 53 | 0 | 0 | 16 |
| 'Dr41L11' | 1 | 1 | 44 | 0 | 0 | 14 |

Table 6.5b Failures of dike ring 41, for scenarios with 22 (set C) and 38 (Set D) breach locations. Grey marked cells indicate locations along Waal, otherwise locations along Meuse.

| | Set C (22 locations, 68 scenario's) | | | Set D (38 locations, 97 scenario's) | | |
|---|---|---|---|---|---|---|
| Location | Without system effects (step3) | With system effects (step 4) | | Without system effects (step 3) | With system effects (step4) | |
| | River side | River side | Dike ring side | River side | River side | Dike ring side |
| 'Dr41L1' | 14 | 9 | 0 | 14 | 9 | 0 |
| 'Dr41L2' | 13 | 6 | 0 | 13 | 6 | 0 |
| 'Dr41L3' | 5 | 1 | 0 | 5 | 1 | 0 |
| 'Dr41L4' | 4 | 0 | 0 | 4 | 0 | 0 |
| 'Dr41L5' | 8 | 0 | 0 | 8 | 0 | 0 |
| 'Dr41L6' | 4 | 1 | 0 | 4 | 1 | 0 |
| 'Dr41L7' | 0 | 0 | 0 | 0 | 0 | 0 |
| 'Dr41L8' | 3 | 1 | 0 | 3 | 0 | 0 |
| 'Dr41L9' | 2 | 0 | 0 | 2 | 0 | 0 |
| 'Dr41L10' | 0 | 0 | 14 | 0 | 0 | 16 |
| 'Dr41L11' | 0 | 0 | 14 | 0 | 0 | 12 |
| 'Dr41L12' | 44 | 38 | 0 | 44 | 39 | 0 |
| 'Dr41L13' | | | | 7 | 2 | 0 |
| 'Dr41L14' | 14 | 10 | 0 | 14 | 10 | 0 |
| 'Dr41L15' | | | | 6 | 0 | 0 |
| 'Dr41L16' | | | | 5 | 2 | 0 |
| 'Dr41L17' | 3 | 0 | 0 | 3 | 0 | 0 |
| 'Dr41L18' | | | | 4 | 0 | 0 |
| 'Dr41L19' | 5 | 1 | 0 | 5 | 1 | 0 |
| 'Dr41L20' | | | | 6 | 1 | 0 |
| 'Dr41L21' | | | | 7 | 2 | 0 |
| 'Dr41L22' | 4 | 0 | 0 | 4 | 0 | 0 |
| 'Dr41L23' | | | | 5 | 0 | 0 |
| 'Dr41L24' | 7 | 1 | 0 | 7 | 2 | 0 |
| 'Dr41L25' | 3 | 0 | 0 | 3 | 0 | 0 |
| 'Dr41L26' | | | | 7 | 6 | 0 |
| 'Dr41L27' | 3 | 2 | 0 | 3 | 0 | 0 |
| 'Dr41L28' | | | | 8 | 5 | 0 |
| 'Dr41L29' | | | | 2 | 0 | 0 |
| 'Dr41L30' | 8 | 6 | 0 | 8 | 3 | 0 |
| 'Dr41L31' | | | | 2 | 0 | 0 |
| 'Dr41L32' | | | | 3 | 2 | 0 |
| 'Dr41L33' | 4 | 3 | 0 | 4 | 3 | 0 |
| 'Dr41L34' | | | | 0 | 0 | 0 |
| 'Dr41L35' | | | | 31 | 27 | 1 |
| 'Dr41L36' | 1 | 3 | 1 | 1 | 2 | 3 |
| 'Dr41L37' | | | | 6 | 0 | 9 |
| 'Dr41L38' | | | | 0 | 0 | 15 |

When categorizing the failure scenarios with respect to failure locations (river Waal or river Meuse) and failure loads (from river or dike ring) the following combinations are realized:

1. **River induced** failure along the *Waal* only
2. **River induced** failure along the *Meuse* only
3. **River induced** failure along the *Waal and Meuse*
4. **River induced** failure along the *Waal* followed by **dike ring induced** failure along the *Meuse*
5. **River induced** failure along the *Waal and Meuse* followed by **dike ring induced** failure along the *Meuse*

Other combinations are (theoretically) possible but were not observed within the sets. The scenarios categorized as above are listed in Table 6.6 along with the mean peak discharges per river in each category (note: river Waal is a tributary of river Rhine). As was seen in the previous tables, there is a significant increase of river Waal induced failures (cat. 1) when going from set B to set C. Next, from set C to set D, there is an increase in river Meuse induced failures (cat. 2. as well as dike ring induced failures in cat. 5).

Table 6.6 Classification of scenarios with respect to failure locations, induced by loads exerted at river side or loads exerted at the dike ring side

| Set | A | B | C | D |
|---|---|---|---|---|
| Number of potential breach locations | 11 | 11 | 22 | 38 |
| Total number of scenarios with failures | 65 | 23 | 68 | 97 |
| Mean $Q_{peak}$ Rhine ($m^3/s$) | (17711) | (15252) | (12431) | (13122) |
| Mean $Q_{peak}$ Meuse ($m^3/s$) | (3918) | (3367) | (2667) | (2923) |
| **1. River induced** failure along the *Waal* only | 6 | 4 | 43 | 41 |
| | (11250) | (9349) | (10490) | (10164) |
| | (2217) | (1861) | (2147) | (2070) |
| **2. River induced** failure along the *Meuse* only | 2 | 0 | 4 | 28 |
| | (17850) | (-) | (14596) | (14846) |
| | (4400) | (-) | (3646) | (3642) |
| **3. River induced** failure along the *Waal and Meuse* | 0 | 0 | 1 | 2 |
| | (-) | (-) | (8913) | (10846) |
| | (-) | (-) | (1906) | (2298) |
| **4. River induced** failure along the *Waal* **followed** by **dike ring induced** failure along the *Meuse* | 44 | 13 | 14 | 15 |
| | (17542) | (14660) | (14575) | (14100) |
| | (3835) | (3216) | (3179) | (2950) |
| **5. River induced** failure along the *Waal and Meuse* **followed** by **dike ring induced** failure along the *Meuse* | 13 | 6 | 6 | 11 |
| | (21185) | (20470) | (20482) | (18844) |
| | (4892) | (4697) | (4678) | (4347) |

An evaluation of the dike ring induced failures along the river Meuse shows that they were all due to 'Overflow and Erosion', i.e. no dike ring induced failure due to 'Heave and Piping' was observed.

### 6.5.5 Step 5 results

The computational framework determines flood risk using the HIS-SMM Damage and Victims module and the hydraulic output computed in the previous step. Flood consequence (both expected damage and expected number of casualties) become available as:

- *A flood risk map* with spatial discretization equal to the SOBEK grid cell size (i.e. 100 m in the present case study), and
- *Tables* of aggregated flood consequence per dike ring area

The flood consequence (i.e. damage and victims) for each set of scenarios are given in Table 6.7.

Table 6.7 Flood consequences for each set of scenarios

| | Victims [-] | | Damage [€] | |
|---|---|---|---|---|
| | Mean | St.Dev | Mean | St.Dev |
| Set A (11 loc.) 65 scenarios | 792 | 436 | $6.2x10^9$ | $2.2x10^9$ |
| Set B (11 loc.) 23 scenarios | 544 | 326 | $5.3x10^9$ | $2.6x10^9$ |
| Set C (22 loc.) 68 scenarios | 248 | 263 | $2.7x10^9$ | $2.5x10^9$ |
| Set D (38 loc.) 97 scenarios | 211 | 241 | $2.4x10^9$ | $2.3x10^9$ |

It can be seen that there is a remarkable drop in mean values for Victims as well as Damage when going from 11 to 22 locations and next to 38 locations. Also the shape of the histograms for these quantities shows a change when the locations are increased, see figure 6.4 and figure 6.5.

The origin of these changes can be found when the consequences are categorized according to the scenario classifications in Table 6.6. Doing so, leads to the mean consequence values as listed in Table 6.8 and Table 6.9. It can be seen that, going from 11 to 22 locations, a substantial number of scenarios arises with relative low mean values for the consequences, namely the 43 scenarios in cat. 1. These are mainly due to failures at location Dr41L12, as already noted in Table 6.5b. The reason why the flood consequence for these 43 scenarios is relatively low is twofold. Firstly, flood consequence is low since the realization for the mean of the river peak discharge for these 43 scenarios is relatively low (see Table 6.6). Secondly, the presence of elevated embankments along the Meuse-Waal canal, that act as an compartmentalizing dike separating dike ring 41 in two parts. These elevated embankments are located directly downstream of potential breach location Dr41L12 and prevent inflowing Waal water to flood a large area in dike ring 41. Of course this reduces the flood consequence of breaches at location Dr41L12. Figure 6.3 shows a typical flow pattern resulting from a failure at location Dr41L12.

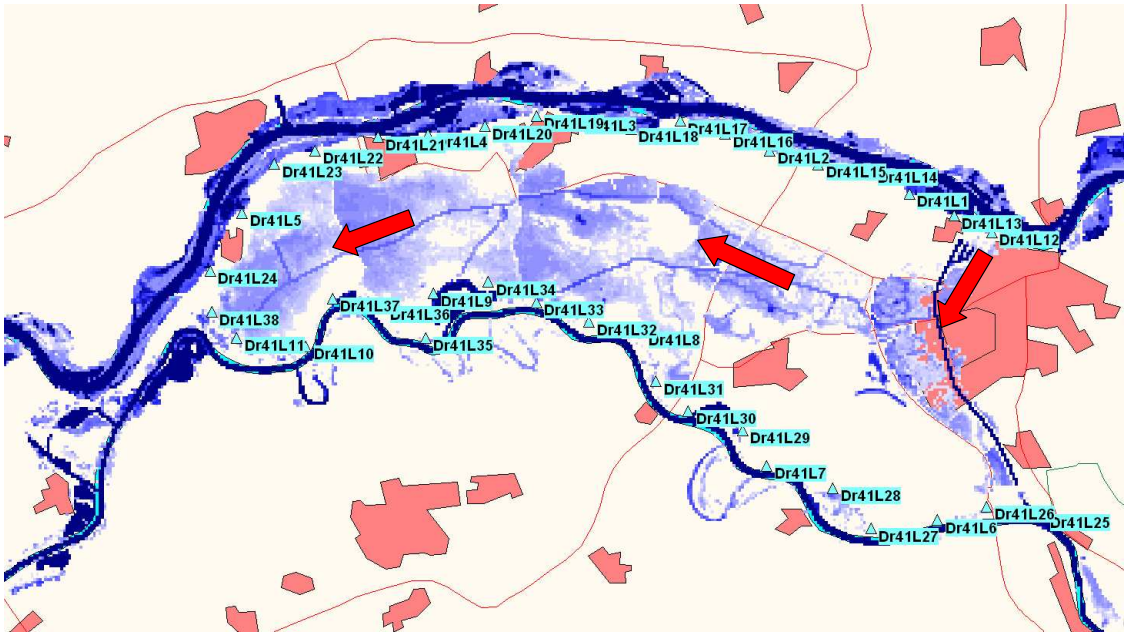


Figure 6.3. Failure of upstream Dr41L12, resulting in reduced hydraulic loads at downstream located potential breach locations

A further reduction for the mean values is obtained when going form 22 to 38 locations. Now a relatively large set of river induced failures at the Meuse is added with relatively low consequence values (28 scenarios of cat. 2.). Location Dr41L35 seems to be involved in most of these scenarios, see Table 6.5b. The reason why the mean flood consequences reduce further, going from 22 to 38 locations (or from 68 to 97 scenarios) is again twofold. Firstly, a number of scenarios are added with predominant breaching at potential Meuse breach locations (see Table 6.5b), whose associated Meuse peak discharges are lower than those associated with the less frequently occurring breaching at potential Waal breach locations. It is obvious that relatively lower peak discharges (weighted average of Waal and Meuse discharges), that effectively flow into dike ring 41 results in a lower flood consequence. Secondly, the surface level in dike ring 41 is sloping from North to South and from East to West. This implies that river water flowing into dike ring 41 at upstream Waal locations (except for Dr41L12) and at upstream Meuse locations (except for Dr41L25) in general flows over a large part of dike ring 41 before reaching the lowest part in front of locations Dr41L10, Dr41L11 and Dr41L35 to Dr41L38. It is obvious that flooding a larger part of dike ring 41 refers to a larger associated flood consequence. In going from 22 to 38 locations, breaching at location Dr41L35 occurs 31 times. Apparently, this location appears to be a weak spot in the Meuse dike along dike ring 41. Location Dr41L35 is located in the middle of dike ring 41 (see figure 4). For the sake of explanation, assume that breaching only occurs at Dr41L35. This means that only a relatively small part of dike ring 41 will be flooded, meaning a very small flood consequence only. This small flood consequence apparently reduces the mean of the flood consequence over the in total 97 scenarios.

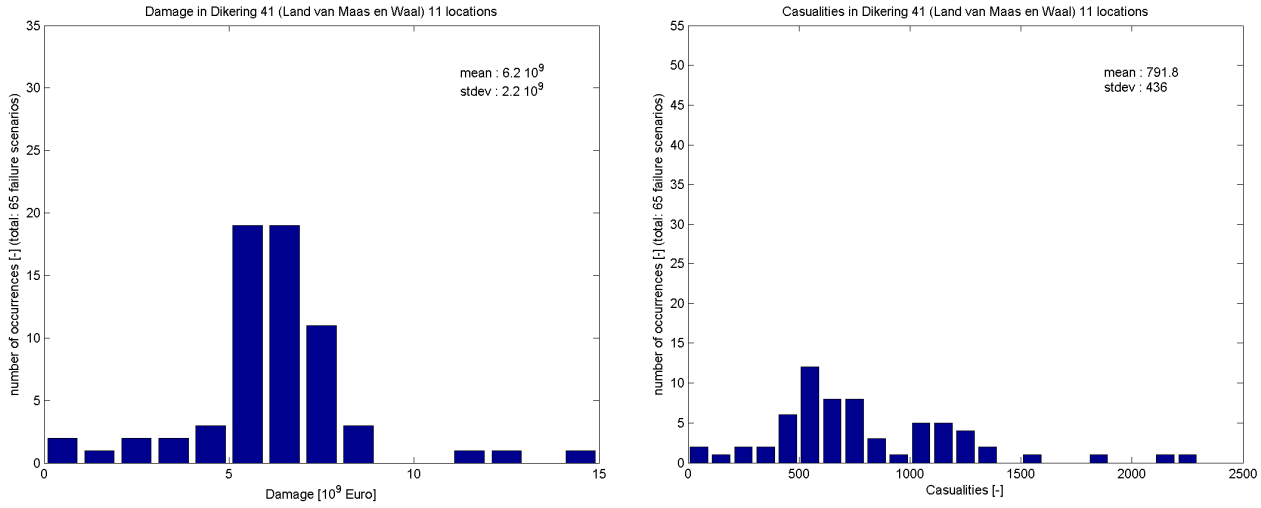


Figure 6.4: Histograms of damage and victims in dike ring 41 for scenario set A (Case 1).

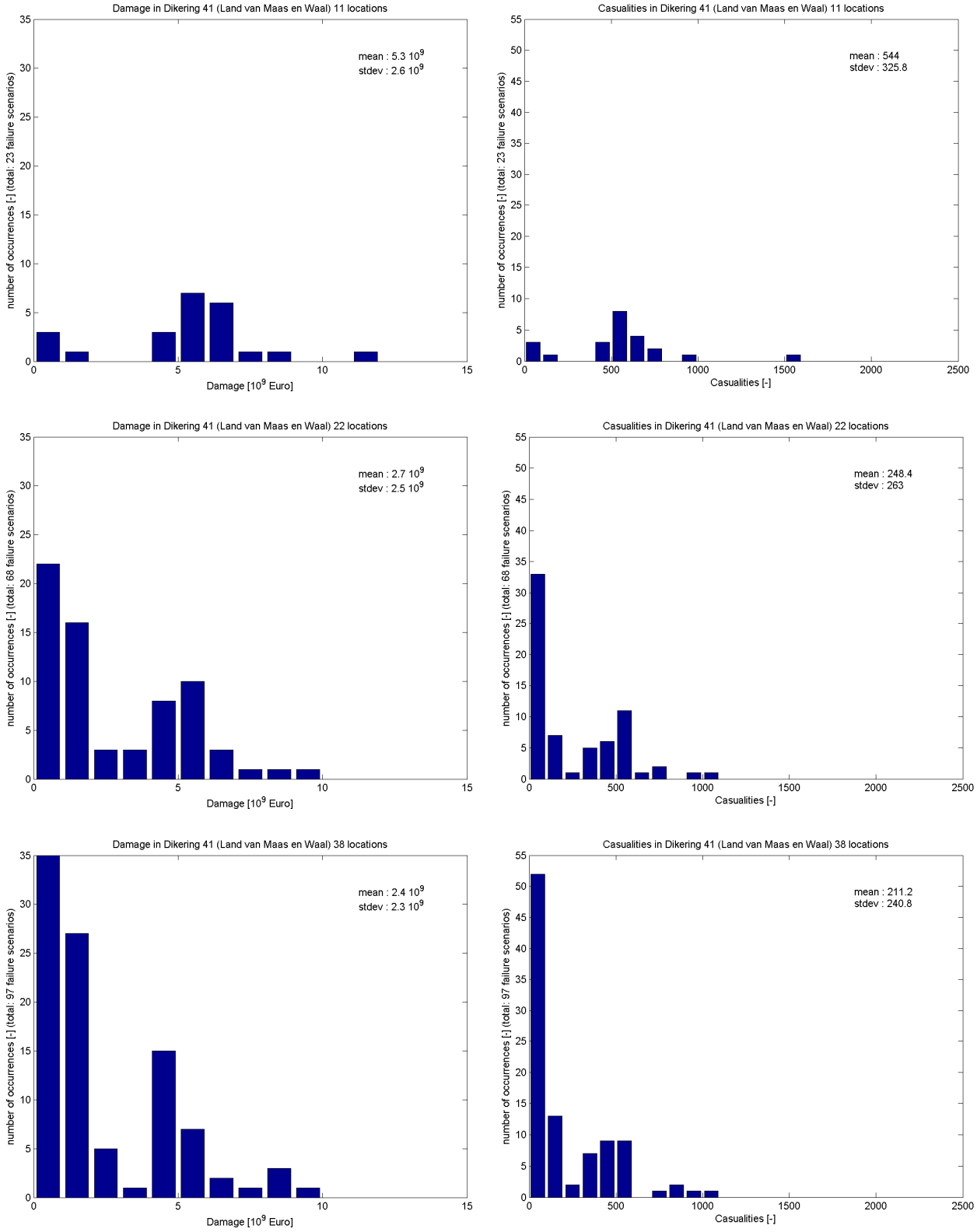


Fig 6.5 Histograms of damage and victims in dike ring 41, scenario set B to D (Case study 2).

Table 6.8 Mean values of victims [-] for subsets of scenarios with respect to failure locations, induced by loads exerted at river side or loads exerted at the dike ring side

| Set | A | B | C | D |
|---|---|---|---|---|
| Number of potential breach locations | 11 | 11 | 22 | 38 |
| All scenarios with failures (Number of scenarios) | 792.0 (65) | 544.0 (23) | 248.4 (68) | 211.2 (97) |
| **1. River induced** failure along the *Waal* only (Number of scenarios) | 176.2 (6) | 50.0 (4) | 99.8 (43) | 83.3 (41) |
| **2. River induced** failure along the *Meuse* only (Number of scenarios) | 304.5 (2) | - (0) | 210.3 (4) | 91.3 (28) |
| **3. River induced** failure along the *Waal and Meuse* (Number of scenarios) | - (0) | - (0) | 10.0 (1) | 96.5 (2) |
| **4. River induced** failure along the *Waal* followed by **dike ring induced** failure along the *Meuse* (Number of scenarios) | 851.4 (44) | 549.5 (13) | 529.8 (14) | 451.7 (15) |
| **5. River induced** failure along the *Waal and Meuse* followed by **dike ring induced** failure along the *Meuse* (Number of scenarios) | 943.8 (13) | 861.5 (6) | 722.3 (6) | 686.1 (11) |

Table 6.9 Mean values of damage [€] for subsets of scenarios with respect to failure locations, induced by loads exerted at river side or loads exerted at the dike ring side

| Set | A | B | C | D |
|---|---|---|---|---|
| Number of potential breach locations | 11 | 11 | 22 | 38 |
| All scenarios with failures (Number of scenarios) | $6.2 \times 10^9$ (65) | $5.3 \times 10^9$ (23) | $2.7 \times 10^9$ (68) | $2.4 \times 10^9$ (97) |
| **1. River induced** failure along the *Waal* only (Number of scenarios) | $2.1 \times 10^9$ (6) | $0.7 \times 10^9$ (4) | $1.4 \times 10^9$ (43) | $1.2 \times 10^9$ (41) |
| **2. River induced** failure along the *Meuse* only (Number of scenarios) | $3.3 \times 10^9$ (2) | - (0) | $2.4 \times 10^9$ (4) | $1.2 \times 10^9$ (28) |
| **3. River induced** failure along the *Waal and Meuse* (Number of scenarios) | - (0) | - (0) | $0.24 \times 10^9$ (1) | $1.3 \times 10^9$ (2) |
| **4. River induced** failure along the *Waal* followed by **dike ring induced** failure along the *Meuse* (Number of scenarios) | $6.2 \times 10^9$ (44) | $5.5 \times 10^9$ (13) | $5.3 \times 10^9$ (14) | $4.7 \times 10^9$ (15) |
| **5. River induced** failure along the *Waal and Meuse* followed by **dike ring induced** failure along the *Meuse* (Number of scenarios) | $8.4 \times 10^9$ (13) | $7.9 \times 10^9$ (6) | $7.1 \times 10^9$ (6) | $6.9 \times 10^9$ (11) |

### 6.5.6 Step 6 results

Finally, the annual flood risk is determined in the dimensions of direct economical damage and human casualties. This (annual) flood risk is determined from the conditional consequences (given failure) multiplied by the failure probability

As Crude Monte Carlo was used, the conditional consequence $E(C|F)$ is simply estimated by its mean value, based on the consequence values of the investigated scenarios with failure.
These conditional consequences then correspond to the mean values presented in Table 6.7.

As calculated with PC-Ring, the probability of failure equals 2.0 $10^{-2}$ [1/year]. Combining this probability of failure with the values in Table 6.7 leads to the annual flood risk values presented in Table 6.10.

Taking the set D results as most elaborate, it shows that the expected damage $R = E[C]$ = 0.48 $10^8$ € per year for dike ring 41. The expected number of victims is equal to 4.2 per year.

Table 6.10 Estimated annual flood risk for Dike ring 41

| | Victims (1/Yr) | Damage (€/Yr) |
|---|---|---|
| Set A (11 loc.) 65 scenarios | 15.8 | 1.24 x$10^8$ |
| Set B (11 loc.) 23 scenarios | 10.9 | 1.06 x$10^8$ |
| Set C (22 loc.) 68 scenarios | 5.0 | 0.54 x$10^8$ |
| Set D (38 loc.) 97 scenarios | 4.2 | 0.48 x$10^8$ |

With reference to Table 6.8 and 6.9, the following observations are made. Starting from set B, the results tend to increase when going to the results of set A for which more scenarios were taken into account. A large number of Waal breach locations with relatively high discharge values are at the origin of this, see Figure 5.3 for an illustration of a flow pattern. However, when the number of locations is increased as for set C and set D, the results decrease significantly For set C this effect is mainly due to a large number of upstream breach locations at the Waal with lower discharge values (see Table 6.6) and with flow patterns (breaching at location Dr41L12) as shown in Figure 6.3. Set D adds a number of scenarios with predominantly breaching at potential Meuse breach locations (see Table 6.5), whose associated discharges are lower than those associated with the breaching at potential Waal breach locations.
The results show a significant influence in the number (and especially location) of potential breach locations as well as the magnitude of the upstream river discharges associated with the scenarios considered. Proper care is thus to be given in selecting the set of potential breach locations as well as scenarios such that they are representative for the modelled geographical area.

## 6.6 Conclusions Case 2

- In case study 2, variations with an increasing number of dike breach locations were performed.
- In general, case study 2 confirms the system behaviour aspects found in case 1 and as such the conclusions from case 1 (section 5.6) also hold for case 2.
- It was also demonstrated that the effects that the geographical properties of the area considered have on flood risk can be accounted for by the computational framework. Properties such as the sloping of dike ring 41 and the presence of the Meuse-Waal canal, acting as a kind of compartmentalizing dike.
- The results for the increasing number of breach locations show a significant change in the calculated estimations for the consequences and hence for the annual risk.
- It can be concluded that a number of 11 locations was not representative for dike ring 41 (an assumption made in case study 1).
- The current results for 22 locations and 38 locations show that they are governed by only a few breach locations. This might suggest that the simulations with 38 locations suffice in order to get a good estimate for the risks. On the other hand, it also shows the sensitivity of the results in (weak) locations being accounted for or not. So, possible locations not yet taken into account could again change the risk estimations.
- It shows that proper care has to be taken in selecting the set of breach locations such that it is representative for the system investigated.

# 7 Outlook

## 7.1 General remarks

There is a long history of risk analysis as a basis for establishing the dike dimensions in the Netherlands. The Delta Law (1957) was based on statistical analysis of local water levels and a rough estimate of the economic optimal design value. Uncertainty at the resistance side was not taken explicitly into account and every dike section was considered as a single entity. Research in later decades was focused on the missing issues. Nowadays software is available to calculate the failure probability of a dike ring.

In order to calculate the risk it was soon realised that one could not simply multiply the failure probability with "the" damage as consequences depend on the amount and type of failures as well as on the water levels and the time of collapse. For that reason the scenario approach was developed. This approach, however, was difficult, time consuming and sometimes doubtful. A careful interpretation of the results was always necessary to prevent misleading results. Clearly there was a need for another method.
Another shortcoming of the approach above is that only dike rings are considered individually. The failure occurring in one dike ring, however, does not only affect other sections of the same ring, but also of other dike rings. It may be important to take this into account.

The approach presented in this report is able to deal with both issues. The approach is possible by the increasing speed of computers and will even be more applicable in future. The present examples are relatively simple as they have more the nature of clarifying the procedures than as an analysis ready to show a practical application. For sure, however, this will be one of the further steps.

This means that research in the next period should focus on issues like:

- dealing consistently with length effects
- treating dike mechanisms when loading is (also) on the inner slopes
- improving efficiency using Importance Sampling methods
- calculating realistic sets of dike rings
- making links to optimal dike improvement strategies

It is not foreseen that in short time the method can be the only tool necessary for flood protection calculations. The present analysis will probably remain on a high level without too many details. Classical procedures will be needed to fill up these gaps.

Apart from the general items for the next period discussed above, a number of specific items are discussed in the following paragraphs.

## 7.2 Failure mechanism, considering the variation of water levels in time

At present in Step 2 of the computational framework (see section 4.4 and 4.5), failure mechanisms are among others evaluated on basis of the maximum water level, that occurs at the potential breach locations. Hence, the variation of water levels in time is not considered. For

some failure mechanisms (e.g. piping**)** advanced formulations are available, that consider the variation of water levels in time. The time dependent variation of water levels at potential breach locations can be made available in the Step 1 hydraulic database. In future, it is considered to use these advanced failure mechanism descriptions in Step 2 of the computational framework.

## 7.3 Residual strength

As mentioned in section 2.3.2 residual strength was not considered in the present (DC2) research project. The reason, here fore, is the lack of adequate formulations that describe the remaining strength of flood protection works after the occurrence of a specific failure mechanism.. Hereunder, reflections regarding residual strength are given, that might be implemented in future enhancements of the computational framework.

Due to the occurrence of a specific failure mechanism, locally the height of a dike might be lowered but not be overtopped (see Fig 6.1). Hence, although a geo-technical dike failure occurred, from a hydraulic point-of-view the dike will not fail. In other words after failure, the residual strength of the dike is sufficient to protect the area behind this dike against flooding. The occurrence of a particular failure mechanism at a later point-in-time or a water level higher than the actual dike height, might result in the hydraulic failure of the dike (see Fig 6.1).

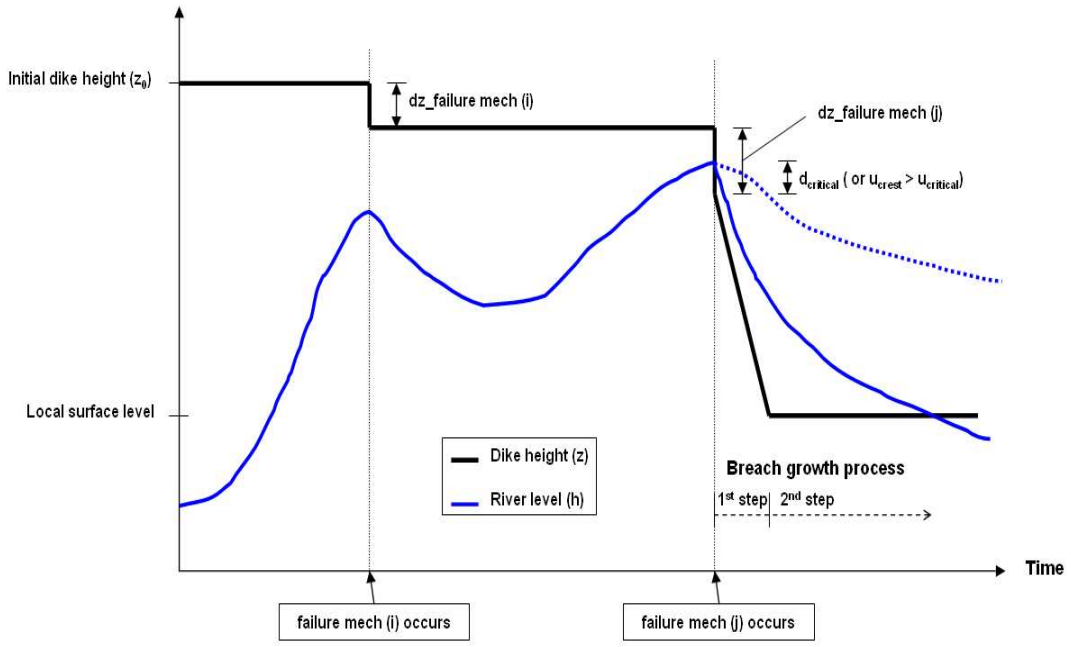


*Figure 6.1 Possible future incorporation of residual strength*

## 7.4 Breaching

As mentioned in section 2.3.2, irrespective of the initiating failure mechanism the same breaching formulation was applied. Furthermore, breaching was modelled as a 1D branch, connected to 2D grid cells, respectively located at the river side and at the dike ring side of the concerning potential breach location (see section 2.1). Hereunder, reflections regarding breaching are given, that might be implemented in future enhancements of the computational framework.

It is considered to replace the 1D-branch-breaching approach by 2D dike grid cells, having the functionality that only a part of their dike height is lowered. In other words that such 2D grid cell is not lowered over its entire area. This would enable the implementation of breach formulations as used in the present study.

It is considered that hydraulic failure and related initiation of breaching might be enabled as follows:

a. A dike is only overtopped (i.e. no erosion of dike material). This possibility is already implemented in the present study
b. A dike is overtopped and dike material is eroded away. So breaching is initiated. Question: Which formulation is most suited to describe the breaching process?
c. Due to a particular failure mechanism a large part of the dike-section collapses, meaning that more or less instantaneously an initial breach occurs. Questions: How large is such instantaneously initial dike-breach?, What is its shape of such initial dike-breach?, Which formulation is most suited to describe the breach process?

**References**


Bouwdienst Rijkswaterstaat en Dienst Weg- en Waterbouwkunde Rijkswaterstaat, *Pilot Case Overstromingsrisico, Deel VI: Eindrapport*, Delft, 2001

Delft Cluster report *Effects of System Behaviour on Flood Risk*,. 2003

Deltares, Klimaatbestendigheid van Nederland Waterland, Knikpunten in beheer en beleid, tussenrapportage, Project T2447, 2008.

Dhondia, J.F. and Stelling, G.S., *Sobek 1D-2D integrated hydraulic model for flood simulation – its capabilities and features explained*, in sixth International Conference on Hydroinformatics, Singapore, Liong Phoon&Babovic (eds), World Scientific Publishing Compagny, ISBN 981-238-787-0.

Diermanse, F.L.M. and Van Vuren, W., *Het samenvallen van pieken op Rijn en Maas in het benedenrivierengebied, WL|Delft Hydraulics memo for RIZA Dordrecht, April 4th, 2002.*

Gudden, J.J, and Overmars J.M.S, Notitie over herhalingstijden (memo concering return periods), Province of Gelderland, february 16th, 2004.

Hohenbichler M., Rackwitz R., *First-order concepts in system reliability*, Structural Safety, 1983, pp. 177-188.

Huizinga, H.J. et al., 2004, *HIS-Schade en Slachtoffermodule*, version 2.1, manual. DWW-2005-004. RWS Dienst Weg- en Waterbouwkunde.

HKV, Aanpassingen golfvormgenerator in opdracht van RWS/RIZA, Lelystad, sept 2004.

Jonkman, S.N., 2007, *Loss of life estimation in flood risk assessment*, dissertation, Delft University of Technology, The Netherlands.

Lammersen, R., 2004, *Grensoverschrijdende effecten van extreem hoogwater op de Niederrhein, Eindrapport, LUA Nordrhein-Westfalen, Province of Gelderland, RIZA The Netherlands, ISBN 9036956390.*

TAW, 1999, report "*Zandmeevoerende wellen*".

TAW, 2001, report *"Technisch Rapport Waterkerende Grondconstructies"*.

Van der Knaap, F.C.M., 2000, *Breach growth as a function of time*; WL|Delft Hydraulics, memo's 2 and 3 of May 21 and September 5 respectively, Q2655, Delft (in Dutch)

Van Manen, S.E., *Pilot Case Overstromingsrisico - Eindrapport*, (In Dutch). Ministerie van Verkeer en Waterstaat, project PICASO, august 2001.

Van Manen, S.E., Brinkhuis, M.M., 2003, *Quantitative flood risk assessment for polders*; Proceedings of ESREL 2003,Bedfort & van Gelder (eds), Swets & Zeitlinger, Lisse, The Netherlands

Van Mierlo, M.C.L.M. et al, 2003, *Effects of River System Behaviour on Flood Risk*, Delft Cluster-publication: DC1-211-1, Delft, The Netherlands.

Van Mierlo, M.C.L.M., 2005, Verkenning van systeemwerking in het bovenrivierengebied van de Rijntakken, WL|Delft Hydraulics report Q4019, December 2005.

Van Mierlo, M.C.L.M., Van Buren, R., 2006a, Uitwerking systeemwerking Maas, WL|Delft Hydraulics report Q4309, December 2006.

Van Mierlo, M.C.L.M., Van Buren, R., 2006b, Verkenning systeemwerking in Nederland, WL|Delft Hydraulics report Q4309, December 2006.

Van Mierlo, M.C.L.M. et al, 2007, *Assessment of floods risk accounting for River System Behaviour*, Intl J. River Basin Management Vol 5, No 2 (2007), pp 93-104.

Verheij, H.J. (2002): Modification breach growth model in HIS-OM; WL|Delft hydraulics, Q3299, November 2002, Delft (in Dutch)

Verheij, H.J. and Van der Knaap, F.C.M., 2002, *Modification Breach Growth Model in HIS-OM*, WL|Delft Hydraulics, Q3299 (in Dutch).

VNK, 2005, *Flood Risk and Safety in the Netherlands* (Floris Study – Full Report), Dutch Ministry of Transport, Public Works and Water Management, , ISBN 90-369-5604-9.

VNK, 2005, *Hoofdrapport Onderzoek Overstromingsrisico's*, ISBN-90-369-5604-8.

VNK-2, *http://www.helpdeskwater.nl/projectvnk/project_vnk2*

Vrouwenvelder, A.C.W.M, Steenbergen, H.M.G.M., 2003, Theoriehandleiding PC-Ring, deel A mechanismen beschrijvingen, TNO rapport 2003-CI-R0020.

Vrouwenvelder, A.C.W.M, Steenbergen, H.M.G.M., 2003, Theoriehandleiding PC-Ring, deel B statistische modellen, TNO rapport 2003-CI-R0021.

## Appendix A
## General Implementation of Failure Mechanisms With Time Dependence

Time effects in failure processes have not been modelled explicitly in this project. The following general description makes a suggestion for modelling time aspects as well as residual strength explicitly in the probabilistic calculation scheme.

### General Formulations of the Simplified Failure Mechanisms

Wherever possible we aggregate the uncertainties of the important design parameters in expressions containing (critical) river heads, critical time durations or other generic uncertainty term like the following:

$$h(t) \geq H_{crit} \cap (t - t_O) \geq T_{crit} \cap re(P_f) = 1 \qquad (1)$$

where:
$h(t)$ = time dependent river head level
$h_{crit}$ = some critical head level, associated with the mechanism (initial failure);
$H_{crit}$ = is either a deterministic quantity, or the realization of a random variable,
$t$ = actual time,
$t_o$ = time point where h(t) initially exceeds $H_{crit}$,
$T_{crit}$ = some critical time interval, which may be either deterministic or the realization of a random variable, and
$re(P_f)$ = some random experiment with possible outcomes 1 or 0 and probability $Pr[RE(P_f)=1]=P_f$

The random experiment criterion may be helpful to specify the effects of components to the probability of failure, which do not (evidently) relate to river head level or duration of discharge wave, e.g. residual strength. Values or random characteristics of $H_{crit}$, $T_{crit}$ and $P_f$ are mechanism type and location specific and should be estimated accordingly, preferably with help of probabilistic failure analysis.

The mechanisms for which the described approach is not applicable, be it due to the desired models to be used, can be described with a response surface type technique, analogously to the implementation of the slope stability failure mechanism (see 2.2.4), by interpolation in time and parameter space. In this case prior reliability results of flood wave scenarios are used to form an expression for an equivalent limit state function:

$$\tilde{Z} = \beta(h, \Delta t) + \sum_{i=1}^{\#\,variables} \alpha_i(h, \Delta t) \frac{(X_i - \mu_{X_i})}{\sigma_i} \qquad (2)$$

where:

| | |
|---|---|
| $\beta(h,\Delta t)$ = | calculated reliability index |
| $\alpha_i(h, \Delta t)$ = | calculated influence factor for random variable $X_i$ |
| $X_i$ = | realization of random variable $X_i$ |
| $\mu_i$ = | mean value of the random variable $X_i$ |
| $\sigma_i$ = | standard deviation of the random variable $X_i$ |

The reliability analysis has to be carried out in a priori determined significant ranges of river heads $h$ and critical head exceedance durations $\Delta t$ for each potential dike breach location. The results can be stored in a table of the following form:

Table A.1: Interpolation table scheme for equivalent LSF

| | $h^* < h_1$ | $h_1 \leq h^* < h_2$ | … |
|---|---|---|---|
| $\Delta t^* < \Delta t_1$ | $[\beta_{01,01}\ \underline{\alpha}'_{01,01}]'$ | $[\beta_{12,01}\ \underline{\alpha}'_{12,01}]'$ | … |
| $\Delta t_1 \leq \Delta t^* < \Delta t_2$ | $[\beta_{01,12}\ \underline{\alpha}'_{01,12}]'$ | $[\beta_{12,12}\ \underline{\alpha}'_{12,12}]'$ | … |
| … | … | … | … |

Alternatively, to pre-defining these limit values one could carry out the reliability analyses for the same discrete values and interpolate the $\beta$ and contingently the $\alpha$-values.

The previous reliability analyses can be carried out with a relatively high number of random variables, e.g. soil properties. The obtained influence factors can be used to reduce the simplified equivalent limit state function and the according table to the significant variables.

**Appendix B**
**Implementation of heave and piping in the hydrodynamic simulations**

The figures on the following pages illustrate the implementation of the heave/piping mechanism in the hydrodynamic simulation, i.e. the decision criteria during a simulation run for whether a dike breaches as a consequence of heave/piping or not. For each possible situation, the calculation water levels upstream and downstream with respect to the mechanism are defined. The main distinctions between the situations are a flooded / not flooded protected area and a flooded respectively "dry" foreshore or winter bed.

In summary, the **DECISION RULES** are:

1. The river side water level h is always taken equal to the river water level being the local surface level on the river or its summer bed's level.
2. The dike ring water level is taken as the:
    - ditch level (local phreatic surface level), if known (from PC-Ring database) and dike ring is not inundated
    - local surface level (at the toe of the dike), if ditch level unknown and dike ring is not inundated
    - inundation level, if dike ring is inundated

**DIFFERENCES** case study 2 with respect to case study 1:

1. *River-induced failure*: In case study 1, the local surface level on the dike ring side was adopted for h_hinter regardless the availability of ditch level information. Consequently, at locations, where there is a ditch level available, the expected value of h_hinter will be lower in case study 2, leading to a higher water level difference. Therefore, the expectation is to obtain higher piping probabilities for river-induced failure in case study 2.
2. *Dike ring-induced failure*: In case study 1, the local surface level on the river side was adopted for h, in case, the river was restricted to its summer bed. Consequently, for situations that fulfil the latter condition, the expected value of h will be lower in case study 2 (being the river water level), leading to a higher water level difference. Therefore, the expectation is to obtain higher piping probabilities for dike ring-induced failure in case study 2.

**REMAINING ISSUES** with respect to current physical insights:

- Piping induced from the dike ring side (towards the river side) is unlikely to occur with and intact (low permeable) cover layer on the dike ring side, i.e. it is practically impossible that heave occurs and therefore no flow could occur and induce piping.

**REMARK**
The above considerations have the underlying assumption that the piping formula is used to calculate a critical head difference $\Delta h_{crit}$ , which is then compared to the absolute value of the difference of water levels: ABS(h-h_hinter), accounting also for eventual model factors.

| Case # | Situation | Sketch | Calculation water levels |
|---|---|---|---|
| 1 | **RIVER**<br>high water level | 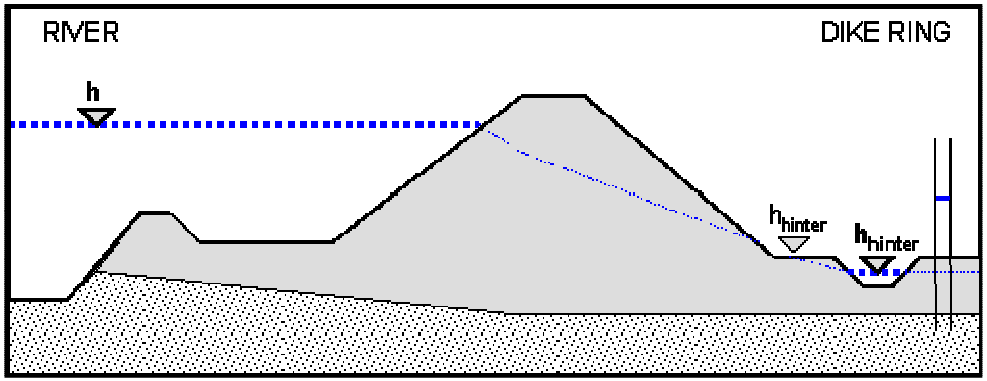 | **h (river):**<br>river water level |
| | **DIKE RING**<br>dry, not inundated | | **h_hinter (dike ring):**<br>phreatic level at the inner toe of the dike<br>(if known, otherwise: local surface level) |
| 2 | **RIVER**<br>low water level<br>(winter bed dry) | 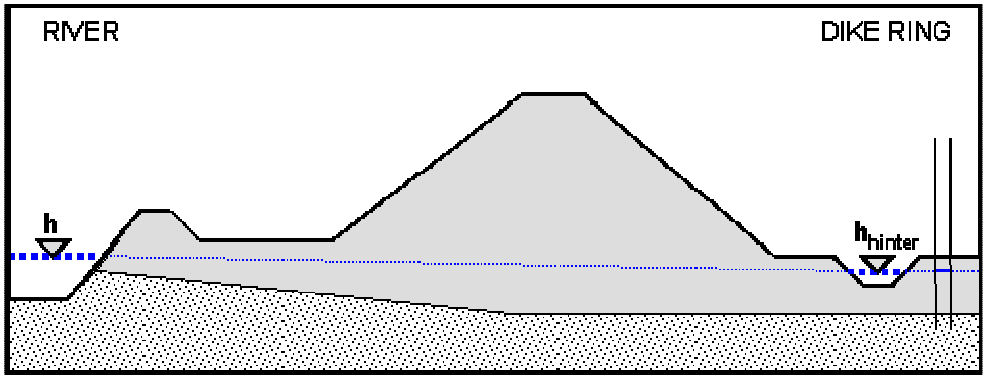 | **h (river):**<br>river water level |
| | **DIKE RING**<br>dry, not inundated | | **h_hinter (dike ring):**<br>phreatic level at the inner toe of the dike<br>(if known, otherwise: local surface level) |

| Case # | Situation | Sketch | Calculation water levels |
|---|---|---|---|
| 3 | **RIVER**<br>low water level<br>(winter bed dry) | 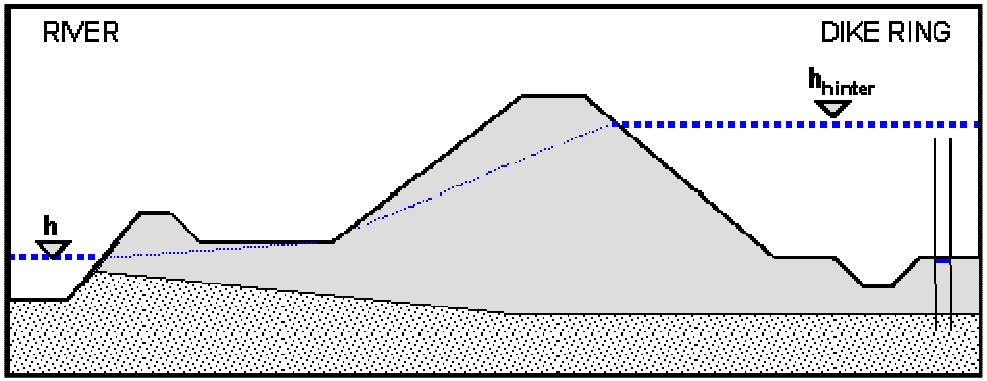 | **h (river):**<br>river water level |
| | **DIKE RING**<br>high water level,<br>dike ring inundated | | **h_hinter (dike ring):**<br>water level at dike toe<br>(inundation level) |
| 4 | **RIVER**<br>high water level | 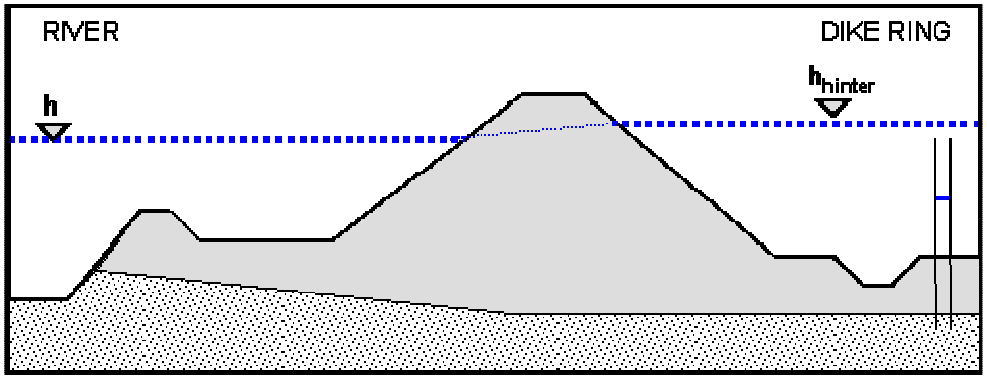 | **h (river):**<br>river water level |
| | **DIKE RING**<br>high water level,<br>dike ring inundated | | **h_hinter (dike ring):**<br>water level at dike toe<br>(inundation level) |

**Appendix C**
**Stochastic properties of parameters used in case study for dijkring41**

This appendix describes the parameter values of the parameters involved in the failure mechanisms of the case studies. The parameter values are given per dike breach location. The values presented are used in case study 2 (chapter 6). In case study 1, different values were used for locations Dr41L1, Dr41L2 and Dr41L6, due to a different procedure followed in matching the breach locations to dike sections from the PCRing data base. Furthermore, in case study 1 the model uncertainty in the head difference for heave (mh) was unintentionally taken as a constant value equal to 0.8.

A number of parameters are taken to be constant and also to be the same for all locations. For some parameters this is based on physical grounds (e.g. gamma_w). For others this is done for pragmatic reasons in order to make the case studies operational despite the lack of reliable data (e.g. breach parameters). These constant values for all dike breach locations are presented in Table C.1.

Table C.1 Parameters with constant values during the present (case) study

| Name | description | value |
|---|---|---|
| Nu | kinematic viscosity | 1.33E-06 |
| Te | exceedance duration (overflow) | 100 |
| gamma_w | volumetric weight of water | 10 |
| B0 | constant breach width (breach growth) | 10 |
| f1 | factor f1 (breach growth) | 1.3 |
| f2 | factor f2 (breach growth) | 0.04 |
| T0 | time period (breach growth) | 0.1 |
| Uc | critical flow-velocity (breach growth) | 0.2 |
| v1 | Velocity of dike height reduction piping) | 0.2 |
| Tp | First time period (piping) | 3 |

The remaining stochastic properties for the dike breach locations are presented from Table C.2 onwards.
The cell labelled as ‘Vaknummer’ refers to the dike segment ID in the ’inwinspreadsheet’ for dijkring 41 as well as to the corresponding ID in de access database (PC-Ring data base) for the dijkring.
The values shown in the tables originate from this database. Except for the standard deviation related to the dike height. This value is increased from 0.1 m (in the original database) to a value of 0.2 m in the current study. Again, this is done for practical reasons in order to force more MC samples leading to failure w.r.t. overflow.

Table C.2 Stochastic properties

| LocatieID | | | | | | |
|---|---|---|---|---|---|---|
| Dr41L1 | | | | | | |
| x | Y | z | WaterstandID | zmin | Vaknummer | |
| 183050 | 431050 | 14.95 | Dr41L1_River | 9.35 | 1410006011 | |
| name | Description | type | mean | stdev | xle | rho_x |
| k_z | specific permeability | LOG | 5.79E-04 | 4.63E-04 | 600 | 0 |
| mh | model uncertainty head difference for heave | LOG | 0.8 | 0.08 | 999999 | 1 |
| mp | model uncertainty Sellmeijer | LOG | 1 | 0.08 | 999999 | 1 |
| m0 | model uncertainty critical head difference for heave | LOG | 1.2 | 0.12 | 999999 | 1 |
| gamma_g | volumetric weight of the grains | NOR | 27 | 1.35 | 300 | 0 |
| gamma_sat | saturated volumetric weight of the impermeable top layer | NOR | 17.68 | 0.384 | 300 | 0 |
| eta | White constant (sleepkrachtfactor) | LOG | 0.3 | 0.045 | 999999 | 1 |
| d_70 | 70th percentile of the grain distribution (sieve curve) | LOG | 4.30E-04 | 6.45E-05 | 180 | 0 |
| h_hinterDefault | hydraulic head hinterland | NOR | 8.75 | 0.26 | 999999 | 1 |
| K | roughness coefficient by Strickler (inner slope) | LOG | 0.015 | 0.00375 | 300 | 0.5 |
| theta | rolling resistance angle | LOG | 43 | 3 | 600 | 0 |
| me | model uncertainty erosion inner slope | LOG | 1 | 0.5 | 1500 | 0.4 |
| l_piping | piping length | LOG | 81.02 | 6.72466 | 200 | 0 |
| tanalphai | inner slope angle | NOR | 0.329943503 | 0.049491525 | 150 | 0 |
| d_aquifer | aquifer thickness | LOG | 50 | 7.5 | 200 | 0 |
| d_topLayer | impermeable top layer thickness | LOG | 2.1 | 0.6552 | 200 | 0 |
| h_d | dike height | NOR | 14.95 | 0.2 | 300 | 0 |
| cg | grass quality coefficient | DET | 1000000 | - | - | - |

| LocatieID | | | | | | |
|---|---|---|---|---|---|---|
| Dr41L2 | | | | | | |
| x | y | z | WaterstandID | zmin | vaknummer | |
| 177850 | 432650 | 14.06 | Dr41L2_River | 9.6 | 1410006015 | |
| name | description | type | mean | stdev | xle | rho_x |
| k_z | specific permeability | LOG | 5.79E-04 | 4.63E-04 | 600 | 0 |
| mh | model uncertainty head difference for heave | LOG | 0.8 | 0.08 | 999999 | 1 |
| mp | model uncertainty Sellmeijer | LOG | 1 | 0.08 | 999999 | 1 |
| m0 | model uncertainty critical head difference for heave | LOG | 1.2 | 0.12 | 999999 | 1 |
| gamma_g | volumetric weight of the grains | NOR | 27 | 1.35 | 300 | 0 |
| gamma_sat | saturated volumetric weight of the impermeable top layer | NOR | 18.36 | 0.418 | 300 | 0 |
| eta | White constant (sleepkrachtfactor) | LOG | 0.3 | 0.045 | 999999 | 1 |
| d_70 | 70th percentile of the grain distribution (sieve curve) | LOG | 4.30E-04 | 6.45E-05 | 180 | 0 |
| h_hinterDefault | hydraulic head hinterland | NOR | 8.21 | 0.49 | 999999 | 1 |
| K | roughness coefficient by Strickler (inner slope) | LOG | 0.015 | 0.00375 | 300 | 0.5 |
| theta | rolling resistance angle | LOG | 43 | 3 | 600 | 0 |
| me | model uncertainty erosion inner slope | LOG | 1 | 0.5 | 1500 | 0.4 |
| l_piping | piping length | LOG | 80.59 | 7.81723 | 200 | 0 |
| tanalphai | inner slope angle | NOR | 0.249501992 | 0.037425299 | 150 | 0 |
| d_aquifer | aquifer thickness | LOG | 50 | 7.5 | 200 | 0 |
| d_topLayer | impermeable top layer thickness | LOG | 0.69 | 0.4209 | 200 | 0 |
| h_d | dike height | NOR | 14.06 | 0.2 | 300 | 0 |
| cg | grass quality coefficient | DET | 1000000 | - | - | - |

| LocatieID | | | | | | |
|---|---|---|---|---|---|---|
| Dr41L3 | | | | | | |
| x | y | z | WaterstandID | zmin | vaknummer | |
| 170750 | 433850 | 13.2 | Dr41L3_River | 7.96 | 1410006026 | |
| name | description | type | mean | stdev | xle | rho_x |
| k_z | specific permeability | LOG | 5.79E-04 | 4.63E-04 | 600 | 0 |
| mh | model uncertainty head difference for heave | LOG | 0.8 | 0.08 | 999999 | 1 |
| mp | model uncertainty Sellmeijer | LOG | 1 | 0.08 | 999999 | 1 |
| m0 | model uncertainty critical head difference for heave | LOG | 1.2 | 0.12 | 999999 | 1 |
| gamma_g | volumetric weight of the grains | NOR | 27 | 1.35 | 300 | 0 |
| gamma_sat | saturated volumetric weight of the impermeable top layer | NOR | 17.86 | 0.393 | 300 | 0 |
| eta | White constant (sleepkrachtfactor) | LOG | 0.3 | 0.045 | 999999 | 1 |
| d_70 | 70th percentile of the grain distribution (sieve curve) | LOG | 5.11E-04 | 7.66E-05 | 180 | 0 |
| h_hinterDefault | hydraulic head hinterland | NOR | 7.48 | 0.31 | 999999 | 1 |
| K | roughness coefficient by Strickler (inner slope) | LOG | 0.015 | 0.00375 | 300 | 0.5 |
| theta | rolling resistance angle | LOG | 43 | 3 | 600 | 0 |
| me | model uncertainty erosion inner slope | LOG | 1 | 0.5 | 1500 | 0.4 |
| l_piping | piping length | LOG | 77.13 | 5.24484 | 200 | 0 |
| tanalphai | inner slope angle | NOR | 0.415011038 | 0.062251656 | 150 | 0 |
| d_aquifer | aquifer thickness | LOG | 40 | 12 | 200 | 0 |
| d_topLayer | impermeable top layer thickness | LOG | 3.96 | 1.67112 | 200 | 0 |
| h_d | dike height | NOR | 13.2 | 0.2 | 300 | 0 |
| cg | grass quality coefficient | DET | 1000000 | - | - | - |

| LocatieID | | | | | | |
|---|---|---|---|---|---|---|
| Dr41L4 | | | | | | |
| x | y | z | WaterstandID | zmin | vaknummer | |
| 165250 | 433250 | 12.8 | Dr41L4_River | 6.49 | 1410006034 | |
| name | description | type | mean | stdev | xle | rho_x |
| k_z | specific permeability | LOG | 5.79E-04 | 4.63E-04 | 600 | 0 |
| mh | model uncertainty head difference for heave | LOG | 0.8 | 0.08 | 999999 | 1 |
| mp | model uncertainty Sellmeijer | LOG | 1 | 0.08 | 999999 | 1 |
| m0 | model uncertainty critical head difference for heave | LOG | 1.2 | 0.12 | 999999 | 1 |
| gamma_g | volumetric weight of the grains | NOR | 27 | 1.35 | 300 | 0 |
| gamma_sat | saturated volumetric weight of the impermeable top layer | NOR | 16.97 | 0.3485 | 300 | 0 |
| eta | White constant (sleepkrachtfactor) | LOG | 0.3 | 0.045 | 999999 | 1 |
| d_70 | 70th percentile of the grain distribution (sieve curve) | LOG | 5.11E-04 | 7.66E-05 | 180 | 0 |
| h_hinterDefault | hydraulic head hinterland | NOR | 6.13 | 0.21 | 999999 | 1 |
| K | roughness coefficient by Strickler (inner slope) | LOG | 0.015 | 0.00375 | 300 | 0.5 |
| theta | rolling resistance angle | LOG | 43 | 3 | 600 | 0 |
| me | model uncertainty erosion inner slope | LOG | 1 | 0.5 | 1500 | 0.4 |
| l_piping | piping length | LOG | 87.36 | 3.14496 | 200 | 0 |
| tanalphai | inner slope angle | NOR | 0.392771084 | 0.058915663 | 150 | 0 |
| d_aquifer | aquifer thickness | LOG | 40 | 12 | 200 | 0 |
| d_topLayer | impermeable top layer thickness | LOG | 5.07 | 0.55263 | 200 | 0 |
| h_d | dike height | NOR | 12.8 | 0.2 | 300 | 0 |
| cg | grass quality coefficient | DET | 1000000 | - | - | - |

| LocatieID |
|---|
| Dr41L5 |

| x | y | z | WaterstandID | zmin | vaknummer |
|---|---|---|---|---|---|
| 158450 | 430350 | 11.75 | Dr41L5_River | 6.88 | 1410006042 |

| name | description | type | mean | stdev | xle | rho_x |
|---|---|---|---|---|---|---|
| k_z | specific permeability | LOG | 5.79E-04 | 4.63E-04 | 600 | 0 |
| mh | model uncertainty head difference for heave | LOG | 0.8 | 0.08 | 999999 | 1 |
| mp | model uncertainty Sellmeijer | LOG | 1 | 0.08 | 999999 | 1 |
| m0 | model uncertainty critical head difference for heave | LOG | 1.2 | 0.12 | 999999 | 1 |
| gamma_g | volumetric weight of the grains | NOR | 27 | 1.35 | 300 | 0 |
| gamma_sat | saturated volumetric weight of the impermeable top layer | NOR | 17.48 | 0.374 | 300 | 0 |
| eta | White constant (sleepkrachtfactor) | LOG | 0.3 | 0.045 | 999999 | 1 |
| d_70 | 70th percentile of the grain distribution (sieve curve) | LOG | 5.11E-04 | 7.66E-05 | 180 | 0 |
| h_hinterDefault | hydraulic head hinterland | NOR | 5.56 | 0.33 | 999999 | 1 |
| K | roughness coefficient by Strickler (inner slope) | LOG | 0.015 | 0.00375 | 300 | 0.5 |
| theta | rolling resistance angle | LOG | 43 | 3 | 600 | 0 |
| me | model uncertainty erosion inner slope | LOG | 1 | 0.5 | 1500 | 0.4 |
| l_piping | piping length | LOG | 84.54 | 4.81878 | 200 | 0 |
| tanalphai | inner slope angle | NOR | 0.375395431 | 0.056309315 | 150 | 0 |
| d_aquifer | aquifer thickness | LOG | 40 | 12 | 200 | 0 |
| d_topLayer | impermeable top layer thickness | LOG | 3.95 | 1.501 | 200 | 0 |
| h_d | dike height | NOR | 11.75 | 0.2 | 300 | 0 |
| cg | grass quality coefficient | DET | 1000000 | - | - | - |

| LocatieID |
|---|
| Dr41L6 |

| x | y | z | WaterstandID | zmin | vaknummer |
|---|---|---|---|---|---|
| 184150 | 419050 | 12.83 | Dr41L6_River | 9.73 | 1410006048 |

| name | description | type | mean | stdev | xle | rho_x |
|---|---|---|---|---|---|---|
| k_z | specific permeability | LOG | 5.79E-04 | 4.63E-04 | 600 | 0 |
| mh | model uncertainty head difference for heave | LOG | 0.8 | 0.08 | 999999 | 1 |
| mp | model uncertainty Sellmeijer | LOG | 1 | 0.08 | 999999 | 1 |
| m0 | model uncertainty critical head difference for heave | LOG | 1.2 | 0.12 | 999999 | 1 |
| gamma_g | volumetric weight of the grains | NOR | 27 | 1.35 | 300 | 0 |
| gamma_sat | saturated volumetric weight of the impermeable top layer | NOR | 17.33 | 0.3665 | 300 | 0 |
| eta | White constant (sleepkrachtfactor) | LOG | 0.3 | 0.045 | 999999 | 1 |
| d_70 | 70th percentile of the grain distribution (sieve curve) | LOG | 3.71E-04 | 5.57E-05 | 180 | 0 |
| h_hinterDefault | hydraulic head hinterland | NOR | 9.5 | 0.41 | 999999 | 1 |
| K | roughness coefficient by Strickler (inner slope) | LOG | 0.015 | 0.00375 | 300 | 0.5 |
| theta | rolling resistance angle | LOG | 43 | 3 | 600 | 0 |
| me | model uncertainty erosion inner slope | LOG | 1 | 0.5 | 1500 | 0.4 |
| l_piping | piping length | LOG | 83.4 | 17.2638 | 200 | 0 |
| tanalphai | inner slope angle | NOR | 0.32987013 | 0.049480519 | 150 | 0 |
| d_aquifer | aquifer thickness | LOG | 14.6 | 1.2848 | 200 | 0 |
| d_topLayer | impermeable top layer thickness | LOG | 4.27 | 1.92577 | 200 | 0 |
| h_d | dike height | NOR | 12.83 | 0.2 | 300 | 0 |
| cg | grass quality coefficient | DET | 1000000 | - | - | - |

| LocatieID |
|---|
| Dr41L7 |

| x | y | z | WaterstandID | zmin | vaknummer |
|---|---|---|---|---|---|
| 177750 | 421050 | 12.42 | Dr41L7_River | 8.09 | 1410006052 |

| name | description | type | mean | stdev | xle | rho_x |
|---|---|---|---|---|---|---|
| k_z | specific permeability | LOG | 5.79E-04 | 4.63E-04 | 600 | 0 |
| mh | model uncertainty head difference for heave | LOG | 0.8 | 0.08 | 999999 | 1 |
| mp | model uncertainty Sellmeijer | LOG | 1 | 0.08 | 999999 | 1 |
| m0 | model uncertainty critical head difference for heave | LOG | 1.2 | 0.12 | 999999 | 1 |
| gamma_g | volumetric weight of the grains | NOR | 27 | 1.35 | 300 | 0 |
| gamma_sat | saturated volumetric weight of the impermeable top layer | NOR | 18 | 0.4 | 300 | 0 |
| eta | White constant (sleepkrachtfactor) | LOG | 0.3 | 0.045 | 999999 | 1 |
| d_70 | 70th percentile of the grain distribution (sieve curve) | LOG | 3.71E-04 | 5.57E-05 | 180 | 0 |
| h_hinterDefault | hydraulic head hinterland | NOR | 7.5 | 0.52 | 999999 | 1 |
| K | roughness coefficient by Strickler (inner slope) | LOG | 0.015 | 0.00375 | 300 | 0.5 |
| theta | rolling resistance angle | LOG | 43 | 3 | 600 | 0 |
| me | model uncertainty erosion inner slope | LOG | 1 | 0.5 | 1500 | 0.4 |
| l_piping | piping length | LOG | 60.6 | 6.969 | 200 | 0 |
| tanalphai | inner slope angle | NOR | 0.43902439 | 0.065853659 | 150 | 0 |
| d_aquifer | aquifer thickness | LOG | 14.4 | 2.1024 | 200 | 0 |
| d_topLayer | impermeable top layer thickness | LOG | 3 | 1.524 | 200 | 0 |
| h_d | dike height | NOR | 12.42 | 0.2 | 300 | 0 |
| cg | grass quality coefficient | DET | 1000000 | - | - | - |

| LocatieID |
|---|
| Dr41L8 |

| x | y | z | WaterstandID | zmin | vaknummer |
|---|---|---|---|---|---|
| 173050 | 425950 | 10.77 | Dr41L8_River | 6.73 | 1410006058 |

| name | description | type | mean | stdev | xle | rho_x |
|---|---|---|---|---|---|---|
| k_z | specific permeability | LOG | 5.79E-04 | 4.63E-04 | 600 | 0 |
| mh | model uncertainty head difference for heave | LOG | 0.8 | 0.08 | 999999 | 1 |
| mp | model uncertainty Sellmeijer | LOG | 1 | 0.08 | 999999 | 1 |
| m0 | model uncertainty critical head difference for heave | LOG | 1.2 | 0.12 | 999999 | 1 |
| gamma_g | volumetric weight of the grains | NOR | 27 | 1.35 | 300 | 0 |
| gamma_sat | saturated volumetric weight of the impermeable top layer | NOR | 17.2 | 0.36 | 300 | 0 |
| eta | White constant (sleepkrachtfactor) | LOG | 0.3 | 0.045 | 999999 | 1 |
| d_70 | 70th percentile of the grain distribution (sieve curve) | LOG | 3.71E-04 | 5.57E-05 | 180 | 0 |
| h_hinterDefault | hydraulic head hinterland | NOR | 6.5 | 0.45 | 999999 | 1 |
| K | roughness coefficient by Strickler (inner slope) | LOG | 0.015 | 0.00375 | 300 | 0.5 |
| theta | rolling resistance angle | LOG | 43 | 3 | 600 | 0 |
| me | model uncertainty erosion inner slope | LOG | 1 | 0.5 | 1500 | 0.4 |
| l_piping | piping length | LOG | 61.9 | 8.4184 | 200 | 0 |
| tanalphai | inner slope angle | NOR | 0.33 | 0.0495 | 150 | 0 |
| d_aquifer | aquifer thickness | LOG | 19.8 | 5.9598 | 200 | 0 |
| d_topLayer | impermeable top layer thickness | LOG | 3.8 | 0.6688 | 200 | 0 |
| h_d | dike height | NOR | 10.77 | 0.2 | 300 | 0 |
| cg | grass quality coefficient | DET | 1000000 | - | - | - |

| LocatieID |
|---|
| Dr41L9 |

| x | y | z | WaterstandID | zmin | vaknummer |
|---|---|---|---|---|---|
| 165450 | 427450 | 10.09 | Dr41L9_River | 5.41 | 1410006065 |

| name | description | type | mean | stdev | xle | rho_x |
|---|---|---|---|---|---|---|
| k_z | specific permeability | LOG | 5.79E-04 | 4.63E-04 | 600 | 0 |
| mh | model uncertainty head difference for heave | LOG | 0.8 | 0.08 | 999999 | 1 |
| mp | model uncertainty Sellmeijer | LOG | 1 | 0.08 | 999999 | 1 |
| m0 | model uncertainty critical head difference for heave | LOG | 1.2 | 0.12 | 999999 | 1 |
| gamma_g | volumetric weight of the grains | NOR | 27 | 1.35 | 300 | 0 |
| gamma_sat | saturated volumetric weight of the impermeable top layer | NOR | 16.7 | 0.335 | 300 | 0 |
| eta | White constant (sleepkrachtfactor) | LOG | 0.3 | 0.045 | 999999 | 1 |
| d_70 | 70th percentile of the grain distribution (sieve curve) | LOG | 3.71E-04 | 5.57E-05 | 180 | 0 |
| h_hinterDefault | hydraulic head hinterland | NOR | 5.4 | 0.29 | 999999 | 1 |
| K | roughness coefficient by Strickler (inner slope) | LOG | 0.015 | 0.00375 | 300 | 0.5 |
| theta | rolling resistance angle | LOG | 43 | 3 | 600 | 0 |
| me | model uncertainty erosion inner slope | LOG | 1 | 0.5 | 1500 | 0.4 |
| l_piping | piping length | LOG | 60.9 | 4.3239 | 200 | 0 |
| tanalphai | inner slope angle | NOR | 0.053399786 | 0.008009968 | 150 | 0 |
| d_aquifer | aquifer thickness | LOG | 41.5 | 6.225 | 200 | 0 |
| d_topLayer | impermeable top layer thickness | LOG | 3.9 | 0.4485 | 200 | 0 |
| h_d | dike height | NOR | 10.09 | 0.2 | 300 | 0 |
| cg | grass quality coefficient | DET | 1000000 | - | - | - |

| LocatieID |
|---|
| Dr41L10 |

| x | y | z | WaterstandID | zmin | vaknummer |
|---|---|---|---|---|---|
| 160850 | 425450 | 8.73 | Dr41L10_River | 6.33 | 1410006072 |

| name | description | type | mean | stdev | xle | rho_x |
|---|---|---|---|---|---|---|
| k_z | specific permeability | LOG | 5.79E-04 | 4.63E-04 | 600 | 0 |
| mh | model uncertainty head difference for heave | LOG | 0.8 | 0.08 | 999999 | 1 |
| mp | model uncertainty Sellmeijer | LOG | 1 | 0.08 | 999999 | 1 |
| m0 | model uncertainty critical head difference for heave | LOG | 1.2 | 0.12 | 999999 | 1 |
| gamma_g | volumetric weight of the grains | NOR | 27 | 1.35 | 300 | 0 |
| gamma_sat | saturated volumetric weight of the impermeable top layer | NOR | 16.6 | 0.33 | 300 | 0 |
| eta | White constant (sleepkrachtfactor) | LOG | 0.3 | 0.045 | 999999 | 1 |
| d_70 | 70th percentile of the grain distribution (sieve curve) | LOG | 3.71E-04 | 5.57E-05 | 180 | 0 |
| h_hinterDefault | hydraulic head hinterland | NOR | 5.1 | 0.62 | 999999 | 1 |
| K | roughness coefficient by Strickler (inner slope) | LOG | 0.015 | 0.00375 | 300 | 0.5 |
| theta | rolling resistance angle | LOG | 43 | 3 | 600 | 0 |
| me | model uncertainty erosion inner slope | LOG | 1 | 0.5 | 1500 | 0.4 |
| l_piping | piping length | LOG | 52.2 | 15.4512 | 200 | 0 |
| tanalphai | inner slope angle | NOR | 0.39488117 | 0.059232176 | 150 | 0 |
| d_aquifer | aquifer thickness | LOG | 21.8 | 0.3924 | 200 | 0 |
| d_topLayer | impermeable top layer thickness | LOG | 4.3 | 1.1352 | 200 | 0 |
| h_d | dike height | NOR | 8.73 | 0.2 | 300 | 0 |
| cg | grass quality coefficient | DET | 1000000 | - | - | - |

| LocatieID |
|---|
| Dr41L11 |

| x | y | z | WaterstandID | zmin | vaknummer |
|---|---|---|---|---|---|
| 158050 | 425850 | 8.91 | Dr41L11_River | 4.28 | 1410006075 |

| name | description | type | mean | stdev | xle | rho_x |
|---|---|---|---|---|---|---|
| k_z | specific permeability | LOG | 5.79E-04 | 4.63E-04 | 600 | 0 |
| mh | model uncertainty head difference for heave | LOG | 0.8 | 0.08 | 999999 | 1 |
| mp | model uncertainty Sellmeijer | LOG | 1 | 0.08 | 999999 | 1 |
| m0 | model uncertainty critical head difference for heave | LOG | 1.2 | 0.12 | 999999 | 1 |
| gamma_g | volumetric weight of the grains | NOR | 27 | 1.35 | 300 | 0 |
| gamma_sat | saturated volumetric weight of the impermeable top layer | NOR | 16.8 | 0.34 | 300 | 0 |
| eta | White constant (sleepkrachtfactor) | LOG | 0.3 | 0.045 | 999999 | 1 |
| d_70 | 70th percentile of the grain distribution (sieve curve) | LOG | 3.71E-04 | 5.57E-05 | 180 | 0 |
| h_hinterDefault | hydraulic head hinterland | NOR | 4.1 | 0.62 | 999999 | 1 |
| K | roughness coefficient by Strickler (inner slope) | LOG | 0.015 | 0.00375 | 300 | 0.5 |
| theta | rolling resistance angle | LOG | 43 | 3 | 600 | 0 |
| me | model uncertainty erosion inner slope | LOG | 1 | 0.5 | 1500 | 0.4 |
| l_piping | piping length | LOG | 58.6 | 12.306 | 200 | 0 |
| tanalphai | inner slope angle | NOR | 0.395069953 | 0.059260493 | 150 | 0 |
| d_aquifer | aquifer thickness | LOG | 23.7 | 0.4503 | 200 | 0 |
| d_topLayer | impermeable top layer thickness | LOG | 3.6 | 1.656 | 200 | 0 |
| h_d | dike height | NOR | 8.91 | 0.2 | 300 | 0 |
| cg | grass quality coefficient | DET | 1000000 | - | - | - |

| LocatieID |
|---|
| Dr41L12 |

| x | y | z | WaterstandID | zmin | vaknummer |
|---|---|---|---|---|---|
| 186150 | 429650 | 15.27 | Dr41L12_River | 11.55 | 1410006046 |

| name | description | type | mean | stdev | xle | rho_x |
|---|---|---|---|---|---|---|
| k_z | specific permeability | LOG | 5.79E-04 | 4.63E-04 | 600 | 0 |
| mh | model uncertainty head difference for heave | LOG | 0.8 | 0.08 | 999999 | 1 |
| mp | model uncertainty Sellmeijer | LOG | 1 | 0.08 | 999999 | 1 |
| m0 | model uncertainty critical head difference for heave | LOG | 1.2 | 0.12 | 999999 | 1 |
| gamma_g | volumetric weight of the grains | NOR | 27 | 1.35 | 300 | 0 |
| gamma_sat | saturated volumetric weight of the impermeable top layer | NOR | 17.83 | 0.3915 | 300 | 0 |
| eta | White constant (sleepkrachtfactor) | LOG | 0.3 | 0.045 | 999999 | 1 |
| d_70 | 70th percentile of the grain distribution (sieve curve) | LOG | 3.71E-04 | 5.57E-05 | 180 | 0 |
| h_hinterDefault | hydraulic head hinterland | NOR | 10 | 1.03 | 999999 | 1 |
| K | roughness coefficient by Strickler (inner slope) | LOG | 0.015 | 0.00375 | 300 | 0.5 |
| theta | rolling resistance angle | LOG | 43 | 3 | 600 | 0 |
| me | model uncertainty erosion inner slope | LOG | 1 | 0.5 | 1500 | 0.4 |
| l_piping | piping length | LOG | 62.2 | 14.3682 | 200 | 0 |
| tanalphai | inner slope angle | NOR | 0.5 | 0.075 | 150 | 0 |
| d_aquifer | aquifer thickness | LOG | 12.3 | 0.8241 | 200 | 0 |
| d_topLayer | impermeable top layer thickness | LOG | 1.87 | 0.92004 | 200 | 0 |
| h_d | dike height | NOR | 15.27 | 0.2 | 300 | 0 |
| cg | grass quality coefficient | DET | 1000000 | - | - | - |

| LocatieID |
|---|
| Dr41L13 |

| x | y | z | WaterstandID | zmin | vaknummer |
|---|---|---|---|---|---|
| 184650 | 430250 | 15.27 | Dr41L13_River | 10.1 | 1410006010 |

| name | description | type | mean | stdev | xle | rho_x |
|---|---|---|---|---|---|---|
| k_z | specific permeability | LOG | 5.79E-04 | 4.63E-04 | 600 | 0 |
| mh | model uncertainty head difference for heave | LOG | 0.8 | 0.08 | 999999 | 1 |
| mp | model uncertainty Sellmeijer | LOG | 1 | 0.08 | 999999 | 1 |
| m0 | model uncertainty critical head difference for heave | LOG | 1.2 | 0.12 | 999999 | 1 |
| gamma_g | volumetric weight of the grains | NOR | 27 | 1.35 | 300 | 0 |
| gamma_sat | saturated volumetric weight of the impermeable top layer | NOR | 18.08 | 0.404 | 300 | 0 |
| eta | White constant (sleepkrachtfactor) | LOG | 0.3 | 0.045 | 999999 | 1 |
| d_70 | 70th percentile of the grain distribution (sieve curve) | LOG | 4.30E-04 | 6.45E-05 | 180 | 0 |
| h_hinterDefault | hydraulic head hinterland | NOR | 9.33 | 0.39 | 999999 | 1 |
| K | roughness coefficient by Strickler (inner slope) | LOG | 0.015 | 0.00375 | 300 | 0.5 |
| theta | rolling resistance angle | LOG | 43 | 3 | 600 | 0 |
| me | model uncertainty erosion inner slope | LOG | 1 | 0.5 | 1500 | 0.4 |
| l_piping | piping length | LOG | 80.19 | 5.05197 | 200 | 0 |
| tanalphai | inner slope angle | NOR | 0.330082136 | 0.04951232 | 150 | 0 |
| d_aquifer | aquifer thickness | LOG | 50 | 7.5 | 200 | 0 |
| d_topLayer | impermeable top layer thickness | LOG | 1.58 | 0.6794 | 200 | 0 |
| h_d | dike height | NOR | 15.27 | 0.2 | 300 | 0 |
| cg | grass quality coefficient | DET | 1000000 | - | - | - |

| LocatieID |
|---|
| Dr41L14 |

| x | y | z | WaterstandID | zmin | vaknummer |
|---|---|---|---|---|---|
| 181550 | 431950 | 14.33 | Dr41L14_River | 10.83 | 1410006011 |

| name | description | type | mean | stdev | xle | rho_x |
|---|---|---|---|---|---|---|
| k_z | specific permeability | LOG | 5.79E-04 | 4.63E-04 | 600 | 0 |
| mh | model uncertainty head difference for heave | LOG | 0.8 | 0.08 | 999999 | 1 |
| mp | model uncertainty Sellmeijer | LOG | 1 | 0.08 | 999999 | 1 |
| m0 | model uncertainty critical head difference for heave | LOG | 1.2 | 0.12 | 999999 | 1 |
| gamma_g | volumetric weight of the grains | NOR | 27 | 1.35 | 300 | 0 |
| gamma_sat | saturated volumetric weight of the impermeable top layer | NOR | 17.68 | 0.384 | 300 | 0 |
| eta | White constant (sleepkrachtfactor) | LOG | 0.3 | 0.045 | 999999 | 1 |
| d_70 | 70th percentile of the grain distribution (sieve curve) | LOG | 4.30E-04 | 6.45E-05 | 180 | 0 |
| h_hinterDefault | hydraulic head hinterland | NOR | 8.75 | 0.26 | 999999 | 1 |
| K | roughness coefficient by Strickler (inner slope) | LOG | 0.015 | 0.00375 | 300 | 0.5 |
| theta | rolling resistance angle | LOG | 43 | 3 | 600 | 0 |
| me | model uncertainty erosion inner slope | LOG | 1 | 0.5 | 1500 | 0.4 |
| l_piping | piping length | LOG | 81.02 | 6.72466 | 200 | 0 |
| tanalphai | inner slope angle | NOR | 0.329943503 | 0.049491525 | 150 | 0 |
| d_aquifer | aquifer thickness | LOG | 50 | 7.5 | 200 | 0 |
| d_topLayer | impermeable top layer thickness | LOG | 2.1 | 0.6552 | 200 | 0 |
| h_d | dike height | NOR | 14.33 | 0.2 | 300 | 0 |
| cg | grass quality coefficient | DET | 1000000 | - | - | - |

| LocatieID | | | | | | |
|---|---|---|---|---|---|---|
| Dr41L15 | | | | | | |
| x | y | z | WaterstandID | zmin | vaknummer | |
| 179650 | 432150 | 14.21 | Dr41L15_River | 10.16 | 1410006013 | |
| name | description | type | mean | stdev | xle | rho_x |
| k_z | specific permeability | LOG | 5.79E-04 | 4.63E-04 | 600 | 0 |
| mh | model uncertainty head difference for heave | LOG | 0.8 | 0.08 | 999999 | 1 |
| mp | model uncertainty Sellmeijer | LOG | 1 | 0.08 | 999999 | 1 |
| m0 | model uncertainty critical head difference for heave | LOG | 1.2 | 0.12 | 999999 | 1 |
| gamma_g | volumetric weight of the grains | NOR | 27 | 1.35 | 300 | 0 |
| gamma_sat | saturated volumetric weight of the impermeable top layer | NOR | 18.7 | 0.435 | 300 | 0 |
| eta | White constant (sleepkrachtfactor) | LOG | 0.3 | 0.045 | 999999 | 1 |
| d_70 | 70th percentile of the grain distribution (sieve curve) | LOG | 4.30E-04 | 6.45E-05 | 180 | 0 |
| h_hinterDefault | hydraulic head hinterland | NOR | 8.25 | 0.21 | 999999 | 1 |
| K | roughness coefficient by Strickler (inner slope) | LOG | 0.015 | 0.00375 | 300 | 0.5 |
| theta | rolling resistance angle | LOG | 43 | 3 | 600 | 0 |
| me | model uncertainty erosion inner slope | LOG | 1 | 0.5 | 1500 | 0.4 |
| l_piping | piping length | LOG | 86 | 4.3 | 200 | 0 |
| tanalphai | inner slope angle | NOR | 0.249501992 | 0.037425299 | 150 | 0 |
| d_aquifer | aquifer thickness | LOG | 50 | 7.5 | 200 | 0 |
| d_topLayer | impermeable top layer thickness | LOG | 0.61 | 0.17446 | 200 | 0 |
| h_d | dike height | NOR | 14.21 | 0.2 | 300 | 0 |
| cg | grass quality coefficient | DET | 1000000 | - | - | - |

| LocatieID | | | | | | |
|---|---|---|---|---|---|---|
| Dr41L16 | | | | | | |
| x | y | z | WaterstandID | zmin | vaknummer | |
| 176250 | 433250 | 13.82 | Dr41L16_River | 9.71 | 1410006016 | |
| name | description | type | mean | stdev | xle | rho_x |
| k_z | specific permeability | LOG | 5.79E-04 | 4.63E-04 | 600 | 0 |
| mh | model uncertainty head difference for heave | LOG | 0.8 | 0.08 | 999999 | 1 |
| mp | model uncertainty Sellmeijer | LOG | 1 | 0.08 | 999999 | 1 |
| m0 | model uncertainty critical head difference for heave | LOG | 1.2 | 0.12 | 999999 | 1 |
| gamma_g | volumetric weight of the grains | NOR | 27 | 1.35 | 300 | 0 |
| gamma_sat | saturated volumetric weight of the impermeable top layer | NOR | 17.18 | 0.359 | 300 | 0 |
| eta | White constant (sleepkrachtfactor) | LOG | 0.3 | 0.045 | 999999 | 1 |
| d_70 | 70th percentile of the grain distribution (sieve curve) | LOG | 4.30E-04 | 6.45E-05 | 180 | 0 |
| h_hinterDefault | hydraulic head hinterland | NOR | 7.53 | 0.37 | 999999 | 1 |
| K | roughness coefficient by Strickler (inner slope) | LOG | 0.015 | 0.00375 | 300 | 0.5 |
| theta | rolling resistance angle | LOG | 43 | 3 | 600 | 0 |
| me | model uncertainty erosion inner slope | LOG | 1 | 0.5 | 1500 | 0.4 |
| l_piping | piping length | LOG | 88.1 | 4.6693 | 200 | 0 |
| tanalphai | inner slope angle | NOR | 0.329943503 | 0.049491525 | 150 | 0 |
| d_aquifer | aquifer thickness | LOG | 50 | 7.5 | 200 | 0 |
| d_topLayer | impermeable top layer thickness | LOG | 2.79 | 0.66123 | 200 | 0 |
| h_d | dike height | NOR | 13.82 | 0.2 | 300 | 0 |
| cg | grass quality coefficient | DET | 1000000 | - | - | - |

| LocatieID | | | | | | |
|---|---|---|---|---|---|---|
| Dr41L17 | | | | | | |
| x | y | z | WaterstandID | zmin | vaknummer | |
| 174550 | 433750 | 13.69 | Dr41L17_River | 10.95 | 1410006017 | |
| name | description | type | mean | stdev | xle | rho_x |
| k_z | specific permeability | LOG | 5.79E-04 | 4.63E-04 | 600 | 0 |
| mh | model uncertainty head difference for heave | LOG | 0.8 | 0.08 | 999999 | 1 |
| mp | model uncertainty Sellmeijer | LOG | 1 | 0.08 | 999999 | 1 |
| m0 | model uncertainty critical head difference for heave | LOG | 1.2 | 0.12 | 999999 | 1 |
| gamma_g | volumetric weight of the grains | NOR | 27 | 1.35 | 300 | 0 |
| gamma_sat | saturated volumetric weight of the impermeable top layer | NOR | 17.55 | 0.3775 | 300 | 0 |
| eta | White constant (sleepkrachtfactor) | LOG | 0.3 | 0.045 | 999999 | 1 |
| d_70 | 70th percentile of the grain distribution (sieve curve) | LOG | 4.30E-04 | 6.45E-05 | 180 | 0 |
| h_hinterDefault | hydraulic head hinterland | NOR | 7.79 | 0.22 | 999999 | 1 |
| K | roughness coefficient by Strickler (inner slope) | LOG | 0.015 | 0.00375 | 300 | 0.5 |
| theta | rolling resistance angle | LOG | 43 | 3 | 600 | 0 |
| me | model uncertainty erosion inner slope | LOG | 1 | 0.5 | 1500 | 0.4 |
| l_piping | piping length | LOG | 133.24 | 12.79104 | 200 | 0 |
| tanalphai | inner slope angle | NOR | 0.330005255 | 0.049500788 | 150 | 0 |
| d_aquifer | aquifer thickness | LOG | 60 | 9 | 200 | 0 |
| d_topLayer | impermeable top layer thickness | LOG | 3.95 | 0.52535 | 200 | 0 |
| h_d | dike height | NOR | 13.69 | 0.2 | 300 | 0 |
| cg | grass quality coefficient | DET | 1000000 | - | - | - |

| LocatieID | | | | | | |
|---|---|---|---|---|---|---|
| Dr41L18 | | | | | | |
| x | y | z | WaterstandID | zmin | vaknummer | |
| 172750 | 433450 | 13.55 | Dr41L18_River | 9.06 | 1410006023 | |
| name | description | type | mean | stdev | xle | rho_x |
| k_z | specific permeability | LOG | 5.79E-04 | 4.63E-04 | 600 | 0 |
| mh | model uncertainty head difference for heave | LOG | 0.8 | 0.08 | 999999 | 1 |
| mp | model uncertainty Sellmeijer | LOG | 1 | 0.08 | 999999 | 1 |
| m0 | model uncertainty critical head difference for heave | LOG | 1.2 | 0.12 | 999999 | 1 |
| gamma_g | volumetric weight of the grains | NOR | 27 | 1.35 | 300 | 0 |
| gamma_sat | saturated volumetric weight of the impermeable top layer | NOR | 18.15 | 0.4075 | 300 | 0 |
| eta | White constant (sleepkrachtfactor) | LOG | 0.3 | 0.045 | 999999 | 1 |
| d_70 | 70th percentile of the grain distribution (sieve curve) | LOG | 5.11E-04 | 7.66E-05 | 180 | 0 |
| h_hinterDefault | hydraulic head hinterland | NOR | 7 | 0.25 | 999999 | 1 |
| K | roughness coefficient by Strickler (inner slope) | LOG | 0.015 | 0.00375 | 300 | 0.5 |
| theta | rolling resistance angle | LOG | 43 | 3 | 600 | 0 |
| me | model uncertainty erosion inner slope | LOG | 1 | 0.5 | 1500 | 0.4 |
| l_piping | piping length | LOG | 151.82 | 1.06274 | 200 | 0 |
| tanalphai | inner slope angle | NOR | 0.330061983 | 0.049509298 | 150 | 0 |
| d_aquifer | aquifer thickness | LOG | 50 | 7.5 | 200 | 0 |
| d_topLayer | impermeable top layer thickness | LOG | 2.43 | 1.35108 | 200 | 0 |
| h_d | dike height | NOR | 13.55 | 0.2 | 300 | 0 |
| cg | grass quality coefficient | DET | 1000000 | - | - | - |

| LocatieID |
|---|
| Dr41L19 |

| x | y | z | WaterstandID | zmin | vaknummer | |
|---|---|---|---|---|---|---|
| 169250 | 433950 | 13.16 | Dr41L19_River | 9.89 | 1410006028 | |
| name | description | type | mean | stdev | xle | rho_x |
| k_z | specific permeability | LOG | 5.79E-04 | 4.63E-04 | 600 | 0 |
| mh | model uncertainty head difference for heave | LOG | 0.8 | 0.08 | 999999 | 1 |
| mp | model uncertainty Sellmeijer | LOG | 1 | 0.08 | 999999 | 1 |
| m0 | model uncertainty critical head difference for heave | LOG | 1.2 | 0.12 | 999999 | 1 |
| gamma_g | volumetric weight of the grains | NOR | 27 | 1.35 | 300 | 0 |
| gamma_sat | saturated volumetric weight of the impermeable top layer | NOR | 18.8 | 0.44 | 300 | 0 |
| eta | White constant (sleepkrachtfactor) | LOG | 0.3 | 0.045 | 999999 | 1 |
| d_70 | 70th percentile of the grain distribution (sieve curve) | LOG | 5.11E-04 | 7.66E-05 | 180 | 0 |
| h_hinterDefault | hydraulic head hinterland | NOR | 7.21 | 0.55 | 999999 | 1 |
| K | roughness coefficient by Strickler (inner slope) | LOG | 0.015 | 0.00375 | 300 | 0.5 |
| theta | rolling resistance angle | LOG | 43 | 3 | 600 | 0 |
| me | model uncertainty erosion inner slope | LOG | 1 | 0.5 | 1500 | 0.4 |
| l_piping | piping length | LOG | 77.16 | 3.70368 | 200 | 0 |
| tanalphai | inner slope angle | NOR | 0.375 | 0.05625 | 150 | 0 |
| d_aquifer | aquifer thickness | LOG | 40 | 12 | 200 | 0 |
| d_topLayer | impermeable top layer thickness | LOG | 1.41 | 0.79101 | 200 | 0 |
| h_d | dike height | NOR | 13.16 | 0.2 | 300 | 0 |
| cg | grass quality coefficient | DET | 1000000 | - | - | - |

| LocatieID |
|---|
| Dr41L20 |

| x | y | z | WaterstandID | zmin | vaknummer | |
|---|---|---|---|---|---|---|
| 167450 | 433550 | 12.94 | Dr41L20_River | 8.32 | 1410006030 | |
| name | description | type | mean | stdev | xle | rho_x |
| k_z | specific permeability | LOG | 5.79E-04 | 4.63E-04 | 600 | 0 |
| mh | model uncertainty head difference for heave | LOG | 0.8 | 0.08 | 999999 | 1 |
| mp | model uncertainty Sellmeijer | LOG | 1 | 0.08 | 999999 | 1 |
| m0 | model uncertainty critical head difference for heave | LOG | 1.2 | 0.12 | 999999 | 1 |
| gamma_g | volumetric weight of the grains | NOR | 27 | 1.35 | 300 | 0 |
| gamma_sat | saturated volumetric weight of the impermeable top layer | NOR | 18.58 | 0.429 | 300 | 0 |
| eta | White constant (sleepkrachtfactor) | LOG | 0.3 | 0.045 | 999999 | 1 |
| d_70 | 70th percentile of the grain distribution (sieve curve) | LOG | 5.11E-04 | 7.66E-05 | 180 | 0 |
| h_hinterDefault | hydraulic head hinterland | NOR | 6.38 | 0.4 | 999999 | 1 |
| K | roughness coefficient by Strickler (inner slope) | LOG | 0.015 | 0.00375 | 300 | 0.5 |
| theta | rolling resistance angle | LOG | 43 | 3 | 600 | 0 |
| me | model uncertainty erosion inner slope | LOG | 1 | 0.5 | 1500 | 0.4 |
| l_piping | piping length | LOG | 87.5 | 5.1625 | 200 | 0 |
| tanalphai | inner slope angle | NOR | 0.392898719 | 0.058934808 | 150 | 0 |
| d_aquifer | aquifer thickness | LOG | 40 | 12 | 200 | 0 |
| d_topLayer | impermeable top layer thickness | LOG | 3.53 | 1.60968 | 200 | 0 |
| h_d | dike height | NOR | 12.94 | 0.2 | 300 | 0 |
| cg | grass quality coefficient | DET | 1000000 | - | - | - |

| LocatieID | | | | | | |
|---|---|---|---|---|---|---|
| Dr41L21 | | | | | | |
| x | y | z | WaterstandID | zmin | vaknummer | |
| 163350 | 433150 | 12.58 | Dr41L21_River | 6.87 | 1410006037 | |
| name | description | type | mean | stdev | xle | rho_x |
| k_z | specific permeability | LOG | 5.79E-04 | 4.63E-04 | 600 | 0 |
| mh | model uncertainty head difference for heave | LOG | 0.8 | 0.08 | 999999 | 1 |
| mp | model uncertainty Sellmeijer | LOG | 1 | 0.08 | 999999 | 1 |
| m0 | model uncertainty critical head difference for heave | LOG | 1.2 | 0.12 | 999999 | 1 |
| gamma_g | volumetric weight of the grains | NOR | 27 | 1.35 | 300 | 0 |
| gamma_sat | saturated volumetric weight of the impermeable top layer | NOR | 18.22 | 0.411 | 300 | 0 |
| eta | White constant (sleepkrachtfactor) | LOG | 0.3 | 0.045 | 999999 | 1 |
| d_70 | 70th percentile of the grain distribution (sieve curve) | LOG | 5.11E-04 | 7.66E-05 | 180 | 0 |
| h_hinterDefault | hydraulic head hinterland | NOR | 6.4 | 0.38 | 999999 | 1 |
| K | roughness coefficient by Strickler (inner slope) | LOG | 0.015 | 0.00375 | 300 | 0.5 |
| theta | rolling resistance angle | LOG | 43 | 3 | 600 | 0 |
| me | model uncertainty erosion inner slope | LOG | 1 | 0.5 | 1500 | 0.4 |
| l_piping | piping length | LOG | 81.51 | 5.62419 | 200 | 0 |
| tanalphai | inner slope angle | NOR | 0.358939186 | 0.053840878 | 150 | 0 |
| d_aquifer | aquifer thickness | LOG | 40 | 12 | 200 | 0 |
| d_topLayer | impermeable top layer thickness | LOG | 1.56 | 0.90168 | 200 | 0 |
| h_d | dike height | NOR | 12.58 | 0.2 | 300 | 0 |
| cg | grass quality coefficient | DET | 1000000 | - | - | - |

| LocatieID | | | | | | |
|---|---|---|---|---|---|---|
| Dr41L22 | | | | | | |
| x | y | z | WaterstandID | zmin | vaknummer | |
| 161050 | 432650 | 12.49 | Dr41L22_River | 8.06 | 1410006039 | |
| name | description | type | mean | stdev | xle | rho_x |
| k_z | specific permeability | LOG | 5.79E-04 | 4.63E-04 | 600 | 0 |
| mh | model uncertainty head difference for heave | LOG | 0.8 | 0.08 | 999999 | 1 |
| mp | model uncertainty Sellmeijer | LOG | 1 | 0.08 | 999999 | 1 |
| m0 | model uncertainty critical head difference for heave | LOG | 1.2 | 0.12 | 999999 | 1 |
| gamma_g | volumetric weight of the grains | NOR | 27 | 1.35 | 300 | 0 |
| gamma_sat | saturated volumetric weight of the impermeable top layer | NOR | 18.73 | 0.4365 | 300 | 0 |
| eta | White constant (sleepkrachtfactor) | LOG | 0.3 | 0.045 | 999999 | 1 |
| d_70 | 70th percentile of the grain distribution (sieve curve) | LOG | 5.11E-04 | 7.66E-05 | 180 | 0 |
| h_hinterDefault | hydraulic head hinterland | NOR | 6.23 | 0.19 | 999999 | 1 |
| K | roughness coefficient by Strickler (inner slope) | LOG | 0.015 | 0.00375 | 300 | 0.5 |
| theta | rolling resistance angle | LOG | 43 | 3 | 600 | 0 |
| me | model uncertainty erosion inner slope | LOG | 1 | 0.5 | 1500 | 0.4 |
| l_piping | piping length | LOG | 81.22 | 3.33002 | 200 | 0 |
| tanalphai | inner slope angle | NOR | 0.392878696 | 0.058931804 | 150 | 0 |
| d_aquifer | aquifer thickness | LOG | 40 | 12 | 200 | 0 |
| d_topLayer | impermeable top layer thickness | LOG | 1.68 | 1.7136 | 200 | 0 |
| h_d | dike height | NOR | 12.49 | 0.2 | 300 | 0 |
| cg | grass quality coefficient | DET | 1000000 | - | - | - |

| LocatieID | | | | | | |
|---|---|---|---|---|---|---|
| Dr41L23 | | | | | | |
| x | y | z | WaterstandID | zmin | vaknummer | |
| 159550 | 432150 | 12.24 | Dr41L23_River | 6.91 | 1410006040 | |
| name | description | type | mean | stdev | xle | rho_x |
| k_z | specific permeability | LOG | 5.79E-04 | 4.63E-04 | 600 | 0 |
| mh | model uncertainty head difference for heave | LOG | 0.8 | 0.08 | 999999 | 1 |
| mp | model uncertainty Sellmeijer | LOG | 1 | 0.08 | 999999 | 1 |
| m0 | model uncertainty critical head difference for heave | LOG | 1.2 | 0.12 | 999999 | 1 |
| gamma_g | volumetric weight of the grains | NOR | 27 | 1.35 | 300 | 0 |
| gamma_sat | saturated volumetric weight of the impermeable top layer | NOR | 18.44 | 0.422 | 300 | 0 |
| eta | White constant (sleepkrachtfactor) | LOG | 0.3 | 0.045 | 999999 | 1 |
| d_70 | 70th percentile of the grain distribution (sieve curve) | LOG | 5.11E-04 | 7.66E-05 | 180 | 0 |
| h_hinterDefault | hydraulic head hinterland | NOR | 6.82 | 0.81 | 999999 | 1 |
| K | roughness coefficient by Strickler (inner slope) | LOG | 0.015 | 0.00375 | 300 | 0.5 |
| theta | rolling resistance angle | LOG | 43 | 3 | 600 | 0 |
| me | model uncertainty erosion inner slope | LOG | 1 | 0.5 | 1500 | 0.4 |
| l_piping | piping length | LOG | 69.79 | 11.58514 | 200 | 0 |
| tanalphai | inner slope angle | NOR | 0.392775229 | 0.058916284 | 150 | 0 |
| d_aquifer | aquifer thickness | LOG | 40 | 12 | 200 | 0 |
| d_topLayer | impermeable top layer thickness | LOG | 3.97 | 1.38156 | 200 | 0 |
| h_d | dike height | NOR | 12.24 | 0.2 | 300 | 0 |
| cg | grass quality coefficient | DET | 1000000 | - | - | - |

| LocatieID | | | | | | |
|---|---|---|---|---|---|---|
| Dr41L24 | | | | | | |
| x | y | z | WaterstandID | zmin | vaknummer | |
| 157150 | 428250 | 11.54 | Dr41L24_River | 5.6 | 1410006044 | |
| name | description | type | mean | stdev | xle | rho_x |
| k_z | specific permeability | LOG | 5.79E-04 | 4.63E-04 | 600 | 0 |
| mh | model uncertainty head difference for heave | LOG | 0.8 | 0.08 | 999999 | 1 |
| mp | model uncertainty Sellmeijer | LOG | 1 | 0.08 | 999999 | 1 |
| m0 | model uncertainty critical head difference for heave | LOG | 1.2 | 0.12 | 999999 | 1 |
| gamma_g | volumetric weight of the grains | NOR | 27 | 1.35 | 300 | 0 |
| gamma_sat | saturated volumetric weight of the impermeable top layer | NOR | 17.53 | 0.3765 | 300 | 0 |
| eta | White constant (sleepkrachtfactor) | LOG | 0.3 | 0.045 | 999999 | 1 |
| d_70 | 70th percentile of the grain distribution (sieve curve) | LOG | 5.11E-04 | 7.66E-05 | 180 | 0 |
| h_hinterDefault | hydraulic head hinterland | NOR | 5.52 | 0.34 | 999999 | 1 |
| K | roughness coefficient by Strickler (inner slope) | LOG | 0.015 | 0.00375 | 300 | 0.5 |
| theta | rolling resistance angle | LOG | 43 | 3 | 600 | 0 |
| me | model uncertainty erosion inner slope | LOG | 1 | 0.5 | 1500 | 0.4 |
| l_piping | piping length | LOG | 77.94 | 5.0661 | 200 | 0 |
| tanalphai | inner slope angle | NOR | 0.259991926 | 0.038998789 | 150 | 0 |
| d_aquifer | aquifer thickness | LOG | 40 | 12 | 200 | 0 |
| d_topLayer | impermeable top layer thickness | LOG | 6.01 | 1.0818 | 200 | 0 |
| h_d | dike height | NOR | 11.54 | 0.2 | 300 | 0 |
| cg | grass quality coefficient | DET | 500000 | - | - | - |

| LocatieID | | | | | | |
|---|---|---|---|---|---|---|
| Dr41L25 | | | | | | |
| x | y | z | WaterstandID | zmin | vaknummer | |
| 187950 | 419250 | 13.36 | Dr41L25_River | 10.14 | 1410006045 | |
| name | description | type | mean | stdev | xle | rho_x |
| k_z | specific permeability | LOG | 5.79E-04 | 4.63E-04 | 600 | 0 |
| mh | model uncertainty head difference for heave | LOG | 0.8 | 0.08 | 999999 | 1 |
| mp | model uncertainty Sellmeijer | LOG | 1 | 0.08 | 999999 | 1 |
| m0 | model uncertainty critical head difference for heave | LOG | 1.2 | 0.12 | 999999 | 1 |
| gamma_g | volumetric weight of the grains | NOR | 27 | 1.35 | 300 | 0 |
| gamma_sat | saturated volumetric weight of the impermeable top layer | NOR | 18 | 0.4 | 300 | 0 |
| eta | White constant (sleepkrachtfactor) | LOG | 0.3 | 0.045 | 999999 | 1 |
| d_70 | 70th percentile of the grain distribution (sieve curve) | LOG | 3.71E-04 | 5.57E-05 | 180 | 0 |
| h_hinterDefault | hydraulic head hinterland | NOR | 9.9 | 0.56 | 999999 | 1 |
| K | roughness coefficient by Strickler (inner slope) | LOG | 0.015 | 0.00375 | 300 | 0.5 |
| theta | rolling resistance angle | LOG | 43 | 3 | 600 | 0 |
| me | model uncertainty erosion inner slope | LOG | 1 | 0.5 | 1500 | 0.4 |
| l_piping | piping length | LOG | 58.6 | 11.72 | 200 | 0 |
| tanalphai | inner slope angle | NOR | 0.330012453 | 0.049501868 | 150 | 0 |
| d_aquifer | aquifer thickness | LOG | 13.9 | 1.5846 | 200 | 0 |
| d_topLayer | impermeable top layer thickness | LOG | 2.07 | 1.45935 | 200 | 0 |
| h_d | dike height | NOR | 13.36 | 0.2 | 300 | 0 |
| cg | grass quality coefficient | DET | 1000000 | - | - | - |

| LocatieID | | | | | | |
|---|---|---|---|---|---|---|
| Dr41L26 | | | | | | |
| x | y | z | WaterstandID | zmin | vaknummer | |
| 185950 | 419550 | 12.85 | Dr41L26_River | 9.64 | 1410006046 | |
| name | description | type | mean | stdev | xle | rho_x |
| k_z | specific permeability | LOG | 5.79E-04 | 4.63E-04 | 600 | 0 |
| mh | model uncertainty head difference for heave | LOG | 0.8 | 0.08 | 999999 | 1 |
| mp | model uncertainty Sellmeijer | LOG | 1 | 0.08 | 999999 | 1 |
| m0 | model uncertainty critical head difference for heave | LOG | 1.2 | 0.12 | 999999 | 1 |
| gamma_g | volumetric weight of the grains | NOR | 27 | 1.35 | 300 | 0 |
| gamma_sat | saturated volumetric weight of the impermeable top layer | NOR | 17.83 | 0.3915 | 300 | 0 |
| eta | White constant (sleepkrachtfactor) | LOG | 0.3 | 0.045 | 999999 | 1 |
| d_70 | 70th percentile of the grain distribution (sieve curve) | LOG | 3.71E-04 | 5.57E-05 | 180 | 0 |
| h_hinterDefault | hydraulic head hinterland | NOR | 10 | 1.03 | 999999 | 1 |
| K | roughness coefficient by Strickler (inner slope) | LOG | 0.015 | 0.00375 | 300 | 0.5 |
| theta | rolling resistance angle | LOG | 43 | 3 | 600 | 0 |
| me | model uncertainty erosion inner slope | LOG | 1 | 0.5 | 1500 | 0.4 |
| l_piping | piping length | LOG | 62.2 | 14.3682 | 200 | 0 |
| tanalphai | inner slope angle | NOR | 0.5 | 0.075 | 150 | 0 |
| d_aquifer | aquifer thickness | LOG | 12.3 | 0.8241 | 200 | 0 |
| d_topLayer | impermeable top layer thickness | LOG | 1.87 | 0.92004 | 200 | 0 |
| h_d | dike height | NOR | 12.85 | 0.2 | 300 | 0 |
| cg | grass quality coefficient | DET | 1000000 | - | - | - |

| LocatieID |
|---|
| Dr41L27 |

| x | y | z | WaterstandID | zmin | vaknummer | |
|---|---|---|---|---|---|---|
| 181550 | 418750 | 12.51 | Dr41L27_River | 9.89 | 1410006049 | |
| name | description | type | mean | stdev | xle | rho_x |
| k_z | specific permeability | LOG | 5.79E-04 | 4.63E-04 | 600 | 0 |
| mh | model uncertainty head difference for heave | LOG | 0.8 | 0.08 | 999999 | 1 |
| mp | model uncertainty Sellmeijer | LOG | 1 | 0.08 | 999999 | 1 |
| m0 | model uncertainty critical head difference for heave | LOG | 1.2 | 0.12 | 999999 | 1 |
| gamma_g | volumetric weight of the grains | NOR | 27 | 1.35 | 300 | 0 |
| gamma_sat | saturated volumetric weight of the impermeable top layer | NOR | 17.86 | 0.393 | 300 | 0 |
| eta | White constant (sleepkrachtfactor) | LOG | 0.3 | 0.045 | 999999 | 1 |
| d_70 | 70th percentile of the grain distribution (sieve curve) | LOG | 3.71E-04 | 5.57E-05 | 180 | 0 |
| h_hinterDefault | hydraulic head hinterland | NOR | 8.74 | 0.81 | 999999 | 1 |
| K | roughness coefficient by Strickler (inner slope) | LOG | 0.015 | 0.00375 | 300 | 0.5 |
| theta | rolling resistance angle | LOG | 43 | 3 | 600 | 0 |
| me | model uncertainty erosion inner slope | LOG | 1 | 0.5 | 1500 | 0.4 |
| l_piping | piping length | LOG | 74.91 | 1.72293 | 200 | 0 |
| tanalphai | inner slope angle | NOR | 0.330088496 | 0.049513274 | 150 | 0 |
| d_aquifer | aquifer thickness | LOG | 21.9 | 1.6644 | 200 | 0 |
| d_topLayer | impermeable top layer thickness | LOG | 1.63 | 1.55828 | 200 | 0 |
| h_d | dike height | NOR | 12.51 | 0.2 | 300 | 0 |
| cg | grass quality coefficient | DET | 1000000 | - | - | - |

| LocatieID |
|---|
| Dr41L28 |

| x | y | z | WaterstandID | zmin | vaknummer | |
|---|---|---|---|---|---|---|
| 180250 | 420250 | 12.36 | Dr41L28_River | 8.68 | 1410006050 | |
| name | description | type | mean | stdev | xle | rho_x |
| k_z | specific permeability | LOG | 5.79E-04 | 4.63E-04 | 600 | 0 |
| mh | model uncertainty head difference for heave | LOG | 0.8 | 0.08 | 999999 | 1 |
| mp | model uncertainty Sellmeijer | LOG | 1 | 0.08 | 999999 | 1 |
| m0 | model uncertainty critical head difference for heave | LOG | 1.2 | 0.12 | 999999 | 1 |
| gamma_g | volumetric weight of the grains | NOR | 27 | 1.35 | 300 | 0 |
| gamma_sat | saturated volumetric weight of the impermeable top layer | NOR | 17.77 | 0.3885 | 300 | 0 |
| eta | White constant (sleepkrachtfactor) | LOG | 0.3 | 0.045 | 999999 | 1 |
| d_70 | 70th percentile of the grain distribution (sieve curve) | LOG | 3.71E-04 | 5.57E-05 | 180 | 0 |
| h_hinterDefault | hydraulic head hinterland | NOR | 8.2 | 0.69 | 999999 | 1 |
| K | roughness coefficient by Strickler (inner slope) | LOG | 0.015 | 0.00375 | 300 | 0.5 |
| theta | rolling resistance angle | LOG | 43 | 3 | 600 | 0 |
| me | model uncertainty erosion inner slope | LOG | 1 | 0.5 | 1500 | 0.4 |
| l_piping | piping length | LOG | 64.5 | 18.447 | 200 | 0 |
| tanalphai | inner slope angle | NOR | 0.329925017 | 0.049488753 | 150 | 0 |
| d_aquifer | aquifer thickness | LOG | 22.3 | 1.4049 | 200 | 0 |
| d_topLayer | impermeable top layer thickness | LOG | 1.93 | 1.26415 | 200 | 0 |
| h_d | dike height | NOR | 12.36 | 0.2 | 300 | 0 |
| cg | grass quality coefficient | DET | 1000000 | - | - | - |

| LocatieID | | | | | | |
|---|---|---|---|---|---|---|
| Dr41L29 | | | | | | |
| x | y | z | WaterstandID | zmin | vaknummer | |
| 176850 | 422350 | 11.79 | Dr41L29_River | 7.31 | 1410006054 | |
| name | description | type | mean | stdev | xle | rho_x |
| k_z | specific permeability | LOG | 5.79E-04 | 4.63E-04 | 600 | 0 |
| mh | model uncertainty head difference for heave | LOG | 0.8 | 0.08 | 999999 | 1 |
| mp | model uncertainty Sellmeijer | LOG | 1 | 0.08 | 999999 | 1 |
| m0 | model uncertainty critical head difference for heave | LOG | 1.2 | 0.12 | 999999 | 1 |
| gamma_g | volumetric weight of the grains | NOR | 27 | 1.35 | 300 | 0 |
| gamma_sat | saturated volumetric weight of the impermeable top layer | NOR | 16.3 | 0.315 | 300 | 0 |
| eta | White constant (sleepkrachtfactor) | LOG | 0.3 | 0.045 | 999999 | 1 |
| d_70 | 70th percentile of the grain distribution (sieve curve) | LOG | 3.71E-04 | 5.57E-05 | 180 | 0 |
| h_hinterDefault | hydraulic head hinterland | NOR | 6.4 | 0.23 | 999999 | 1 |
| K | roughness coefficient by Strickler (inner slope) | LOG | 0.015 | 0.00375 | 300 | 0.5 |
| theta | rolling resistance angle | LOG | 43 | 3 | 600 | 0 |
| me | model uncertainty erosion inner slope | LOG | 1 | 0.5 | 1500 | 0.4 |
| l_piping | piping length | LOG | 89 | 3.026 | 200 | 0 |
| tanalphai | inner slope angle | NOR | 0.314897413 | 0.047234612 | 150 | 0 |
| d_aquifer | aquifer thickness | LOG | 13.5 | 0.5535 | 200 | 0 |
| d_topLayer | impermeable top layer thickness | LOG | 4.2 | 1.6548 | 200 | 0 |
| h_d | dike height | NOR | 11.79 | 0.2 | 300 | 0 |
| cg | grass quality coefficient | DET | 1000000 | - | - | - |

| LocatieID | | | | | | |
|---|---|---|---|---|---|---|
| Dr41L30 | | | | | | |
| x | y | z | WaterstandID | zmin | vaknummer | |
| 174850 | 423050 | 11.38 | Dr41L30_River | 7.92 | 1410006056 | |
| name | description | type | mean | stdev | xle | rho_x |
| k_z | specific permeability | LOG | 5.79E-04 | 4.63E-04 | 600 | 0 |
| mh | model uncertainty head difference for heave | LOG | 0.8 | 0.08 | 999999 | 1 |
| mp | model uncertainty Sellmeijer | LOG | 1 | 0.08 | 999999 | 1 |
| m0 | model uncertainty critical head difference for heave | LOG | 1.2 | 0.12 | 999999 | 1 |
| gamma_g | volumetric weight of the grains | NOR | 27 | 1.35 | 300 | 0 |
| gamma_sat | saturated volumetric weight of the impermeable top layer | NOR | 17.3 | 0.365 | 300 | 0 |
| eta | White constant (sleepkrachtfactor) | LOG | 0.3 | 0.045 | 999999 | 1 |
| d_70 | 70th percentile of the grain distribution (sieve curve) | LOG | 3.71E-04 | 5.57E-05 | 180 | 0 |
| h_hinterDefault | hydraulic head hinterland | NOR | 7.5 | 0.69 | 999999 | 1 |
| K | roughness coefficient by Strickler (inner slope) | LOG | 0.015 | 0.00375 | 300 | 0.5 |
| theta | rolling resistance angle | LOG | 43 | 3 | 600 | 0 |
| me | model uncertainty erosion inner slope | LOG | 1 | 0.5 | 1500 | 0.4 |
| l_piping | piping length | LOG | 51 | 8.109 | 200 | 0 |
| tanalphai | inner slope angle | NOR | 0.327464789 | 0.049119718 | 150 | 0 |
| d_aquifer | aquifer thickness | LOG | 15.1 | 3.4881 | 200 | 0 |
| d_topLayer | impermeable top layer thickness | LOG | 3.4 | 0.986 | 200 | 0 |
| h_d | dike height | NOR | 11.38 | 0.2 | 300 | 0 |
| cg | grass quality coefficient | DET | 1000000 | - | - | - |

| LocatieID | | | | | | |
|---|---|---|---|---|---|---|
| Dr41L31 | | | | | | |
| x | y | z | WaterstandID | zmin | vaknummer | |
| 173650 | 424150 | 11.07 | Dr41L31_River | 6.99 | 1410006057 | |
| name | description | type | mean | stdev | xle | rho_x |
| k_z | specific permeability | LOG | 5.79E-04 | 4.63E-04 | 600 | 0 |
| mh | model uncertainty head difference for heave | LOG | 0.8 | 0.08 | 999999 | 1 |
| mp | model uncertainty Sellmeijer | LOG | 1 | 0.08 | 999999 | 1 |
| m0 | model uncertainty critical head difference for heave | LOG | 1.2 | 0.12 | 999999 | 1 |
| gamma_g | volumetric weight of the grains | NOR | 27 | 1.35 | 300 | 0 |
| gamma_sat | saturated volumetric weight of the impermeable top layer | NOR | 17.5 | 0.375 | 300 | 0 |
| eta | White constant (sleepkrachtfactor) | LOG | 0.3 | 0.045 | 999999 | 1 |
| d_70 | 70th percentile of the grain distribution (sieve curve) | LOG | 3.71E-04 | 5.57E-05 | 180 | 0 |
| h_hinterDefault | hydraulic head hinterland | NOR | 7.3 | 0.53 | 999999 | 1 |
| K | roughness coefficient by Strickler (inner slope) | LOG | 0.015 | 0.00375 | 300 | 0.5 |
| theta | rolling resistance angle | LOG | 43 | 3 | 600 | 0 |
| me | model uncertainty erosion inner slope | LOG | 1 | 0.5 | 1500 | 0.4 |
| l_piping | piping length | LOG | 61.1 | 15.5194 | 200 | 0 |
| tanalphai | inner slope angle | NOR | 0.329969728 | 0.049495459 | 150 | 0 |
| d_aquifer | aquifer thickness | LOG | 14.1 | 2.4675 | 200 | 0 |
| d_topLayer | impermeable top layer thickness | LOG | 3 | 1.278 | 200 | 0 |
| h_d | dike height | NOR | 11.07 | 0.2 | 300 | 0 |
| cg | grass quality coefficient | DET | 1000000 | - | - | - |

| LocatieID | | | | | | |
|---|---|---|---|---|---|---|
| Dr41L32 | | | | | | |
| x | y | z | WaterstandID | zmin | vaknummer | |
| 171250 | 426350 | 10.55 | Dr41L32_River | 8.18 | 1410006060 | |
| name | description | type | mean | stdev | xle | rho_x |
| k_z | specific permeability | LOG | 5.79E-04 | 4.63E-04 | 600 | 0 |
| mh | model uncertainty head difference for heave | LOG | 0.8 | 0.08 | 999999 | 1 |
| mp | model uncertainty Sellmeijer | LOG | 1 | 0.08 | 999999 | 1 |
| m0 | model uncertainty critical head difference for heave | LOG | 1.2 | 0.12 | 999999 | 1 |
| gamma_g | volumetric weight of the grains | NOR | 27 | 1.35 | 300 | 0 |
| gamma_sat | saturated volumetric weight of the impermeable top layer | NOR | 17.9 | 0.395 | 300 | 0 |
| eta | White constant (sleepkrachtfactor) | LOG | 0.3 | 0.045 | 999999 | 1 |
| d_70 | 70th percentile of the grain distribution (sieve curve) | LOG | 3.71E-04 | 5.57E-05 | 180 | 0 |
| h_hinterDefault | hydraulic head hinterland | NOR | 6.4 | 0.51 | 999999 | 1 |
| K | roughness coefficient by Strickler (inner slope) | LOG | 0.015 | 0.00375 | 300 | 0.5 |
| theta | rolling resistance angle | LOG | 43 | 3 | 600 | 0 |
| me | model uncertainty erosion inner slope | LOG | 1 | 0.5 | 1500 | 0.4 |
| l_piping | piping length | LOG | 57.6 | 11.9808 | 200 | 0 |
| tanalphai | inner slope angle | NOR | 0.329877474 | 0.049481621 | 150 | 0 |
| d_aquifer | aquifer thickness | LOG | 18.6 | 8.5188 | 200 | 0 |
| d_topLayer | impermeable top layer thickness | LOG | 2.5 | 1.1125 | 200 | 0 |
| h_d | dike height | NOR | 10.55 | 0.2 | 300 | 0 |
| cg | grass quality coefficient | DET | 1000000 | - | - | - |

| LocatieID |
|---|
| Dr41L33 |

| x | y | z | WaterstandID | zmin | vaknummer | |
|---|---|---|---|---|---|---|
| 169250 | 427050 | 10.13 | Dr41L33_River | 7.44 | 1410006061 | |
| name | description | type | mean | stdev | xle | rho_x |
| k_z | specific permeability | LOG | 5.79E-04 | 4.63E-04 | 600 | 0 |
| mh | model uncertainty head difference for heave | LOG | 0.8 | 0.08 | 999999 | 1 |
| mp | model uncertainty Sellmeijer | LOG | 1 | 0.08 | 999999 | 1 |
| m0 | model uncertainty critical head difference for heave | LOG | 1.2 | 0.12 | 999999 | 1 |
| gamma_g | volumetric weight of the grains | NOR | 27 | 1.35 | 300 | 0 |
| gamma_sat | saturated volumetric weight of the impermeable top layer | NOR | 17.2 | 0.36 | 300 | 0 |
| eta | White constant (sleepkrachtfactor) | LOG | 0.3 | 0.045 | 999999 | 1 |
| d_70 | 70th percentile of the grain distribution (sieve curve) | LOG | 3.71E-04 | 5.57E-05 | 180 | 0 |
| h_hinterDefault | hydraulic head hinterland | NOR | 6.4 | 0.83 | 999999 | 1 |
| K | roughness coefficient by Strickler (inner slope) | LOG | 0.015 | 0.00375 | 300 | 0.5 |
| theta | rolling resistance angle | LOG | 43 | 3 | 600 | 0 |
| me | model uncertainty erosion inner slope | LOG | 1 | 0.5 | 1500 | 0.4 |
| l_piping | piping length | LOG | 51.7 | 15.0447 | 200 | 0 |
| tanalphai | inner slope angle | NOR | 0.704590818 | 0.105688623 | 150 | 0 |
| d_aquifer | aquifer thickness | LOG | 17 | 2.55 | 200 | 0 |
| d_topLayer | impermeable top layer thickness | LOG | 3.8 | 1.3034 | 200 | 0 |
| h_d | dike height | NOR | 10.13 | 0.2 | 300 | 0 |
| cg | grass quality coefficient | DET | 1000000 | - | - | - |

| LocatieID |
|---|
| Dr41L34 |

| x | y | z | WaterstandID | zmin | vaknummer | |
|---|---|---|---|---|---|---|
| 167450 | 427750 | 10.68 | Dr41L34_River | 6.26 | 1410006063 | |
| name | description | type | mean | stdev | xle | rho_x |
| k_z | specific permeability | LOG | 5.79E-04 | 4.63E-04 | 600 | 0 |
| mh | model uncertainty head difference for heave | LOG | 0.8 | 0.08 | 999999 | 1 |
| mp | model uncertainty Sellmeijer | LOG | 1 | 0.08 | 999999 | 1 |
| m0 | model uncertainty critical head difference for heave | LOG | 1.2 | 0.12 | 999999 | 1 |
| gamma_g | volumetric weight of the grains | NOR | 27 | 1.35 | 300 | 0 |
| gamma_sat | saturated volumetric weight of the impermeable top layer | NOR | 16.9 | 0.345 | 300 | 0 |
| eta | White constant (sleepkrachtfactor) | LOG | 0.3 | 0.045 | 999999 | 1 |
| d_70 | 70th percentile of the grain distribution (sieve curve) | LOG | 3.71E-04 | 5.57E-05 | 180 | 0 |
| h_hinterDefault | hydraulic head hinterland | NOR | 5.2 | 0.14 | 999999 | 1 |
| K | roughness coefficient by Strickler (inner slope) | LOG | 0.015 | 0.00375 | 300 | 0.5 |
| theta | rolling resistance angle | LOG | 43 | 3 | 600 | 0 |
| me | model uncertainty erosion inner slope | LOG | 1 | 0.5 | 1500 | 0.4 |
| l_piping | piping length | LOG | 67.4 | 4.1114 | 200 | 0 |
| tanalphai | inner slope angle | NOR | 0.32996633 | 0.049494949 | 150 | 0 |
| d_aquifer | aquifer thickness | LOG | 30.5 | 4.575 | 200 | 0 |
| d_topLayer | impermeable top layer thickness | LOG | 2.8 | 0.2016 | 200 | 0 |
| h_d | dike height | NOR | 10.68 | 0.2 | 300 | 0 |
| cg | grass quality coefficient | DET | 1000000 | - | - | - |

| LocatieID | | | | | | |
|---|---|---|---|---|---|---|
| Dr41L35 | | | | | | |
| x | y | z | WaterstandID | zmin | vaknummer | |
| 165150 | 425750 | 8.95 | Dr41L35_River | 6.95 | 1410006068 | |
| name | description | type | mean | stdev | xle | rho_x |
| k_z | specific permeability | LOG | 5.79E-04 | 4.63E-04 | 600 | 0 |
| mh | model uncertainty head difference for heave | LOG | 0.8 | 0.08 | 999999 | 1 |
| mp | model uncertainty Sellmeijer | LOG | 1 | 0.08 | 999999 | 1 |
| m0 | model uncertainty critical head difference for heave | LOG | 1.2 | 0.12 | 999999 | 1 |
| gamma_g | volumetric weight of the grains | NOR | 27 | 1.35 | 300 | 0 |
| gamma_sat | saturated volumetric weight of the impermeable top layer | NOR | 17 | 0.35 | 300 | 0 |
| eta | White constant (sleepkrachtfactor) | LOG | 0.3 | 0.045 | 999999 | 1 |
| d_70 | 70th percentile of the grain distribution (sieve curve) | LOG | 3.71E-04 | 5.57E-05 | 180 | 0 |
| h_hinterDefault | hydraulic head hinterland | NOR | 5.4 | 0.22 | 999999 | 1 |
| K | roughness coefficient by Strickler (inner slope) | LOG | 0.015 | 0.00375 | 300 | 0.5 |
| theta | rolling resistance angle | LOG | 43 | 3 | 600 | 0 |
| me | model uncertainty erosion inner slope | LOG | 1 | 0.5 | 1500 | 0.4 |
| l_piping | piping length | LOG | 55 | 4.4 | 200 | 0 |
| tanalphai | inner slope angle | NOR | 0.395079595 | 0.059261939 | 150 | 0 |
| d_aquifer | aquifer thickness | LOG | 14.5 | 1.0875 | 200 | 0 |
| d_topLayer | impermeable top layer thickness | LOG | 3.6 | 1.098 | 200 | 0 |
| h_d | dike height | NOR | 8.95 | 0.2 | 300 | 0 |
| cg | grass quality coefficient | DET | 1000000 | - | - | - |

| LocatieID | | | | | | |
|---|---|---|---|---|---|---|
| Dr41L36 | | | | | | |
| x | y | z | WaterstandID | zmin | vaknummer | |
| 163550 | 426850 | 9.46 | Dr41L36_River | 6.33 | 1410006069 | |
| name | description | type | mean | stdev | xle | rho_x |
| k_z | specific permeability | LOG | 5.79E-04 | 4.63E-04 | 600 | 0 |
| mh | model uncertainty head difference for heave | LOG | 0.8 | 0.08 | 999999 | 1 |
| mp | model uncertainty Sellmeijer | LOG | 1 | 0.08 | 999999 | 1 |
| m0 | model uncertainty critical head difference for heave | LOG | 1.2 | 0.12 | 999999 | 1 |
| gamma_g | volumetric weight of the grains | NOR | 27 | 1.35 | 300 | 0 |
| gamma_sat | saturated volumetric weight of the impermeable top layer | NOR | 16.9 | 0.345 | 300 | 0 |
| eta | White constant (sleepkrachtfactor) | LOG | 0.3 | 0.045 | 999999 | 1 |
| d_70 | 70th percentile of the grain distribution (sieve curve) | LOG | 3.71E-04 | 5.57E-05 | 180 | 0 |
| h_hinterDefault | hydraulic head hinterland | NOR | 5.1 | 0.46 | 999999 | 1 |
| K | roughness coefficient by Strickler (inner slope) | LOG | 0.015 | 0.00375 | 300 | 0.5 |
| theta | rolling resistance angle | LOG | 43 | 3 | 600 | 0 |
| me | model uncertainty erosion inner slope | LOG | 1 | 0.5 | 1500 | 0.4 |
| l_piping | piping length | LOG | 57 | 8.265 | 200 | 0 |
| tanalphai | inner slope angle | NOR | 0.394822006 | 0.059223301 | 150 | 0 |
| d_aquifer | aquifer thickness | LOG | 18.9 | 1.3608 | 200 | 0 |
| d_topLayer | impermeable top layer thickness | LOG | 3.8 | 1.2654 | 200 | 0 |
| h_d | dike height | NOR | 9.46 | 0.2 | 300 | 0 |
| cg | grass quality coefficient | DET | 1000000 | - | - | - |

| LocatieID | | | | | | |
|---|---|---|---|---|---|---|
| Dr41L37 | | | | | | |
| x | y | z | WaterstandID | zmin | vaknummer | |
| 161750 | 427250 | 8.95 | Dr41L37_River | 5.87 | 1410006070 | |
| name | description | type | mean | stdev | xle | rho_x |
| k_z | specific permeability | LOG | 5.79E-04 | 4.63E-04 | 600 | 0 |
| mh | model uncertainty head difference for heave | LOG | 0.8 | 0.08 | 999999 | 1 |
| mp | model uncertainty Sellmeijer | LOG | 1 | 0.08 | 999999 | 1 |
| m0 | model uncertainty critical head difference for heave | LOG | 1.2 | 0.12 | 999999 | 1 |
| gamma_g | volumetric weight of the grains | NOR | 27 | 1.35 | 300 | 0 |
| gamma_sat | saturated volumetric weight of the impermeable top layer | NOR | 17.1 | 0.355 | 300 | 0 |
| eta | White constant (sleepkrachtfactor) | LOG | 0.3 | 0.045 | 999999 | 1 |
| d_70 | 70th percentile of the grain distribution (sieve curve) | LOG | 3.71E-04 | 5.57E-05 | 180 | 0 |
| h_hinterDefault | hydraulic head hinterland | NOR | 4.9 | 0.43 | 999999 | 1 |
| K | roughness coefficient by Strickler (inner slope) | LOG | 0.015 | 0.00375 | 300 | 0.5 |
| theta | rolling resistance angle | LOG | 43 | 3 | 600 | 0 |
| me | model uncertainty erosion inner slope | LOG | 1 | 0.5 | 1500 | 0.4 |
| l_piping | piping length | LOG | 57.2 | 7.3788 | 200 | 0 |
| tanalphai | inner slope angle | NOR | 0.395209581 | 0.059281437 | 150 | 0 |
| d_aquifer | aquifer thickness | LOG | 20.9 | 0.6479 | 200 | 0 |
| d_topLayer | impermeable top layer thickness | LOG | 3.8 | 0.9956 | 200 | 0 |
| h_d | dike height | NOR | 8.95 | 0.2 | 300 | 0 |
| cg | grass quality coefficient | DET | 1000000 | - | - | - |

| LocatieID | | | | | | |
|---|---|---|---|---|---|---|
| Dr41L38 | | | | | | |
| x | y | z | WaterstandID | zmin | vaknummer | |
| 157350 | 426650 | 8.72 | Dr41L38_River | 4.37 | 1410006076 | |
| name | description | type | mean | stdev | xle | rho_x |
| k_z | specific permeability | LOG | 5.79E-04 | 4.63E-04 | 600 | 0 |
| mh | model uncertainty head difference for heave | LOG | 0.8 | 0.08 | 999999 | 1 |
| mp | model uncertainty Sellmeijer | LOG | 1 | 0.08 | 999999 | 1 |
| m0 | model uncertainty critical head difference for heave | LOG | 1.2 | 0.12 | 999999 | 1 |
| gamma_g | volumetric weight of the grains | NOR | 27 | 1.35 | 300 | 0 |
| gamma_sat | saturated volumetric weight of the impermeable top layer | NOR | 16.2 | 0.31 | 300 | 0 |
| eta | White constant (sleepkrachtfactor) | LOG | 0.3 | 0.045 | 999999 | 1 |
| d_70 | 70th percentile of the grain distribution (sieve curve) | LOG | 3.71E-04 | 5.57E-05 | 180 | 0 |
| h_hinterDefault | hydraulic head hinterland | NOR | 4.5 | 0.47 | 999999 | 1 |
| K | roughness coefficient by Strickler (inner slope) | LOG | 0.015 | 0.00375 | 300 | 0.5 |
| theta | rolling resistance angle | LOG | 43 | 3 | 600 | 0 |
| me | model uncertainty erosion inner slope | LOG | 1 | 0.5 | 1500 | 0.4 |
| l_piping | piping length | LOG | 47.6 | 7.0924 | 200 | 0 |
| tanalphai | inner slope angle | NOR | 0.5 | 0.075 | 150 | 0 |
| d_aquifer | aquifer thickness | LOG | 23.7 | 0.474 | 200 | 0 |
| d_topLayer | impermeable top layer thickness | LOG | 4.9 | 0.7791 | 200 | 0 |
| h_d | dike height | NOR | 8.72 | 0.2 | 300 | 0 |
| cg | grass quality coefficient | DET | 1000000 | - | - | - |

**Appendix D**
**An estimator for the consequences upon failure**

In the case studies, a Crude Monte Carlo sampling was used for deriving the failure scenarios. A corresponding estimator for the conditional consequence E(*D*|*F*) is simply obtained by:

$$E(D|F) = 1/N \, \Sigma \, C_i \qquad (D.1)$$

with N failure scenarios and with $C_i$ the consequences for failure scenario i.
In this estimator no explicit weight is put on the consequences as a result of a breach location. A first order approximation is obviously present for approximately constant values of $C_j$ for breach locations j in combination with breach locations failing separately (i.e. not simultaneously within one scenario). In that case the expression above can be written as:

$$E(D|F) = (1/N \, \Sigma \, n_j \, C_j \,)/ \, (\Sigma \, n_j \, /N \,) \qquad (D.2)$$

This equation can be seen as a weighted average for the consequences, with weights equal to the probability of occurrence for failure at breach location j.

In the Monte Carlo Sampling applied in the case studies, no length effects were applied, i.e. the breach location was modelled as infinitesimally small locations. A breach location might in reality be representing a section of 0.1 km and another breach location a section of 1 km. These length effects are thus not present in the expressions above. Although the absence of this effect will be nihilated when using a sufficiently large amount of locations homogeneously distributed along the dike circumference.
In the PCRing approach, on the other hand, a dike ring is divided in a number of sections of a certain length, each with distinct properties. In the PCring calculations the probability of failures per mechanism and per dike section are available as intermediate results before combining them into the overall failure probability for the dike ring.
Using this information one might adopt the following estimator for the conditional consequences:

$$E(D|F) = (\Sigma \, \Pi_{ij} \, C_{ij} \,)/ \, (\Sigma \, \Pi_{ij} \,) \qquad (D.3)$$

With $\Pi_{ij}$ the product of failure probabilities of sections i to j (due to a mechanism) and $C_{ij}$ the consequence value when the corresponding scenarios involving sections i to j occurs. This is again but an approximation as no account is given for the correlations between the failure probabilities of the different sections. They are treated here as independent for the sake of simplicity. Also system effects with there impact on the failure probabilities are not taken into account. A full analysis would involve a scenario analysis as in section 4.2, with the same drawbacks.

Nevertheless the approach is tested for case study 2. Table D.1 presents the intermediate results from the PCRing calculations in terms of beta values.

Table D.1 Intermediate results of PCRing calculation

| | β [-] (48 hrs) | |
|---|---|---|
| Location | Piping | Overloop |
| Dr41L1 | 2.76 | 4.21 |
| Dr41L10 | 3.49 | 4.31 |
| Dr41L11 | 3.34 | 6.43 |
| Dr41L12 | 3.08 | 3.7 |
| Dr41L13 | 2.78 | 3.83 |
| Dr41L14 | 2.76 | 4.21 |
| Dr41L15 | 3.27 | 6.11 |
| Dr41L16 | 2.88 | 10.34 |
| Dr41L17 | 4.57 | 3.41 |
| Dr41L18 | 4.98 | 6.69 |
| Dr41L19 | 3.22 | 4.82 |
| Dr41L2 | 2.67 | 6.17 |
| Dr41L20 | 3.52 | 4.84 |
| Dr41L21 | 3.49 | 4.69 |
| Dr41L22 | 3.35 | 4.35 |
| Dr41L23 | 3.02 | 4.09 |
| Dr41L24 | 4.81 | 4.68 |
| Dr41L25 | 3.5 | 3.81 |
| Dr41L26 | 3.08 | 3.7 |
| Dr41L27 | 3.74 | 3.69 |
| Dr41L28 | 2.63 | 4.14 |
| Dr41L29 | 4.79 | 4 |
| Dr41L3 | 3.92 | 4.12 |
| Dr41L30 | 3.24 | 3.56 |
| Dr41L31 | 3.36 | 3.54 |
| Dr41L32 | 3.07 | 4.16 |
| Dr41L33 | 2.77 | 3.76 |
| Dr41L34 | 3.77 | 4.63 |
| Dr41L35 | 4.1 | 3.62 |
| Dr41L36 | 3.65 | 4.49 |
| Dr41L37 | 3.78 | 3.89 |
| Dr41L38 | 4.25 | 6.72 |
| Dr41L4 | 4.07 | 4.49 |
| Dr41L5 | 3.76 | 4.52 |
| Dr41L6 | 5.02 | 4.16 |
| Dr41L7 | 3.56 | 5.39 |
| Dr41L8 | 3.83 | 3.47 |
| Dr41L9 | 3.68 | 3.96 |

These values were used in obtaining the values depicted Table D.2, calculated according to eq. D.3 (see Table 6.7 for comparison).

Table D.2: Flood consequences for each set of scenarios in case study 2, according to eq. D.3

| | Set A (11 loc.) | Set B (22 loc.) | Set C (38 loc.) |
|---|---|---|---|
| | | | |
| *Victims [-]* | 386 | 218 | 168 |
| *Damage [€]* | $4.03 \times 10^9$ | $2.48 \times 10^9$ | $1.96 \times 10^9$ |

www.deltares.nl
www.tno.nl

Deltares